Input output selection based on robust performance

Input Output Selection Based on Robust Performance: An Active Suspension Application

Marc van de Wal

WFW report 96.048

M. M. J. van de Wal
Faculty of Mechanical Engineering
Eindhoven University of Technology
April 1996

Input Output Selection Based on Robust Performance: An Active Suspension Application

Marc van de Wal

Faculty of Mechanical Engineering
Eindhoven University of Technology
Eindhoven, The Netherlands

April 16, 1996

Summary

In [45], a method for selection of actuators and sensors (Input Output (IO) selection) in linear control systems was studied. Its main shortcoming was the inability to effectively deal with structured uncertainties and robust performance. This is partially resolved by two IO selection methods studied here. The key idea is to eliminate actuator/sensor combinations (IO sets) for which a controller meeting a guaranteed level of robust stability or robust performance cannot be designed. The structured singular value plays a key role, so the report starts with a discussion on this concept and how it can be employed for control system design.

The first method is closely related to the one in [45], *i.e.*, for each IO set six conditions are checked for existence of a stabilizing $\mathcal{H}_\infty$ controller. However, these "viability conditions" now apply for a generalized plant extended with scaling filters, which are introduced to account for structure in the uncertainty block. The resulting condition for IO set viability is a sufficient one, mainly because the scalings are only determined for the IO set including all actuators and sensors and so may not be optimal for other IO sets. The second method is based on a necessary condition, which is mainly due to the fact that the stabilizing property of the controller is dropped. The viability conditions (in the form of linear matrix inequalities) are checked for various frequencies, using transfer matrix data of the generalized plant. A major shortcoming is the inability to effectively deal with uncertainties consisting of more than two full blocks.

The two IO selection methods have been implemented in MATLAB and an active suspension control problem for a tractor-semitrailer combination served to evaluate them. A total number of 45 candidate IO sets are assessed for their ability to meet a specified level of robust performance under one scalar uncertainty. Due to its sufficiency, the first IO selection method rejects two viable IO sets, while, due to its necessity, the second method accepts two non-viable IO sets. Based on this single example, it is impossible to conclude on the methods' effectiveness in general. In the current implementation, the second IO selection method takes considerably more computation time than the first one; improvement of the efficiency of both methods merits further investigation.

A major topic for future research is IO selection for nonlinear systems. First, it must be revealed if the investigated methods can be applied successfully to linearizations of nonlinear systems, accounting for the neglected nonlinearities via the uncertainty block. Second, it must be investigated if the theory of nonlinear $\mathcal{H}_\infty$ control offers prospects in case of nominal performance or robust stability against unstructured uncertainties.

Contents

Chapter 1

Introduction

Preceding the design of a controller, an appropriate number, place, and type of actuators and sensors must be selected. This process is here referred to as "Input Output (IO) selection." Compared to modeling and controller design techniques, relatively little attention has been paid to IO selection. Nevertheless, it is a crucial step in control system design. First, the IO set may put fundamental limitations on the system's performance, *e.g.*, it may introduce right-half-plane transmission zeros, which impose restrictions on the achievable bandwidth, regardless of the controller type, see, *e.g.*, [11]. Second, the IO set partially determines aspects like system complexity, hardware expenses, and maintenance effort. Due to the combinatorial nature of the problem, the number of "candidate" IO sets may be huge and favorable ones are easily overlooked. So, an efficient and effective IO selection is desired.

The goal for IO selection in this report is stated as follows (see also [47]): *minimize the number of inputs and outputs, subject to the achievement of a specified Robust Performance (RP) level.* Thus, with the IO set it must be possible to design a controller which stabilizes the system and meets the performance specifications in the presence of a particular class of uncertainties. Candidate IO sets for which it is possible to design such a controller are termed "viable."

Various IO selection methods are surveyed in [42,46,47]. Three commonly encountered limitations are the following. First, IO selection is often restricted to systems with an equal number of inputs and outputs. Second, the controlled and measured variables are not always treated separately: it is frequently assumed that controlled variables can either directly be measured, or suitably be represented by measured variables. Third, quantitative performance specifications and uncertainty characterizations (if employed at all) are usually restricted to one particular frequency (range). In [45], a new IO selection approach for *linear* systems is discussed, which avoids these limitations, but which is only able to deal with RP in a conservative way. Instead, the method employs criteria based on Nominal Performance (NP) and Robust Stability (RS) against separate uncertainties, which are properties necessary for RP. Fundamentally, the conservativeness of the method is due to the inability to account for structured uncertainty representations, arising in systems with multiple uncertainty sources.

Two IO selection methods for *linear* control systems will be compared. Both are able to handle structured uncertainties and RP. For this purpose, the structured singular value μ is employed. The first, newly proposed, method gives a *sufficient* condition for IO set viability. After extending the generalized plant with particular scaling filters, the method essentially checks six conditions for existence of an $\mathcal{H}_\infty$ controller, as discussed in [45, Section 2.4]. Via the scaling filters, the structure of the uncertainty block can, to some extent, be accounted for. The secondly investigated method is adopted from [22]. It is based on *necessary* conditions for viability, formulated as Linear Matrix Inequalities (LMIs). Unfortunately, it is not guaranteed that a *stabilizing* controller can be designed for an accepted IO set.

The report is organized as follows. Chapter 2 discusses the structured singular value concept and the way in which it is applied for RP analysis and RP design. The two IO selection methods to be investigated are treated in Chapter 3. An active suspension control problem is proposed in Chapter 4 as an example to evaluate the IO selection methods; performance specifications and a parametric uncertainty model are given. For 45 candidate IO sets, Chapter 5 compares the results for the IO selection methods. In Chapter 6, the pros and cons of both methods are discussed and Chapter 7 provides needs for future research on IO selection for *linear* systems. As a special topic for further study, the final chapter explores the (im)possibilities to generalize the IO selection method based on existence of an $\mathcal{H}_\infty$ controller (as discussed in [45]) to *nonlinear* systems.

Chapter 2

Robust Performance

A disadvantage of the IO selection method studied in [45] is the inability to account for *structured* uncertainty representations in an adequate way. This is due to the fact that $\mathcal{H}_\infty$ theory relies on the small gain theorem [59, Section 9.2], which is conservative in case of structured uncertainties, see [45, Section 2.2]. To resolve this shortcoming, the two IO selection methods to be compared employ the so-called structured singular value, abbreviated μ, which was first introduced in [6]. Section 2.1 discusses μ in a purely algebraic context; with slight modifications, the treatment is adopted from [33, Section 3] and [51, Section 2.2]. This is followed by discussions on how to use μ for Robust Performance (RP) analysis (Section 2.2) and RP design (Section 2.3) for linear control systems.

2.1 The Structured Singular Value

In this section, the structured singular value μ will be treated as a matrix function operating on complex matrices $M \in \mathbb{C}^{n\times m}$. In the definition of μ, there is an underlying structure $\mathbf{\Delta}$, which is a set of block diagonal matrices. As will become clear in Section 2.2, for control systems the structure $\mathbf{\Delta}$ depends on uncertainty characterizations *and* performance specifications. Defining the structure involves specifying three things: 1) the total number of blocks, 2) the type of each block (repeated scalar or full, real or complex), and 3) the dimension of each block.

In this report, only *full complex* blocks making up $\mathbf{\Delta}$ will be considered, leaving out full real, repeated complex and repeated real blocks. The restriction to *full* blocks not only simplifies the notation, but appears also appropriate for the truck example, see Section 4.3. The restriction to *complex* blocks is motivated by the avoidance of extra complications in the first exploration of the IO selection methods. Since some algorithms in the MATLAB μ-Synthesis and Analysis Toolbox [1] (abbreviated "μ-Toolbox") can also deal with mixed real and complex, full and repeated blocks *and* since real blocks are more appropriate for the uncertainty model in the truck example, IO selection involving more general uncertainties

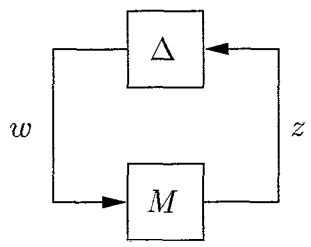

Figure 2.1: Constant matrix feedback connection $M - \Delta$

is certainly a need for future research (see also Chapter 7). Hence, the structure $\mathbf{\Delta}$ to be considered here is as follows:

$$\mathbf{\Delta} = \{\text{diag}(\Delta_1, \Delta_2, \ldots, \Delta_l) : \ \Delta_i \in \mathbb{C}^{m_i \times n_i}\}; \ \sum_{i=1}^{l} m_i = m; \ \sum_{i=1}^{l} n_i = n. \tag{2.1}$$

Contrary to the treatments in [33,51], each block Δ_i is allowed to be nonsquare. Often, a norm bounded subset of $\mathbf{\Delta}$ is used, denoted as:

$$\boldsymbol{B}_{\mathbf{\Delta}} = \left\{\Delta \in \mathbf{\Delta} : \ \bar{\sigma}(\Delta) \leq \frac{1}{\gamma}\right\}, \tag{2.2}$$

with $\bar{\sigma}$ the largest singular value of a matrix. The structured singular value is now defined as follows, see, *e.g.*, [33, Section 3]:

Definition of μ: *Given a matrix $M \in \mathbb{C}^{n \times m}$ and a compatible block diagonal structure $\mathbf{\Delta}$, the structured singular value $\mu_{\mathbf{\Delta}}(M)$ of M with respect to $\mathbf{\Delta}$ is defined as:*

$$\mu_{\mathbf{\Delta}}(M) := \frac{1}{\min\{\bar{\sigma}(\Delta) : \ \Delta \in \mathbf{\Delta}, \ \det(I - M\Delta) = 0\}}, \tag{2.3}$$

unless no $\Delta \in \mathbf{\Delta}$ makes $I - M\Delta$ singular, in which case $\mu_{\mathbf{\Delta}}(M) := 0$.

Note, that $\mu_{\mathbf{\Delta}}(M)$ not only depends on M, but on $\mathbf{\Delta}$ as well. It is illustrative to give a "feedback" interpretation of the μ definition [33]. Consider Fig. 2.1, which represents the loop equations $z = Mw$ and $w = \Delta z$. As long as $I - M\Delta$ is nonsingular, the only solutions z and w to these equations are $z = w = 0$. However, if $I - M\Delta$ is singular there are infinitely many solutions and the norms of z and w can be arbitrarily large, *i.e.*, the constant matrix feedback system in Fig. 2.1 is "unstable." Likewise, the system is "stable" when the only solutions are zero. Thus, $\mu_{\mathbf{\Delta}}(M)$ provides a measure of the smallest structured Δ causing instability. The "magnitude" of this Δ is $1/\mu_{\mathbf{\Delta}}(M)$.

Unfortunately, exact computation of μ cannot be performed efficiently in general. Instead, μ is approximated by lower and upper bounds, based on the following inequalities:

$$\rho(M) \leq \mu_{\mathbf{\Delta}}(M) \leq \bar{\sigma}(M), \tag{2.4}$$

with ρ the spectral radius of a matrix, *i.e.*, the magnitude of the largest eigenvalue (in magnitude). Since the gap between the upper and lower bounds can be arbitrarily large (see [59, Section 11.2.2] for an analytical example), these bounds are not directly suitable

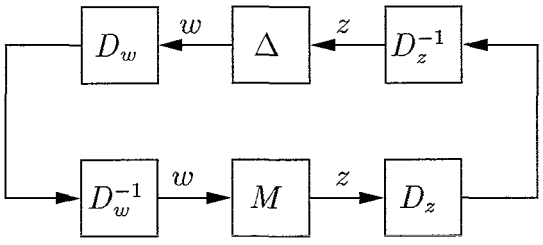

Figure 2.2: Scaled, constant matrix feedback connection $M - \Delta$

for μ computation. To (partially) solve this, transformations on M are used, which *do not affect* $\mu_{\mathbf{\Delta}}$, but which *do affect* ρ and $\bar{\sigma}$. The computation of the lower bound will not be further addressed here (see, *e.g.*, [33] for details), because only the upper bound is used for the IO selection methods. To compute a better upper bound, two sets of invertible scaling matrices ("D-scales") are defined, see also Fig. 2.2:

$$\boldsymbol{D_z} = \{\mathrm{diag}(d_1 I_{m_1}, d_2 I_{m_2}, \ldots, d_l I_{m_l}) : \; d_i \in \mathbb{R}^+\}, \tag{2.5}$$

$$\boldsymbol{D_w} = \{\mathrm{diag}(d_1 I_{n_1}, d_2 I_{n_2}, \ldots, d_l I_{n_l}) : \; d_i \in \mathbb{R}^+\}. \tag{2.6}$$

Note, that the sets $\boldsymbol{D_z}$ and $\boldsymbol{D_w}$ are such that each full block Δ_i in $\mathbf{\Delta}$ is accompanied by diagonal scaling matrices $d_i I_{m_i}$ and $d_i I_{n_i}$ with positive real numbers d_i as diagonal entries. These numbers are collected in the set $\boldsymbol{d}$:

$$\boldsymbol{d} = \{(d_1, d_2, \ldots, d_l) : \; d_i \in \mathbb{R}^+\} \tag{2.7}$$

Without loss of generality, the scaling matrices will be normalized with respect to the last diagonal matrices in $\boldsymbol{D_z}$ and $\boldsymbol{D_w}$, *i.e.*, $d_l = 1$ [33]. For any $\Delta \in \mathbf{\Delta}$, $D_z \in \boldsymbol{D_z}$, and $D_w \in \boldsymbol{D_w}$ (*e.g.*, [59, Section 11.2.2]):

$$D_w \Delta D_z^{-1} = \Delta, \tag{2.8}$$

$$\mu_{\mathbf{\Delta}}(M) = \mu_{\mathbf{\Delta}}(D_z M {D_w}^{-1}), \tag{2.9}$$

and hence the upper bound for μ can be tightened to:

$$\mu_{\mathbf{\Delta}}(M) \leq \inf_{d \in \boldsymbol{d}} \bar{\sigma}(D_z M {D_w}^{-1}). \tag{2.10}$$

This bound can be reformulated as a convex optimization problem (in fact, a Linear Matrix Inequality (LMI), see [33, Section 3]), so the global optimum can in principle be found.

The upperbound in (2.10) is only an *equality* for some special cases of the uncertainty structure (so-called "μ-simple structures," [33]). For the structure in (2.1), μ computation is exact if the number of blocks is *less* than four, *i.e.*, $l \leq 3$. Fortunately, computational experimentation has shown, that in most cases the upper bound is nearly equal to $\mu_{\mathbf{\Delta}}(M)$ [1, Chapter 2]. The use of the upperbound instead of μ itself is also justified by the following two reasons. First, in the context of control systems, μ is essentially a stability measure (see Section 2.2) and it would be more dangerous to underestimate μ than to overestimate it. Second, robustness against arbitrarily slowly time-varying uncertainties is covered by the upperbound [36].

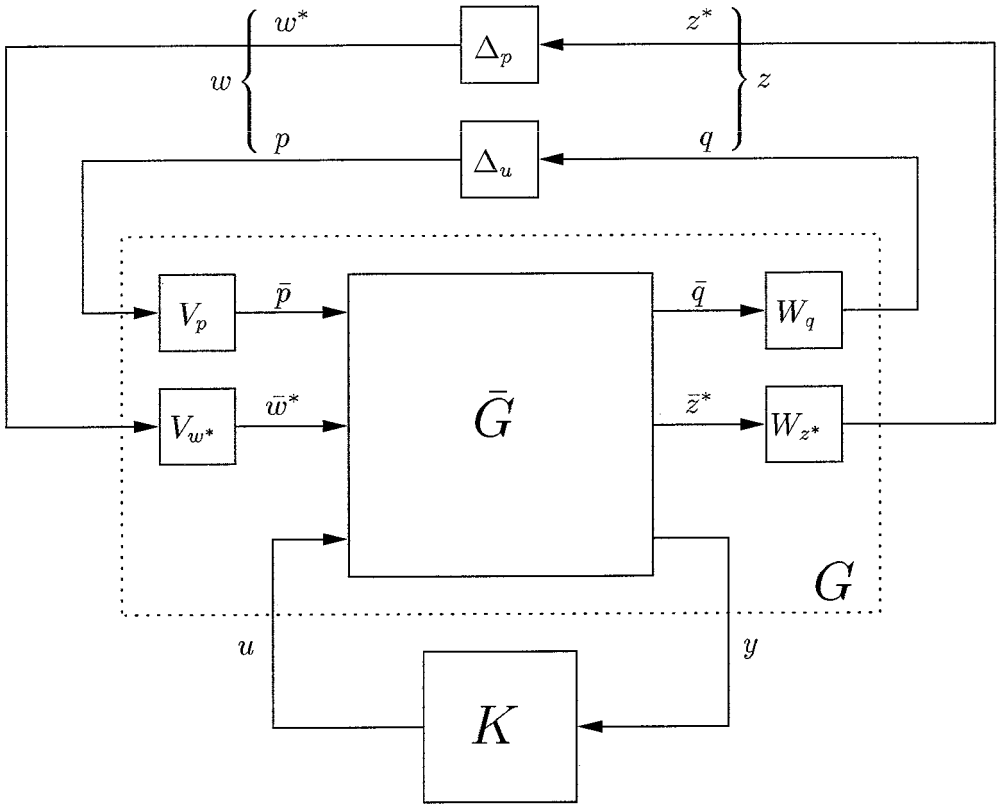

G	:	generalized plant
$\bar{G}$	:	nominal plant (system model)
K	:	controller
Δ_u	:	scaled uncertainty block
Δ_p	:	scaled performance block
V_{w^*}	:	shaping filter for exogenous variables
W_{z^*}	:	weighting filter for controlled variables
V_p, W_q	:	scaling filters for uncertainties
$\bar{p}/p$	:	unscaled/scaled output from uncertainty block
$\bar{q}/q$	:	unscaled/scaled input to uncertainty block
$\bar{w}^*/w^*$	:	unshaped/shaped exogenous variables
$\bar{z}^*/z^*$	:	unweighted/weighted controlled variables
u	:	manipulated variables (inputs)
y	:	measured variables (outputs)

Figure 2.3: Standard control system set-up

2.2 μ-Analysis

While in the previous section μ was related with *constant* matrices, in this section μ will be discussed in the context of Transfer Function Matrices (TFMs) for *dynamic* control systems.

To start with, the standard set-up for finite dimensional, linear, time-invariant control systems in Fig. 2.3 is considered. Block G is called the generalized plant, which includes nominal system data via $\bar{G}$ and which may also include TFMs reflecting performance specifications (V_{w^*}, W_{z^*}) and uncertainty characterizations (V_p, W_q), see [45, Section 2.1] for more details. Uncertainties are represented by the block Δ_u, while a *fictitious* uncertainty block Δ_p is introduced to account for performance specifications; in general, Δ_p is an unstructured complex block. It is assumed, that Δ_u and Δ_p are stable, *i.e.*, that all poles are in the open left-half-plane $\mathbb{C}^-$. The controller is denoted K. In the sequel, it is assumed that G and K are real-rational and proper and that their state-space descriptions are stabilizable and detectable, see [59, Section 16.1]. Controllers K with the additional property of being internally stabilizing are termed "*admissible*" ([7], [59, Section 16.1]) and the set of all admissible controllers is denoted $\mathcal{K}_A$.

From Fig. 2.3, the open-loop TFM G can be written as follows:

$$\begin{bmatrix} q \\ z^* \\ y \end{bmatrix} = \begin{bmatrix} z \\ y \end{bmatrix} = \begin{bmatrix} G_{11} & G_{12} \\ G_{21} & G_{22} \end{bmatrix} \begin{bmatrix} w \\ u \end{bmatrix} = G \begin{bmatrix} p \\ w^* \\ u \end{bmatrix}. \tag{2.11}$$

Figure 2.4 is obtained from Fig. 2.3 by closing the control loop. The generalized closed-loop TFM M can be written as a so-called lower linear fractional transformation of G and K:

$$\begin{aligned} M &= \mathcal{F}_l(G, K) := G_{11} + G_{12}K(I - G_{22}K)^{-1}G_{21}, \\ z &= \begin{bmatrix} q \\ z^* \end{bmatrix} = \begin{bmatrix} M_{11} & M_{12} \\ M_{21} & M_{22} \end{bmatrix} \begin{bmatrix} p \\ w^* \end{bmatrix} = Mw. \end{aligned} \tag{2.12}$$

The nominal closed-loop $\bar{M}$ can be found in a similar way via $\bar{M} = \mathcal{F}_l(\bar{G}, K)$. Note that the system in Fig. 2.4 can be viewed as a *dynamic* equivalent of the feedback interconnection in Fig. 2.1. The following feedback interpretation of $\mu_{\mathbf{\Delta}}(M)$ in the *frequency domain* can now be given [3, Section 5.7.1].

Consider the loop in Fig. 2.4 as the feedback of a nominally stable closed-loop control system $M(s)$ and a set of stable uncertainty TFMs $\Delta(s)$ with structure like $\mathbf{\Delta}$. According to the multivariable Nyquist criterion (see, *e.g.*, [3, Section 1.3.4]), the feedback loop is stable if and only if the plot of $\det\{I - M(j\omega)\Delta(j\omega)\}$ does not pass through or encircle the origin. Suppose that a given uncertainty Δ destabilizes the system, so $\det\{I - M\Delta\}$ passes through the origin or encircles it at least once. Also consider $\det\{I - M \cdot \epsilon\Delta\}$, with ϵ between zero and one. For $\epsilon = 1$ the original Nyquist plot is retained, while for $\epsilon = 0$ the plot reduces to the point 1. Since the Nyquist plot depends continuously on ϵ, there is an $\epsilon \in (0, 1]$ such that $\det\{I - M \cdot \epsilon\Delta\}$ passes through the origin. Hence, if Δ destabilizes the perturbed system,

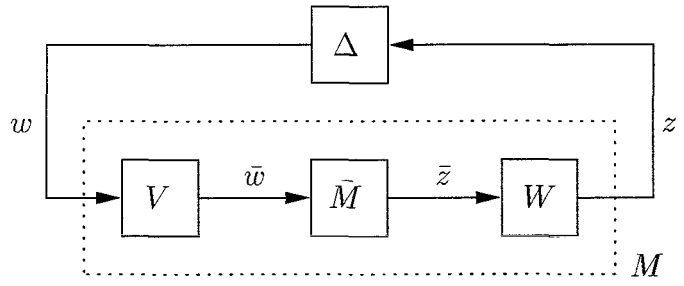

M : generalized closed-loop control system
$\bar{M}$: nominal closed-loop control system
Δ : $\Delta = \text{diag}(\Delta_u, \Delta_p)$
V : $V = \text{diag}(V_p, V_{w^*})$
W : $W = \text{diag}(W_q, W_{z^*})$

$w,\ \bar{w}$: $w = \binom{p}{w^*},\ \bar{w} = \binom{\bar{p}}{\bar{w}^*}$
$z,\ \bar{z}$: $z = \binom{q}{z^*},\ \bar{z} = \binom{\bar{q}}{\bar{z}^*}$

Figure 2.4: Standard closed-loop control system set-up

there exist an $\omega \in \mathbb{R}$ and a "smaller" uncertainty $\epsilon\Delta$ such that $\det\{I - M(j\omega) \cdot \epsilon\Delta(j\omega)\} = 0$. Thus, under the specified uncertainty structure $\mathbf{\Delta}$, the feedback loop is destabilized if and only if for some $\omega \in \mathbb{R}$

$$\det\{I - M(j\omega)\Delta(j\omega)\} = 0. \tag{2.13}$$

Involving the definition of μ in (2.3) in this reasoning, the frequency dependent $\mu_{\mathbf{\Delta}}\{M(j\omega)\}$ is the reciprocal of the smallest structured uncertainty Δ causing instability of the feedback loop, if such an uncertainty exists. The peak value of μ over the frequency domain determines the size of uncertainties the loop is robustly stable against.

With μ it is possible to test, *e.g.*, the RP properties of a control system, *i.e.*, it can be used to test if a system is stable, at the same time meeting the performance specifications in the face of a prescribed set of uncertainties. To arrive at a normalized test, the set $\mathbf{\Delta}$ will be restricted to the subset $\boldsymbol{B}_{\mathbf{\Delta}}$ in (2.2). It is emphasized, that with a slight abuse of notation $\boldsymbol{B}_{\mathbf{\Delta}}$ now represents the stable, $\mathcal{H}_\infty$ norm bounded rational TFMs with a block structure like $\mathbf{\Delta}$. The following provides a *necessary and sufficient* condition for RP [33]:

Robust Performance: *Consider Fig. 2.4, Given that Δ and M are stable, stability of the uncertain system for all $\Delta \in \boldsymbol{B}_{\mathbf{\Delta}}$ is achieved if and only if*

$$\|M\|_\mu < \gamma, \tag{2.14}$$

with

$$\|M\|_\mu := \sup_\omega \mu_{\mathbf{\Delta}}\{M(j\omega)\}. \tag{2.15}$$

Testing this condition is referred to as "μ-analysis." Though $\|M\|_\mu$ lacks the positive-definiteness and triangle properties of norms (see, *e.g.*, [3, Section 5.4.2]), the notation is similar to

the $\mathcal{H}_\infty$ norm:

$$\|M\|_\infty := \sup_\omega \bar{\sigma}\{M(j\omega)\}. \tag{2.16}$$

The value $\|M\|_\mu$ could be seen as a multivariable stability margin, since it indicates how "far" the uncertain closed-loop is from instability with the worst case uncertainty $\Delta \in \mathbf{\Delta}$. The reciprocal of an $\|M\|_\mu$ smaller than one yields the value with which the worst case uncertainty can be multiplied before it causes instability.

The RP test (2.14) is a stability test against an uncertainty block Δ, composed of a true uncertainty block Δ_u and a *fictitious* uncertainty block Δ_p. Hence, the requirement of combined *stability* and *performance* under a class of uncertainties (RP requirement) has been transformed into a single *stability* test. An analogous test for Robust Stability (RS) can be given, in which case only the block Δ_u in Δ and the subsystem M_{11} in the generalized closed-loop M are considered.

To conclude this section, it is recalled that $\|M\|_\mu$ in (2.15) is usually not computed exactly. Instead, the upper and lower bounds for μ are computed. If the upper bound "$\|M\|_{\bar{\mu}}$" for $\|M\|_\mu$ is used, replacing (2.14) and (2.15) by

$$\|M\|_{\bar{\mu}} < \gamma, \tag{2.17}$$

with

$$\|M\|_{\bar{\mu}} := \sup_\omega \inf_{d \in \boldsymbol{d}} \bar{\sigma}\{D_z(j\omega)M(j\omega)D_w^{-1}(j\omega)\}, \tag{2.18}$$

a *sufficient* condition for RP is provided, which is generally tight, *i.e.*, $\|M\|_{\bar{\mu}} \approx \|M\|_\mu$. In practice (see also [1]), $\|M\|_{\bar{\mu}}$ is computed by successively choosing a suitable frequency range and frequency grid, optimizing the D-scales at each considered frequency, and computing the supremum of $\bar{\sigma}(D_z M D_w^{-1})$ over all considered frequencies. Note, that the obtained $\|M\|_{\bar{\mu}}$ value is too small if "critical" frequencies are absent in the specified grid.

Comparing (2.18) with the definition of the $\mathcal{H}_\infty$ norm (2.16), the μ upperbound is simply the $\mathcal{H}_\infty$ norm of a *scaled* system. This will be employed by the first IO selection method in Section 3.1 and the μ-synthesis in the next section.

2.3 μ-Synthesis

In the previous section, μ-analysis served to check if a plant G closed with a *given* controller K achieves RP. In this section, the problem of *designing* a controller achieving (the best possible level of) RP is considered, which is referred to as μ-synthesis. The goal of "optimal" μ-synthesis can be expressed as follows:

$$\min_{K \in \mathcal{K}_A} \|M(G,K)\|_\mu. \tag{2.19}$$

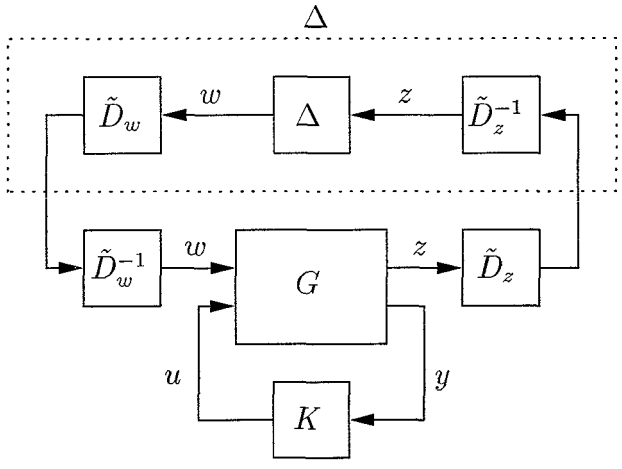

Figure 2.5: Extending G with rational D-scales for D-K iteration

Recall that $\mathcal{K}_A$ is the set of all admissible controllers. Unfortunately, this problem is currently unsolved. Instead, (2.19) is replaced by the following "approximate" goal [59, Section 11.4]:

$$\min_{K \in \mathcal{K}_A} \inf_{\tilde{d} \in \tilde{\boldsymbol{d}}} \|\tilde{D}_z M(G,K) \tilde{D}_w^{-1}\|_\infty, \tag{2.20}$$

with "$\tilde{x}$, $\tilde{X}$" denoting stable, minimum phase, real-rational approximations of the frequency dependent variables x, X. It is remarked, that compared to the unstructured optimal $\mathcal{H}_\infty$-synthesis, this structured μ-synthesis problem has extra freedom via the scalings $\tilde{D}_z$ and $\tilde{D}_w$. This is exploited to lead to lower achievable closed-loop "norms."

The approximate μ-synthesis problem in (2.20) is nonconvex for K and $\tilde{d}$ simultaneously and the global optimum may be hard to find. Instead, a *sequence* of convex minimizations can be performed, which is often called "D-K iteration," see, *e.g.*, [1, Chapter 3], [3, Section 6.9.3], and [59, Section 11.4]. This process is summarized as follows, see also Fig. 2.5:

0. *Compute an initial controller.*
   An initial, stabilizing controller K is designed (*e.g.*, an $\mathcal{H}_\infty$ controller for the unstructured version of $\boldsymbol{B}_\Delta$) and the corresponding nominal closed-loop M is computed.

1. *Perform μ-analysis.*
   For the given M, the convex optimization problem $\inf_{d \in \boldsymbol{d}} \bar{\sigma}\{D_z(j\omega) M(j\omega) D_w^{-1}(j\omega)\}$ is solved for a finite number of frequencies ω in a representative frequency range. The supremum over the frequency grid of this μ upper bound yields $\|M\|_\mu$, see (2.18).

2. *Find rational D-scaling approximations.*
   Over the frequencies of interest, stable, minimum phase, rational transfer functions are fit (in magnitude) to d from the previous step. The data in d are replaced by their rational approximations $\tilde{d}$.

3. *Perform $\mathcal{H}_\infty$ optimization.*
   Given the rational approximation $\tilde{d}$, $\|\tilde{D}_z M(G,K)\tilde{D}_w^{-1}\|_\infty$ is minimized with respect to all stabilizing K, see Fig. 2.5. With the newly obtained M, the μ-analysis in step 1 is repeated.

This iteration could be repeated until $\|M\|_{\bar{\mu}}$ in step 1 does not further decrease ("optimal D-K iteration"), or until $\|M\|_{\bar{\mu}} < \gamma$, *e.g.*, for $\gamma = 1$ ("suboptimal D-K iteration"). Other stopping criteria are that the plot of $\mu_{\mathbf{\Delta}}(M)$ in step 1 does not change anymore, or that the plot of the D-scales remains the same [59, Section 11.4]. Although the D-K iteration is not guaranteed to converge, it usually does in practice [59, Section 11.4].

The controller order is equal to the order of G plus twice the order of $\tilde{d}$ which was lastly used in step 3. To limit the controller order, it may thus be preferred to use low order D-scaling approximations in the final iteration step. It is however advisable to perform a μ-analysis for the resulting M, to check if the D-K iteration has not diverged in the final step.

Chapter 3

Input Output Selection Methods

One way to check if IO sets are viable in the sense of RP is to perform D-K iteration for all candidates. However, for a large number of candidates, this "brute force" approach is undesirable. More efficient, but probably less effective, IO selection methods are discussed in this chapter. To our knowledge, the first method (Section 3.1) has not been investigated elsewhere in literature. The second method (Section 3.2) was proposed in [22] and is further studied in [35]. While the first IO selection approach is based on a sufficient condition for IO set viability, the second one relies on a necessary condition.

3.1 Input Output Selection Based on D-Scale Estimates

Suppose that optimal D-K iteration is performed for the *overall* IO set, *i.e.*, the IO set including all candidate actuators and sensors. Call the closed-loop for the overall IO set $M^\star$. If $\|M^\star\|_{\bar{\mu}}$ from step 1 in the *final* iteration is smaller than γ, the overall IO set is guaranteed to achieve an RP level γ. Note, that in case $\|M^\star\|_{\bar{\mu}} > \gamma$, the overall IO set may still be viable in the sense that it achieves the desired RP level, since $\|M^\star\|_{\mu} \leq \|M^\star\|_{\bar{\mu}}$. For the finally obtained $M^\star$, a μ-analysis is performed and the associated D-scales D_z and D_w are fit with rational approximations denoted by $\hat{D}_z$ and $\hat{D}_w$. With $\hat{D}_z$ and $\hat{D}_w$, an "estimate" $\|M^\star\|_{\hat{\mu}}$ for the upperbound $\|M^\star\|_{\bar{\mu}}$ is defined as:

$$\|M^\star\|_{\hat{\mu}} := \|\hat{D}_z M^\star \hat{D}_w^{-1}\|_\infty. \tag{3.1}$$

Comparing equations (2.15), (2.18), and (3.1), three different "norms" related to the overall IO set's closed-loop $M^\star$ can be computed, for which the following inequalities apply:

$$\|M^\star\|_{\mu} \leq \|M^\star\|_{\bar{\mu}} \leq \|M^\star\|_{\hat{\mu}}. \tag{3.2}$$

The higher the order of $\hat{D}_z$ and $\hat{D}_w$, the better $\inf_{d\in\boldsymbol{d}} \bar{\sigma}(D_z M^\star D_w^{-1})$ and $\bar{\sigma}(\hat{D}_z M^\star \hat{D}_w^{-1})$ will match and the closer $\|M^\star\|_{\bar{\mu}}$ and $\|M^\star\|_{\hat{\mu}}$ will be.

The rational D-scales $\hat{D}_z$ and $\hat{D}_w$ for the overall IO set play a crucial role in the IO selection method proposed in this section. Suppose that w and z in Fig. 2.5 represent the same goals for all candidate IO sets, implying that w does not contain measurement noise ("y-noise") and z does not include input weights ("u-weights"). The following notion provides the key idea for IO selection. An optimal closed-loop M for an IO set which is "almost as good" as the overall IO set will have approximately the same dynamic behavior as $M^\star$, *i.e.*, $M^\star(s) \approx M(s)$. The following measure will serve to quantify the closeness of M and $M^\star$:

$$\Omega = \frac{\|M^\star - M\|_\infty}{\|M^\star\|_\infty}. \tag{3.3}$$

If $\Omega \ll 1$, M and $M^\star$ behave approximately the same, $\mu_{\boldsymbol{\Delta}}(M) \approx \mu_{\boldsymbol{\Delta}}(M^\star)$, *and* the D-scales for M are roughly the same as those for $M^\star$. In that case, $\hat{D}_z$ and $\hat{D}_w$ are good estimates for the D-scales associated with M, provided $\hat{D}_z$ and $\hat{D}_w$ are good estimates for the D-scales associated with $M^\star$. If so, $\|\hat{D}_z M \hat{D}_w^{-1}\|_\infty \approx \|M\|_{\bar{\mu}}$.

For each IO set, G can be extended with the rational scalings $\hat{D}_z$ and $\hat{D}_w^{-1}$ arising from the overall IO set's optimal closed-loop $M^\star$. An estimate of the achievable $\|M\|_{\bar{\mu}}$ value for each IO set can be obtained by computing an *optimal* $\mathcal{H}_\infty$ controller for each IO set's extended G (compare with the 3rd step in D-K iteration). It is emphasized, that this may be a *conservative* estimate, since $\hat{D}_z$ and $\hat{D}_w$ might not be the best approximations for other IO sets than the overall one. This is expressed by the following inequality:

$$\min_{K \in \mathcal{K}_A} \inf_{\tilde{d} \in \tilde{\boldsymbol{d}}} \|\tilde{D}_z(\tilde{d}) M(G,K) \tilde{D}_w^{-1}(\tilde{d})\|_\infty \leq \min_{K \in \mathcal{K}_A} \|\hat{D}_z M(G,K) \hat{D}_w^{-1}\|_\infty. \tag{3.4}$$

For the purpose of IO selection, the rational D-scales $\hat{D}_z$ and $\hat{D}_w$ are now used as follows:

IO Selection with D-Scale Estimates: *Consider Fig. 2.5. For each candidate IO set, G is scaled with $\hat{D}_z$, $\hat{D}_w^{-1}$ and it is tested if an admissible K can be designed achieving $\|M(G,K)\|_{\bar{\mu}} := \|\hat{D}_z M(G,K) \hat{D}_w^{-1}\|_\infty < \gamma$. Since this is a* sufficient *condition for existence of an admissible controller achieving $\|M(G,K)\|_\mu < \gamma$, IO sets for which this condition is met are guaranteed to achieve RP against all $\Delta \in \boldsymbol{B}_{\boldsymbol{\Delta}}$.*

Unfortunately, due to sufficiency, IO sets which are actually viable might be eliminated. This shortcoming is expected to be more serious if y-noise is included in w and u-weights in z. The presence of u-weights and y-noise is reflected in the lower right blocks of the D-scales (associated with Δ_p), which are normalized to identity ($d_l = 1$ in (2.7)). To subject other IO sets than the overall one to the viability tests, identity diagonal entries in $\hat{D}_z$ and $\hat{D}_w$ corresponding to non-considered inputs and outputs must be skipped. It is expected, that the larger the y-noise and u-weights are, the less "close" $\hat{D}_z$ and $\hat{D}_w$ are to the optimal D-scales for each IO set, *i.e.*, the gap in inequality (3.4) will be larger. After all, D-K iteration for the overall IO set accounts for u-weights on *all* inputs and y-noises on *all* outputs. The IO selection example in Chapter 5 will be used to investigate the severity of this problem (Section 5.2).

Essentially, the IO selection proposal amounts to the same approach as in [45, Section 2.4], where six conditions test the existence of an admissible controller achieving a desired closed-loop $\mathcal{H}_\infty$ norm. It was already noted in the explanation of D-K iteration (Section 2.3), that

by extending the generalized plant G with rational D-scales, a new $\mathcal{H}_\infty$ control problem can be formulated. For IO selection, the existence of an admissible controller achieving RP is checked via the same six conditions. For the sake of completeness, these conditions will be summarized here.

The generalized plant G in Fig. 2.3 can be represented as:

$$G: \begin{cases} \dot{x} = Ax + B_1 w + B_2 u \\ z = C_1 x + D_{11} w + D_{12} u \\ y = C_2 x + D_{21} w + D_{22} u, \end{cases} \tag{3.5}$$

with $x \in \mathbb{R}^{n_x}$ the state vector and the inputs and outputs as defined in Fig. 2.3 and Fig. 2.4: $w \in \mathbb{R}^{n_w}$, $u \in \mathbb{R}^{n_u}$, $z \in \mathbb{R}^{n_z}$, and $y \in \mathbb{R}^{n_y}$. For the state-space parameterization of $\mathcal{H}_\infty$ controllers in [12], six assumptions on (3.5) are made. These must be satisfied for $\mathcal{H}_\infty$ design via the Riccati equation approach (*e.g.*, with [1]) *and* for the suggested IO selection method:

1,2. (A, B_2) is stabilizable and (C_2, A) detectable,

3,4. D_{12} has full column rank and D_{21} has full row rank,

5,6. $\begin{bmatrix} A - j\omega I & B_2 \\ C_1 & D_{12} \end{bmatrix}$ has full column rank $\forall\, \omega$ and $\begin{bmatrix} A - j\omega I & B_1 \\ C_2 & D_{21} \end{bmatrix}$ has full row rank $\forall\, \omega$.

In the derivation of the controller parameterization in [12], u and y are scaled and unitary transformations on w and z are performed. Without loss of generality, these manipulations are such, that

$$D_{12} = \begin{bmatrix} 0_{(n_z - n_u)\times(n_u)} \\ I_{n_u} \end{bmatrix}, \quad D_{21} = \begin{bmatrix} 0_{(n_y)\times(n_w - n_y)} & I_{n_y} \end{bmatrix} \tag{3.6}$$

(by assumptions 3 and 4), and

$$D_{11} = \begin{bmatrix} D_{11_{11}} & D_{11_{12}} \\ D_{11_{21}} & D_{11_{22}} \end{bmatrix}, \text{ with } \begin{array}{l} D_{11_{11}} \in \mathbb{R}^{(n_z - n_u)\times(n_w - n_y)} \\ D_{11_{12}} \in \mathbb{R}^{(n_z - n_u)\times n_y} \\ D_{11_{21}} \in \mathbb{R}^{n_u \times (n_w - n_y)} \\ D_{11_{22}} \in \mathbb{R}^{n_u \times n_y} \end{array}. \tag{3.7}$$

For more details on the involved transformations, it is referred to, *e.g.*, [30, Section 6.7] and [59, Section 17.2]. To obtain an admissible controller achieving $\|M\|_\infty < \gamma$, two Riccati equations must be solved, see, *e.g.*, [12], [30, Section 6.7], or [59, Section 17.1] for documentation of these equations. One of them is related with a state-feedback-like problem ("state-feedback Riccati"), the other with an observer-like problem ("observer Riccati"). The following lays the foundation for the IO selection method:

There exists an admissible controller such that $\|M\|_\infty < \gamma$ if and only if *the following conditions hold [59, Section 17.1]:*

1. $\max\{\overline{\sigma}(D_{11_{11}}, D_{11_{12}}), \overline{\sigma}(D_{11_{11}}^T, D_{11_{21}}^T)\} < \gamma$,

2,3. The two Hamiltonians H_X and H_Y associated with the state-feedback Riccati and the observer Riccati respectively do not have $j\omega$-axis eigenvalues. Moreover, $\mathrm{Im}\binom{0_{n\times n}}{I_{n\times n}}$ is complementary to each Hamiltonian's invariant subspace corresponding to the stable eigenvalues.

4,5. The solutions X_∞ and Y_∞ to the state-feedback and observer Riccati respectively are positive semi-definite: $X_\infty \geq 0$ and $Y_\infty \geq 0$

6. The spectral radius of the product $X_\infty Y_\infty$ is smaller than γ^2: $\rho(X_\infty Y_\infty) < \gamma^2$.

In the context of IO selection, the conditions 1–6 will be called the "viability conditions." Note, that condition 1 also depends on the IO set under consideration, since (possible very small) input weights and measurement noises are included in z and w respectively to meet assumptions 3 and 4. However, if $D_{11} = 0$ for the overall IO set, it will also be zero for the other IO sets and so condition 1 need not be checked. For an elaboration on conditions 2–6, it is referred to [45, Section 2.4] and Chapter 7.

For the RP based IO selection, the viability conditions are checked for the generalized plant G *extended* with the rational approximations for the overall IO set's D-scales $\hat{D}_z$ and $\hat{D}_w^{-1}$. It is remarked, that once the standard *assumptions* are met for G, they will also be met for the extended generalized plant, thanks to the properties of the rational D-scales, see Section 2.3. Having obtained the state-space formulation of the extended generalized plant, each IO set is subjected to the viability conditions. As soon as one condition fails, the rest need not be checked.

3.2 Input Output Selection Based on Linear Matrix Inequalities

This section discusses the *key ideas* of the IO selection method proposed in [22] and summarized in [44]. For a more detailed treatment of the theory, it is referred to [35].

Consider the control system set-up in Fig. 2.3. Although not explicitly mentioned in [22], it will be assumed here that the generalized plant meets the six assumptions listed in Section 3.1. First, assumptions 1 and 2 guarantee the entire closed-loop being stable and not just the loop around G_{22} (see (2.11) for the partitioning of G). Second, assumptions 3 and 4 guarantee K to be proper (and hence physically realizable) and, third, assumptions 5 and 6 guarantee G_{12} and G_{21} to have full column rank n_u and full row rank n_y respectively for all frequencies, which is needed in the derivation of the IO selection formulas, see (3.12). A more detailed discussion on these assumptions is found in [45, Section 2.3].

Another difference with [22] is, that Δ is not restricted to consist of square diagonal blocks. The formulas for *nonsquare* uncertainty blocks are straightforwardly obtained by following the derivation in [22].

The basic idea for the IO selection approach in [22] is to check if $\min_{K\in\mathcal{K}_S}\|M(G,K)\|_\mu < \gamma$, with $\mathcal{K}_S$ the set of all proper, real-rational, and stabilizing controllers (actually, $\gamma = 1$ in [22]). Due to the inability to exactly compute μ, this inequality is replaced in [22] by:

$$\min_{K\in\mathcal{K}_S}\inf_{d\in\boldsymbol{d}}\|D_z(d)M(G,K)D_w^{-1}(d)\|_\infty < \gamma, \tag{3.8}$$

yielding a *sufficient* (but generally tight) condition for existence of a robustly performing controller. The so-called Youla controller parameterization (see, *e.g.*, [10, Chapter 4], [30, Chapter 6] for elaboration) is invoked to create an expression for the closed-loop M which is affine in the "new controller" Q, whereas the expression (2.12) is not affine in K. Inequality (3.8) is then replaced by its *equivalent*

$$\min_{Q\in\mathcal{RH}_\infty}\inf_{d\in\boldsymbol{d}}\|D_z(d)M(N,Q)D_w^{-1}(d)\|_\infty < \gamma, \tag{3.9}$$

with $\mathcal{RH}_\infty$ the set of all proper, real-rational, and stable transfer functions and N a modified version of G. Note, that the requirement of K being *stabilizing* (K itself not necessarily stable) is replaced by the requirement of Q itself being *stable*.

Unfortunately and in analogy to (2.20), the optimization (3.9) in the parameters Q and d jointly is nonconvex [22] and it also requires controller design. Both problems are circumvented in [22] by replacing $Q \in \mathcal{RH}_\infty$ with $Q \in \mathcal{RM}$. Here, $\mathcal{RM}$ is the set of all proper, real-rational transfer functions, which need *not* be stable ($\mathcal{RH}_\infty \subset \mathcal{RM}$). Hence, due to this modification, the requirement that the controller must be stabilizing is dropped. It is claimed in [22], that dropping the stability requirement on Q is equivalent to dropping the causality requirement on Q; see also [59, Section 4.3], where a TFM which is analytic (*i.e.*, all of its entries are differentiable in the considered space) and bounded in the open left-half-plane is defined as antistable *or* anticausal.

Without going into detail here, the following "screening tool" for IO selection can be derived:

A necessary *condition for existence of a proper, real-rational, stabilizing controller achieving the μ upperbound specification $\|M\|_{\bar{\mu}} < \gamma$ is the existence of a D-scaling "d" such that:*

$$\hat{G}_{21_\perp}\{G_{11}^* X_z(d) G_{11} - \gamma^2 X_w(d)\}\hat{G}_{21_\perp}^* < 0\ \forall\ \omega \qquad \text{(output selection)}, \tag{3.10}$$

$$\hat{G}_{12_\perp}^*\{G_{11} X_w^{-1}(d) G_{11}^* - \gamma^2 X_z^{-1}(d)\}\hat{G}_{12_\perp} < 0\ \forall\ \omega \qquad \text{(input selection)}, \tag{3.11}$$

with

$$\hat{G}_{12} = G_{12}(G_{12}^* G_{12})^{-1/2}, \qquad \hat{G}_{21} = (G_{21}G_{21}^*)^{-1/2} G_{21}, \tag{3.12}$$

$$X_z(d) = D_z^*(d)D_z(d), \qquad X_w(d) = D_w^*(d)D_w(d), \tag{3.13}$$

and $\{\}^*$ denoting the complex conjugate transpose and $\{\}_\perp$ the orthogonal complement. Note, that if μ and its upperbound are the same, the above is also necessary for existence of a K achieving the exact μ specification $\|M\|_\mu < \gamma$. In [22], $X_z = X_w = X$, due to the restriction to square blocks in Δ.

With respect to conditions (3.10) and (3.11), a few remarks are made. First, suppose that y-noise is not included in w and u-weights are not included in z. It is obvious, that condition

(3.10) is now independent of the input set and hence is referred to as "output selection condition," while (3.11) is now independent of the output set and is referred to as "input selection condition." This also holds true if y-noise and u-weights are incorporated in the design. Suppose, u-weights are accounted for by extending z with $z_u = W_u u$ and y-noise is accounted for by extending w with w_y and adding $V_y w_y$ to y. In that case, G_{11}, G_{12} and G_{21} in conditions (3.10) and (3.11) are replaced by G'_{11}, G'_{12}, and G'_{21} respectively:

$$G'_{11} = \begin{bmatrix} G_{11} & 0 \\ 0 & 0 \end{bmatrix}, \; G'_{12} = \begin{bmatrix} G_{12} \\ W_u \end{bmatrix}, \; G'_{21} = \begin{bmatrix} G_{21} & V_y \end{bmatrix}$$

(see also Appendix D). Again, screening tool (3.10) is independent of the input set and (3.11) of the output set. It is emphasized however, that for an IO set to be viable, the two conditions must be met jointly, *i.e.*, for the same d.

In [22], it is remarked that (3.11) drops out if $\hat{G}_{12}$ has full row rank, for which it is necessary that $n_z \leq n_u$. However, to meet the full column rank assumption on G_{12}, $n_z \geq n_u$ is required. So, (3.11) can only drop out if $n_z = n_u$. In analogy, (3.10) drops out if $\hat{G}_{21}$ has full column rank. Under the full row rank requirement for G_{21}, this situation can only occur if $n_w = n_y$.

The individual conditions (3.10) and (3.11) are convex feasibility problems; (3.10) in the squared D-scale entries and (3.11) in the reciprocals of the squared D-scale entries. Unfortunately, testing the two conditions jointly is a *nonconvex* feasibility problem and therefore more difficult. According to [22], this problem is currently only solved if Δ consists of two full blocks, *e.g.*, one full block Δ_u and one full block Δ_p. In that case, the following results:

$$X_z(s) = \begin{bmatrix} sI_{n_q} & 0 \\ 0 & I_{n_{z^*}} \end{bmatrix}, \quad X_w(s) = \begin{bmatrix} sI_{n_p} & 0 \\ 0 & I_{n_{w^*}} \end{bmatrix}, \tag{3.14}$$

$$X_z^{-1}(t) = \begin{bmatrix} tI_{n_q} & 0 \\ 0 & I_{n_{z^*}} \end{bmatrix}, \quad X_w^{-1}(t) = \begin{bmatrix} tI_{n_p} & 0 \\ 0 & I_{n_{w^*}} \end{bmatrix}, \tag{3.15}$$

with $s = d^2$ and $t = 1/d^2$. Further, $n_q = \dim(q)$, $n_p = \dim(p)$, $n_{z^*} = \dim(z^*)$, $n_{w^*} = \dim(w^*)$, see also Fig. 2.3. It can now be checked if the solution intervals of s and $1/t$ intersect, *i.e.*, if (3.10) and (3.11) are jointly met.

Note, that G_{11}, $\hat{G}_{12_\perp}$, and $\hat{G}_{21_\perp}$ in (3.10) and (3.11) are *complex* matrices. Therefore, these conditions are *not* Linear Matrix Inequalities (LMIs) according to the definition in [4]. However, noting that both conditions can be written in the form $\Sigma_1(d) + j\Sigma_2(d) < 0$ with Σ_1 and Σ_2 real matrices and noting that $\Sigma_1 = \Sigma_1^T$, $\Sigma_2 = -\Sigma_2^T$, the following is employed to rewrite (3.10) and (3.11) as LMIs:

$$\Sigma_1 + j\Sigma_2 < 0 \Leftrightarrow \begin{bmatrix} \Sigma_1 & -\Sigma_2 \\ \Sigma_2 & \Sigma_1 \end{bmatrix} < 0. \tag{3.16}$$

Appendix A proves this equivalence and further details the transformation into LMIs. For each frequency in a specified grid, the resulting LMI feasibility problems can be tackled with `lmisolver` from the MATLAB Toolbox LMITOOL [9]. In fact, a (constrained) LMI problem is transformed into a so-called semidefinite programming problem, which is solved with the MEX-file `sp` from [53]. For details on how (in)feasibility is established, see [53, Section 2] and [52, Section 3.3].

Chapter 4

Active Suspension Control Problem

The two IO selection methods discussed in Chapter 3 will be evaluated for an active suspension control problem. First, the system model is introduced (Section 4.1), second, the control objectives are quantified via shaping and weighting filters (Section 4.2), and third, a parametric uncertainty model model is given (Section 4.3). Though this was also done in [45, Chapter 3], there are some important differences with respect to motivations for filter parameter choices and uncertainties.

4.1 Tractor-Semitrailer System

The 4 Degree-Of-Freedom (DOF) model of the vehicle in Fig. 4.1 will serve as an example for IO selection. Its state-space description is documented in Appendix B. This system was also used to evaluate the IO selection proposal in [45], while in [43] a 6 DOF model illustrated the IO selection method of [37]. Compared to the model in [45], small tire dampings are included, see Appendix C for the motivation of this modification.

For the active suspension control problem, two actuators u_1 and u_2 placed between the axles and the chassis are proposed as candidate inputs, while measurements of the suspension deflections (y_1, y_2) and the chassis accelerations (y_3, y_4) are suggested as candidate outputs. This yields 45 candidate IO sets, among which the 4×2 overall IO set $y_1y_2y_3y_4/u_1u_2$ and eight 1×1 IO sets.

4.2 Performance Specifications

In this section, shaping and weighting filters V_{w^*}, W_{z^*} are proposed to quantify the performance specifications in the control system set-up of Fig. 2.3.

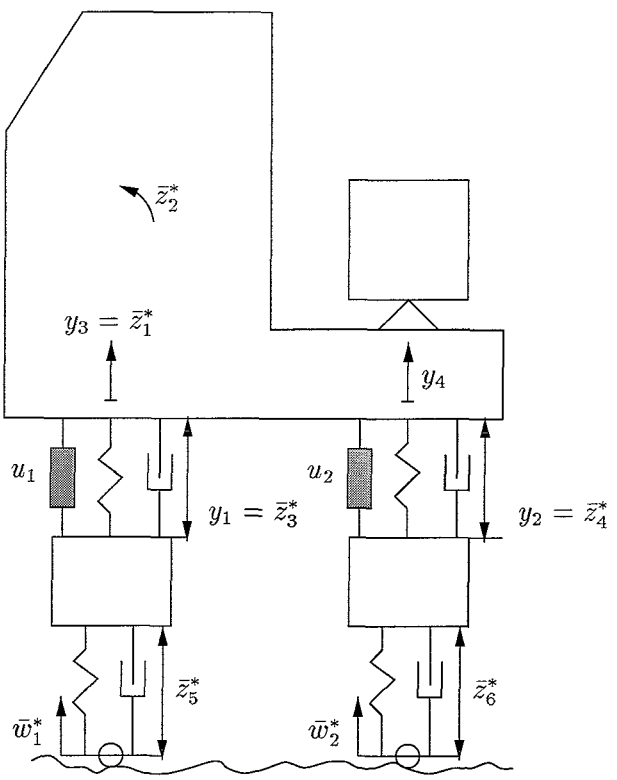

Figure 4.1: 4 DOF tractor-semitrailer combination

The exogenous input $\bar{w}^*$ includes the excitation by the road surface ($\bar{w}_1^*$, $\bar{w}_2^*$) and the measurement noises ($\bar{w}_3^*, \ldots, \bar{w}_6^*$). Due to the presence of tire dampings, $\bar{w}_1^*$ and $\bar{w}_2^*$ represent the *derivatives* of the road surface height. Assuming the road surface height to be lowpass-filtered white noise, its derivative is a highpass-filtered version. The corresponding shaping filter in V_{w^*} is chosen as:

$$V_{w_1^*} = V_{w_2^*} = V_{w_{1,2}^*} = \frac{v_0 s}{s/\omega_0 + 1}, \tag{4.1}$$

see also Fig. 4.2. For a fair motorway and a forward vehicle speed of 25 m/s, $\omega_0 = 2\pi \cdot 0.25$ rad/s and $v_0 = 8.0 \cdot 10^{-3}$ are representative choices [14, Section 2.2.2].

The four measurements are assumed to be disturbed with zero-mean, white noises with an intensity of θ times the order of magnitude of each measurement. So, parameter θ can be interpreted as the error fraction in the measured variables. The associated magnitudes are obtained by computing the $\mathcal{H}_2$ norms of the TFMs from w^* (*not* $\bar{w}^*$) to each measurement. For the road surface modeled by (4.1), this results in the following choice of the shaping filters incorporated in V_{w^*}:

$$V_{w_3^*} = 3.3 \cdot 10^{-3}\theta, \tag{4.2}$$
$$V_{w_4^*} = 3.3 \cdot 10^{-3}\theta, \tag{4.3}$$
$$V_{w_5^*} = 5.7 \cdot 10^{-1}\theta, \tag{4.4}$$
$$V_{w_6^*} = 8.7 \cdot 10^{-1}\theta. \tag{4.5}$$

Four main design goals are distinguished [5,14]. First, good driver comfort must be guaranteed (as well as cargo comfort, but this will not be considered). The tractor's vertical acceleration at the front $\bar{z}_1^*$ and the rotational acceleration $\bar{z}_2^*$ are used to quantitatively represent driver comfort. Though the limitation of accelerations due to stochastic road surfaces actually involves limiting the $\mathcal{H}_2$ norm [5], this goal must as well as possible be transformed in the $\mathcal{H}_\infty$ norm setting by the choice of suitable weighting filters in W_{z^*}. These filters are based on human sensitivity plots for vertical and *horizontal* accelerations provided in [5]. However, since the driver's horizontal acceleration can be approximated by a constant times $\bar{z}_2^*$, the horizontal sensitivity will be used to represent rotational sensitivity. The sensitivity contour for $\bar{z}_1^*$ is approximated by the magnitude of $W_{z_1^*}$:

$$W_{z_1^*} = \rho_1 {\omega_1}^2 \frac{s/\omega_2 + w_{1_0}}{s^2 + 2\zeta\omega_1 s + {\omega_1}^2}, \tag{4.6}$$

with $w_{1_0} = 0.4$, $\zeta = 1$, $\omega_1 = 2\pi \cdot 10$ rad/s, and $\omega_2 = 2\pi \cdot 5$ rad/s. Via ρ_1, the attenuation of the most crucial accelerations can be specified. The sensitivity contour for $\bar{z}_2^*$ is approximated by the magnitude of $W_{z_2^*}$:

$$W_{z_2^*} = \rho_2 \frac{w_{2_0}}{s/\omega_3 + 1}, \tag{4.7}$$

with $w_{2_0} = 1$ and $\omega_3 = 2\pi \cdot 2$ rad/s. The acceleration weights in (4.6) and (4.7) are also depicted in Fig. 4.2.

The second and third design goals are limiting the suspension deflections (due to space limitations) and the tire deflections (for good handling and minimum road surface damage) respectively. This means that the $\mathcal{L}_1$ norm of the corresponding TFMs must be restricted and suitable weights in the $\mathcal{H}_\infty$ norm setting are hard to give. Here, the front and rear weights are chosen equal and constant:

$$W_{z_3^*} = W_{z_4^*} = W_{z_{3,4}^*} = \rho_3 \qquad \text{(suspension deflections)}, \tag{4.8}$$

$$W_{z_5^*} = W_{z_6^*} = W_{z_{5,6}^*} = \rho_4 \qquad \text{(tire deflections)}. \tag{4.9}$$

Finally, weights for the inputs u must be formulated. In general, the bandwidth of actuators is limited and high-frequency inputs cannot be realized. To account for this, the following bi-proper weighting filter for $\bar{z}_7^* = u_1$ and $\bar{z}_8^* = u_2$ is used (see also Fig. 4.2):

$$W_{z_7^*} = W_{z_8^*} = W_{z_{7,8}^*} = \rho_5 \frac{s/\omega_4 + 1}{s/\omega_5 + 1}. \tag{4.10}$$

It is assumed, that the bandwidth of the actuators is 5 Hz, *i.e.*, $\omega_4 = 2\pi \cdot 5$ rad/s. Furthermore, $\omega_5 = 100 \cdot \omega_4$ is used.

Up till now, it has only been decided on the shape of the filters, while numerical values for the parameters θ, $\rho_1, \ldots, \rho_5$ still have to be chosen. This will be done to conclude this section. The $\mathcal{H}_\infty$ controllers are designed for the overall IO set $y_1 y_2 y_3 y_4 / u_1 u_2$.

- **Acceleration Weights:** In accordance with the original sensitivity contours in [5], ρ_1 and ρ_2 in (4.6) and (4.7) are "normalized" at one.

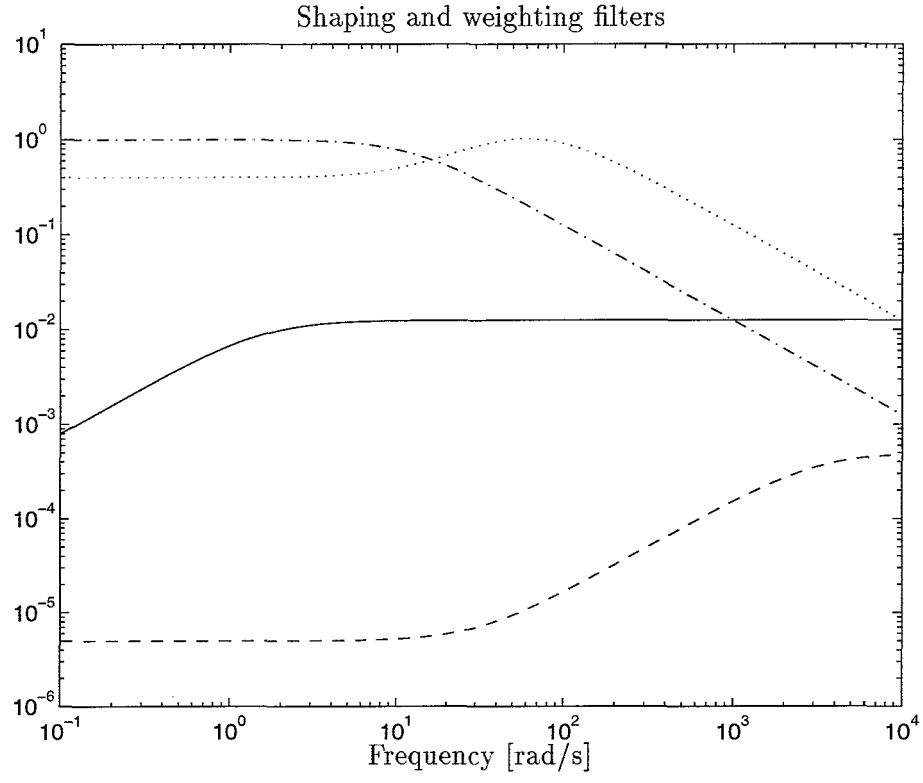

Figure 4.2: Performance specifications $V_{w^*_{1,2}}$ (−), $W_{z^*_1}$ (··), $W_{z^*_2}$ (−·), and $W_{z^*_{7,8}}$ (- -)

- **Measurement Noise:** To represent a 5% error in each measured variable, $\theta = 5 \cdot 10^{-2}$ is used. Designing an $\mathcal{H}_\infty$ optimal controller aimed at minimizing $\bar{z}^*_1$ and $\bar{z}^*_2$ in the presence of y-noise yields $\|M\|_\infty = 0.0259$, which equals 23% of the corresponding open-loop $\mathcal{H}_\infty$ norm: 0.1123.

- **Actuator Weights:** Next, ρ_5 in (4.10) is fixed at $5 \cdot 10^{-6}$. For an $\mathcal{H}_\infty$ optimal design accounting for $\bar{z}^*_1$, $\bar{z}^*_2$, but without y-noise, $\|M\|_\infty = 0.0700$ results (62% of the open-loop norm). If both y-noise *and* u-weights are included, $\|M\|_\infty = 0.0700$.

- **Suspension and Tire Deflections:** Though the suspension and tire deflection limits will not be exceeded for stochastic road surfaces [5], this might happen for *deterministic* disturbances. It is decided to set ρ_3 and ρ_4 such, that $\mathcal{H}_\infty$ optimal designs with u-weights and y-noise aimed at minimizing $\bar{z}^*_3$, $\bar{z}^*_4$ or $\bar{z}^*_5$, $\bar{z}^*_6$ achieve approximately the same $\|M\|_\infty$ as a design for $\bar{z}^*_1$, $\bar{z}^*_2$. In this way, accelerations, suspension deflections, and tire deflections are specified "equally important." The values $\rho_3 = 90$ and $\rho_4 = 330$ result.

An $\mathcal{H}_\infty$ optimal controller design with all controlled variables $z^*_1, \ldots, z^*_8$ and y-noise included gives $\|M\|_\infty = 0.1479$ (open-loop norm equals 0.2784). In [14], rounded pulses are proposed as a class of deterministic road profiles. Five rounded pulses with specific characteristic lengths and heights are suggested in [5] and classified from "tiny" to "huge." If the maximum height of each rounded pulse is such, that for the uncontrolled system at least one of the suspension

or tire deflections hits its limits, it is observed that for the controlled system only the front suspension deflection slightly exceeds its lower limit for a "large" rounded pulse and exceeds its limit by 28% for a "huge" rounded pulse. Apparently, with the proposed parameters the controlled system fairly well accounts for deterministic road profiles. An attempt to find constant weights for $z_3^*, \ldots, z_6^*$ with which the controlled system does not exceed any of its limits results in large weights and the other controlled variables become of minor importance.

4.3 Uncertainties

In the 4 DOF truck model, various uncertain parameters play a role for which an uncertainty model is developed, see Appendix B. The following uncertainties are accounted for:

- k_{tf}, k_{tr}, k_{sf}, k_{sr}: tire and suspension stiffnesses at the front and rear,
- b_{tf}, b_{tr}, b_{sf}, b_{sr}: tire and suspension dampings at the front and rear,
- m_{af}, m_{ar}: axle mass at the front and rear,
- M_{ch}, J_{ch}: chassis mass and inertia,
- M_t: semi-trailer *effective* mass.

The approach for modeling uncertain spring and damper parameters is described in [38] (see also [45, Section 3.3]), while [34, Section 4] provides an example for an uncertain mass. Suppose a is the nominal value of an uncertain parameter a', which are related as $a' = a + w_a\delta_a$, $\|\delta_a\|_\infty \leq 1$. The δ_a's for the uncertain parameters together build the uncertainty block, resulting in a 13×13 *structured*, diagonal Δ_u; the w_a's express the amount of uncertainty included in W_q, while V_p is fixed at identity.

With respect to the uncertainty model, an important remark must be made. Though the uncertainties are modeled as time-invariant, *real parametric* ones, in this report the IO selection *and* the controller design with μ-Tools [1] will treat them as time-invariant, *complex* uncertainties, see also the restriction in (2.1). Thus, the IO selection and controller design account for a too large class of uncertainties, introducing conservativeness. Therefore, in the current approach w_a should be interpreted as a specification for the maximum *complex* uncertainty in the real nominal parameter a. For the tractor-semitrailer this means, that real parametric uncertainties are covered with $\mathcal{H}_\infty$ norm bounded *dynamical* uncertainties. Recent research has been aimed on solving μ-analysis [55,56], [8, Chapter 4] and μ-synthesis [40,54] for mixed real and complex uncertainties. Thus, the development of an IO selection method for mixed uncertainties certainly merits further investigation, see also Chapter 7.

Finally it is remarked, that in [35] an uncertainty model for a 6 DOF truck model is derived in terms of perturbed natural frequencies and damping ratios.

Chapter 5

Input Output Selection for the Active Suspension Problem

The two IO selection methods proposed in Chapter 3 are illustrated for the active suspension control problem sketched in the previous chapter. To start with, μ-synthesis will be performed for some "typical" IO sets (Section 5.1) aimed at achieving performance under uncertain semitrailer mass. This is followed by IO selection with the methods based on D-scale estimates in Section 5.2 and linear matrix inequalities in Section 5.3. Finally, some results for the two methods are shortly compared in Section 5.4.

5.1 μ-Synthesis for Typical Input Output Sets

In this section, optimal D-K iterations will be performed for the same nine "typical" IO sets as in [45, Section 4.2], see Table 5.1. In this way, insight is acquired on the importance of each sensor and actuator for RP. This information will be used to assess the results of the two IO selection methods.

To serve an easier interpretation, only the uncertain effective mass of the semi-trailer (M_t) will be incorporated in the uncertainty block Δ_u. In practice, this parametric uncertainty is probably dominant over the other ones in Section 4.3, since M_t strongly depends on the transported cargo; the semitrailer might even be empty or absent. Here, M_t is assumed to vary between its value for an empty and a fully loaded semitrailer. The nominal value is taken the mean of these two, allowing a 90% variation in the nominal M_t. Figure 5.1 depicts the effect of this uncertainty on the *open-loop* TFM between the road inputs $\bar{w}_1^*$, $\bar{w}_2^*$ and the controlled variables $\bar{z}_1^*, \ldots, \bar{z}_6^*$. Note, that the difference between the TFMs for the mean and minimum M_t is clearly visible, but *not* for the mean and maximum value.

In Table 5.1, closed-loop norms $\|M\|_\infty$ from $\mathcal{H}_\infty$ optimal controller designs aimed at achieving Nominal Performance (NP) are listed for the cases *with* and "*without*" measurement noise

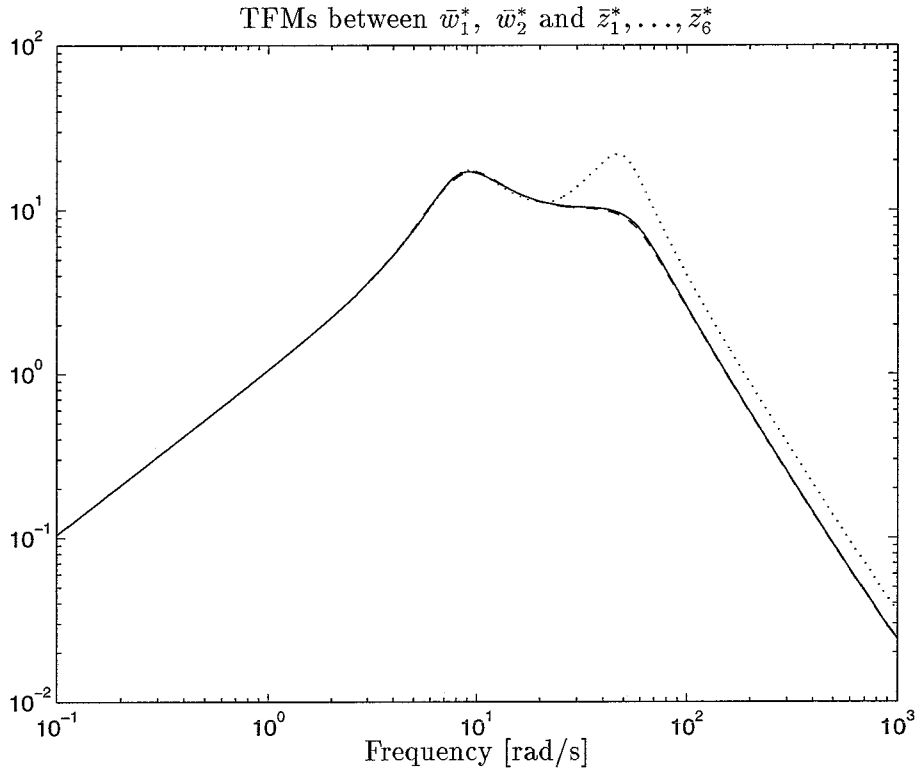

Figure 5.1: Influence of uncertain M_t on the maximum singular value of the TFM between road input and controlled variables: (–) mean M_t; (··) minimum M_t; (- -) maximum M_t.

Table 5.1: Optimal controller design for some typical IO sets.

IO set	Outputs	Inputs	Excluding y-noise and u-weights			Including y-noise and u-weights		
			$\|M\|_\infty$ (NP)	$\|M\|_{\bar{\mu}}$ (RP)	Ω	$\|M\|_\infty$ (NP)	$\|M\|_{\bar{\mu}}$ (RP)	Ω
1	$y_1\ y_2\ y_3\ y_4$	$u_1\ u_2$	0.13	0.75	0.00	0.15	0.76	0.00
2	$y_1\ y_2\ y_3\ y_4$	u_1	0.17	1.06	0.48	0.17	1.06	0.65
3	$y_1\ y_2\ y_3\ y_4$	u_2	0.27	0.76	0.40	0.27	0.76	0.10
4	$y_1\ y_2$	$u_1\ u_2$	0.13	0.76	0.90	0.15	0.77	1.11
5	$y_3\ y_4$	$u_1\ u_2$	0.13	0.76	0.50	0.16	0.76	0.54
6	y_1	$u_1\ u_2$	0.16	1.01	1.52	0.16	1.01	1.70
7	y_2	$u_1\ u_2$	0.27	0.76	0.98	0.27	0.77	1.11
8	y_3	$u_1\ u_2$	0.17	0.82	2.93	0.17	0.83	4.51
9	y_4	$u_1\ u_2$	0.27	0.76	0.59	0.28	0.77	0.53

and input weights. To meet assumptions 3 and 4 in Section 3.1, y-noise and u-weights must always be included here. Therefore, "no" y-noise and "no" u-weights refer to their effects being negligible, *i.e.*, $\theta = 10^{-6}$ and $\rho_5 = 10^{-8}$. For the RP problem, Table 5.1 also shows $\|M\|_{\bar{\mu}}$ values for the optimal closed-loops.

The D-K iteration is performed with the μ-Toolbox [1]. In the $\mathcal{H}_\infty$ design part (`hinfsyn`) of D-K iteration, the tolerance for the γ-iteration is fixed at `tol`$= 10^{-2}$ to avoid potential numerical problems if the optimum is approached too closely [3, Section 6.6.1]. The μ-analysis part (`mu`) of D-K iteration is performed in the interesting frequency range between 10^{-1} and 10^3 rad/s, using 100 logarithmically spaced frequency points. For computation of the μ upperbound, the LMI-based algorithm is selected in `mu`. For the purpose of finding rational D-scaling approximations, two algorithms are available in μ-Tools: `musynfit` and `musynflp`. In previous research ([45, Section 5.2], [48]), `musynfit` sometimes caused convergence problems, which might be due to incorrectly returned constant D-scales, see Section 5.2. Therefore, `musynflp` was used instead. In this research, D-K iterations for each IO set are checked with *both* options, using second order rational D-scales. In general, the D-K iteration with `musynfit` better converges and tends to give more reliable results than with `musynflp`. The $\|M\|_{\bar{\mu}}$ values listed in Table 5.1 are therefore computed with `musynfit`. The D-K iteration is stopped if the reduction in consecutive $\|M\|_{\bar{\mu}}$ values is no larger than `tol`$= 10^{-2}$.

The first observation from Table 5.1 is, that both the optimal NP level *and* the optimal RP level are approximately the same for the cases with and without y-noise and u-weights. Apparently, the influence of measurement noises $\bar{w}_3^*, \ldots, \bar{w}_6^*$ and input weights $\bar{z}_7^*$, $\bar{z}_8^*$ is negligible compared to the other exogenous variables $\bar{p}$, $\bar{w}_1^*$, $\bar{w}_2^*$ and the other controlled variables $\bar{q}$, $\bar{z}_1^*, \ldots, \bar{z}_6^*$ respectively.

Comparing IO sets 1, 2, and 3, a second and third conclusion follow from Table 5.1. First, IO set 2, based on the front actuator u_1, is not viable for RP under the imposed performance

specifications and uncertainty. This implies, that also the other 14 IO sets which employ u_1 as the single actuator are nonviable. Second, the overall IO set 1 and IO set 3 are equally best for RP and IO set 3 is better for RP than IO set 2. While IO set 1 is better than IO set 3 if only NP is considered, adding u_1 is not beneficial in the case of RP. This is due to the control of $\bar{q}$ being dominant over the control of $\bar{z}^*$. So, adding u_1 may be advantageous for $\bar{z}^*$, but the effect on $\bar{q}$ is negligible. Moreover, if only one actuator is used, the rear actuator u_2 is better for RP than the front actuator u_1. This is also felt intuitively, since u_2 is physically "closer to the uncertainty source" M_t than u_1; see [45, Section 5.2], where a similar conclusion is drawn with respect to the ease of achieving robust stability against uncertain springs and dampers.

A fourth observation from Table 5.1 is, that for IO set 4 and 5 the achievable NP *and* RP level are the same. Apparently, a set of two suspension deflection measurements is equally best as a set of two acceleration measurements.

In case of two actuators and a *single* sensor (IO sets 6–9), the acceleration measurement at the front y_3 is preferred (for RP) over the displacement measurement at the front y_1. The IO sets based on the front suspension deflection y_1, *i.e.*, y_1/u_1u_2, y_1/u_1, and y_1/u_2 are not even viable for RP. The rear displacement and acceleration measurements y_2 and y_4 are equally best and better for RP than the front measurements. Again, it seems preferable to use measurements close to the uncertainty.

In Fig. 5.2, the frequency-dependent upperbounds for $\mu_{\mathbf{\Delta}}(M)$ are plotted for IO sets 3–5, 7, and 9, which achieve "the same" RP level $\|M\|_{\bar{\mu}}$ as the overall IO set. The case without y-noise and u-weights is considered. Though the $\|M\|_{\bar{\mu}}$ values are the same and also occur around the same frequency ($\sqrt{(k_{tr}/m_{ar})} = 57.74$ rad/s), the *shapes* of the upperbounds and the associated D-scales are considerably different. Recall from Section 3.1, that the Ω-values in Table 5.1 are a measure for the "closeness" in dynamic behavior between the overall IO set's optimal closed-loop and those for the other IO sets. The fact that none of the Ω's for IO sets 3–5, 7, and 9 are close to zero is in line with the fact that the D-scales are considerably different. Note that IO set 3, which has the smallest $\Omega = 0.40$, also has a D-scale which best matches the overall IO set's D-scale. The above is a crucial observation to bear in mind for the forthcoming IO selection based on D-scale estimates. For this IO selection, rational D-scales $\hat{D}_z$ and $\hat{D}_w$ obtained via the overall IO set's optimal closed-loop $M^\star$ are employed. If $\hat{D}_z$ and $\hat{D}_w$ are significantly different from the other IO sets' D-scales with the optimal M's, the IO selection may yield conservative results.

5.2 Input Output Selection with D-Scale Estimates

This section investigates the perspectives for the IO selection method based on D-scale estimates as suggested in Section 3.1. To start with, the case without y-noise and u-weights is studied. The overall IO set then achieves an optimal RP level of 0.75, see Table 5.1. A plot of the μ upperbound of the associated closed-loop $M^\star$ is depicted in Fig. 5.3. To be on the safe side for IO selection, a larger range and denser grid of frequencies are used than for

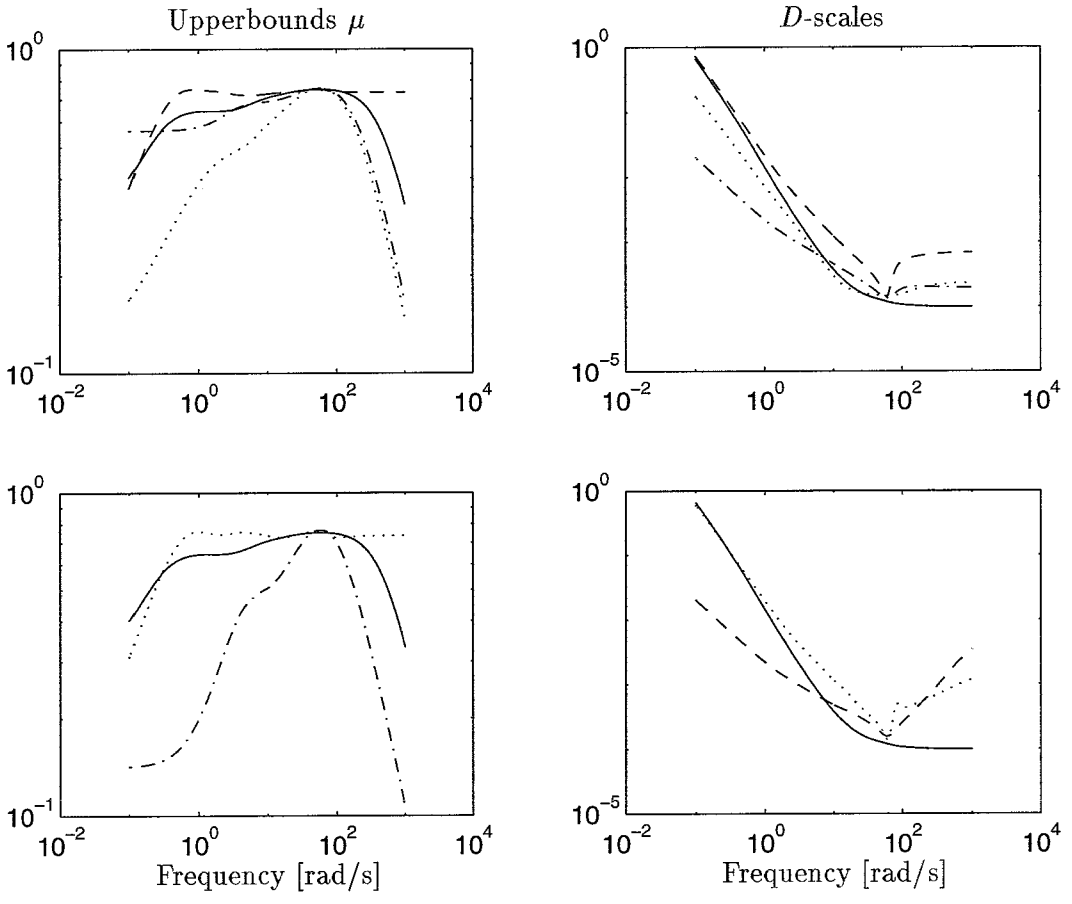

Figure 5.2: Upperbounds for $\mu_{\Delta}(M)$ and frequency-dependent D-scales for IO sets achieving $\|M\|_{\bar{\mu}} \approx 0.75$ in the case without y-noise and u-weights: *upper plots:* (–) IO set 1, (··) IO set 3, (- -) IO set 4, (–·) IO set 5; *lower plots:* (–) IO set 1, (··) IO set 7, (- -) IO set 9.

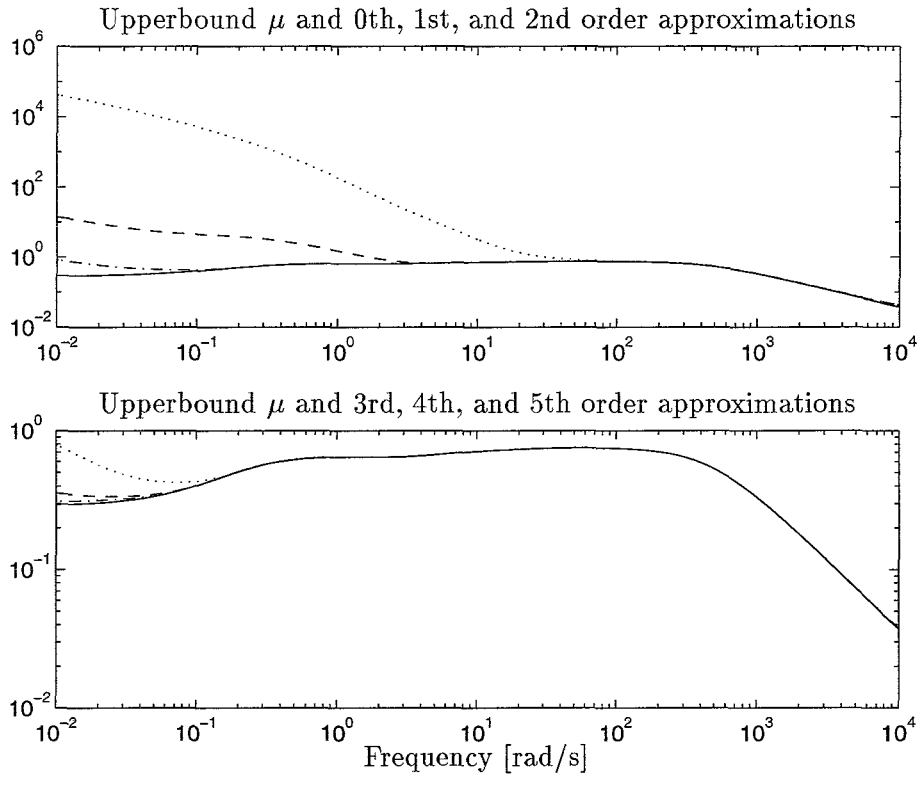

Figure 5.3: The frequency-dependent upperbound of μ for the overall IO set and some approximations using rational D-scales (`musynfit`) in the case without y-noise and u-weights: *upper plot:* (–) μ upperbound and approximations via 0th order (··), 1st order (- -), and 2nd order (–·) D-scales; *lower plot:* (–) μ upperbound and approximations via 3rd order (··), 4th order (- -), and 5th order (–·) D-scales.

μ-synthesis: 200 logarithmically spaced frequencies between 10^{-2} and 10^4 rad/s. Figure 5.3 also shows plots of $\bar{\sigma}\{\hat{D}_z(j\omega)M^\star(j\omega)\hat{D}_w^{-1}(j\omega)\}$ for 0th till 5th order rational D-scales, obtained with `musynfit`. For the problem considered here, only the first entry $\hat{d}_1$ of $\hat{D}_z$ and $\hat{D}_w$ (associated with the 1×1 Δ_u block) is used to fit the optimal, frequency-dependent D-scales computed with `mu`; the other entry $\hat{d}_2$ (associated with the Δ_p block) is equal to one. The magnitudes of the investigated rational transfer functions $\hat{d}_1$ are depicted in Fig. 5.4. Note, that `musynfit` returns an *incorrect* 0th order D-scale; if `musynflp` is used, a more plausible constant D-scale is returned. Obviously, the higher the order, the better the D-scale approximations. Table 5.2 lists the corresponding values $\|M^\star\|_{\hat{\mu}} = \|\hat{D}_z M^\star \hat{D}_w^{-1}\|_\infty$. Note, that only for 4th and 5th order D-scales, $\|M^\star\|_{\hat{\mu}} \approx \|M^\star\|_{\bar{\mu}} = 0.75$. For the 0th–3rd order D-scales, the $\|M^\star\|_{\hat{\mu}}$ values are achieved near $\omega = 0$. If more emphasis were put on the fit in the low-frequency region (by specifying a denser frequency grid in this region), the results for $\|M^\star\|_{\hat{\mu}}$ with low order D-scales would become better.

The generalized plants G for the nine IO sets in Table 5.1 are extended with rational D-scale estimates $\hat{D}_z$ and $\hat{D}_w^{-1}$ of various orders obtained via the overall IO set (see Fig. 2.5), followed by $\mathcal{H}_\infty$ *optimal* controller designs. The computed closed-loop norms provide (conservative) estimates of the achievable $\|M\|_{\bar{\mu}}$ values for each IO set. The results are depicted in Table 5.3,

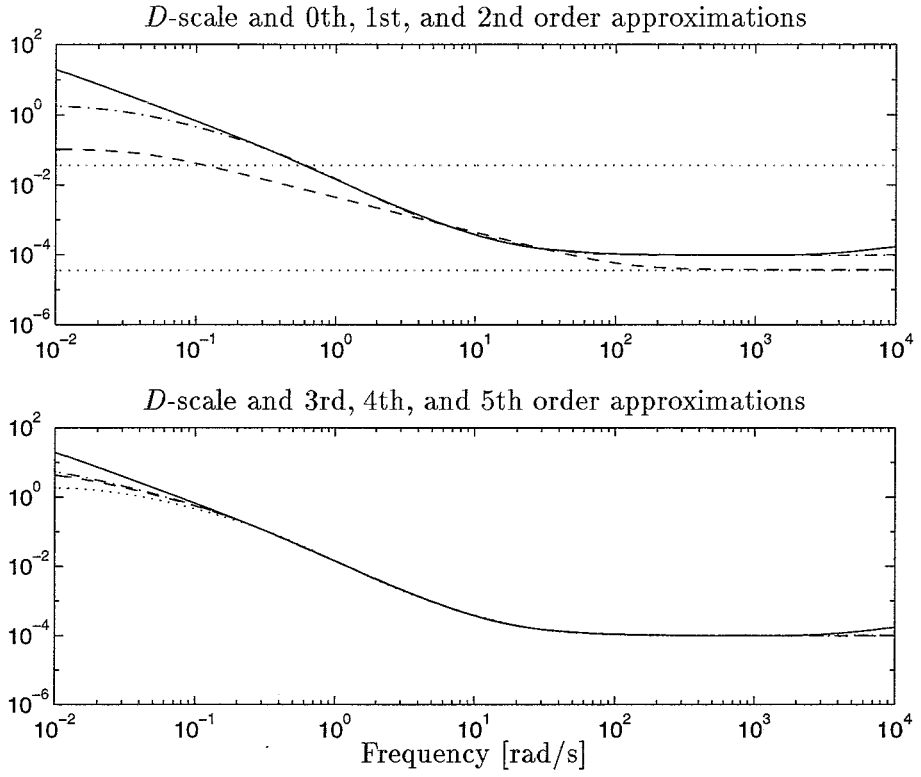

Figure 5.4: The frequency-dependent D-scale for the overall IO set and some rational approximations in the case without y-noise and u-weights: *upper plot:* (–) D-scale, (··) 0th order (lower line with `musynfit`, upper line with `musynflp`), (- -) 1st order, and (–·) 2nd order D-scale; *lower plot:* (–) D-scale, (··) 3rd order, (- -) 4th order, and (–·) 5th order D-scale.

Table 5.2: Rational D-scale orders (`musynfit`) and resulting $\|M^\star\|_{\hat{\mu}}$ for the overall IO set.

	Order of $\hat{D}_z$, $\hat{D}_w$					
	0	1	2	3	4	5
$\|M^\star\|_{\hat{\mu}}$, excluding y-noise & u-weights	$6.56 \cdot 10^4$	21.54	1.23	1.16	0.75	0.75
$\|M^\star\|_{\hat{\mu}}$, including y-noise & u-weights	73.73	0.77	0.76	0.76	0.76	0.76

Table 5.3: Influence of the rational D-scale order (`musynfit`) on the optimal $\mathcal{H}_\infty$ norm of the scaled, generalized plant for some typical IO sets; *excluding* y-noise and u-weights.

IO set	Outputs	Inputs	$\|M\|_{\bar{\mu}}$	$\min_{K\in\mathcal{K}_A} \|\hat{D}_z M(G,K)\hat{D}_w^{-1}\|_\infty$							
				D-scale orders							
				×	0		1	2	3	4	5
					`musynflp`	`musynfit`					
1	$y_1\ y_2\ y_3\ y_4$	$u_1\ u_2$	0.75	3.49	3.47	1.84	0.76	0.76	0.76	0.76	0.76
2	$y_1\ y_2\ y_3\ y_4$	u_1	1.06	187.86	34.30	6.07	1.09	1.12	1.13	1.13	1.13
3	$y_1\ y_2\ y_3\ y_4$	u_2	0.76	3.73	3.70	2.48	0.76	0.76	0.76	0.76	0.76
4	$y_1\ y_2$	$u_1\ u_2$	0.76	3.49	3.47	1.88	0.77	0.76	0.76	0.76	0.76
5	$y_3\ y_4$	$u_1\ u_2$	0.76	3.49	3.47	4.58	0.76	0.76	0.76	0.76	0.76
6	y_1	$u_1\ u_2$	1.01	972.35	35.02	2.56	1.03	1.03	1.03	1.02	1.02
7	y_2	$u_1\ u_2$	0.76	53.33	3.47	1.88	0.77	0.76	0.76	0.76	0.76
8	y_3	$u_1\ u_2$	0.82	946.19	34.08	4.58	0.98	0.95	0.94	0.93	0.93
9	y_4	$u_1\ u_2$	0.76	202.97	7.31	4.58	0.76	0.76	0.76	0.76	0.76

leading to the following conclusions.

If G is *not* extended with rational D-scales (indicated with "×"), a "conventional" $\mathcal{H}_\infty$ optimization is performed. From Table 5.3, it is observed that the optimal closed-loop norms $\|M\|_\infty$ are between 3.49 (overall IO set 1 and IO sets 4 and 5) and 972 (IO set 6). Comparing these $\|M\|_\infty$ values with the $\|M\|_{\bar{\mu}}$ values illustrates the conservativeness of the $\mathcal{H}_\infty$ design, which is due to its inability to deal with the structure in Δ. By extending the generalized plant with the D-scale estimates $\hat{D}_z$ and $\hat{D}_w$, it is attempted to account for the structure in Δ to some extent.

The optimal $\mathcal{H}_\infty$ norms of the *overall* IO set 1 considerably differ from $\|M^\star\|_{\bar{\mu}} = 0.75$ if 0th order rational D-scales are used, while they do not for higher order approximations. Since the $\mathcal{H}_\infty$ optimization for the overall IO set in fact completes an *additional* step of the formerly performed D-K iteration, this means that the D-K iteration would not converge anymore for 0th order D-scales. Also note, that the RP levels for the overall IO set are 0.76 instead of 0.75. This slight difference is due to limited numerical accuracy: for further D-K iterations with 2nd order D-scales the RP level varies between 0.75 and 0.76. Note, that also for the other IO sets the *optimal* $\mathcal{H}_\infty$ norms are larger than one for 0th order D-scales. Though the constant D-scale obtained with `musynflp` looks better (Fig. 5.4), the gap between the optimal $\mathcal{H}_\infty$ norms and the $\|M\|_{\bar{\mu}}$ values are smaller for the D-scale obtained with `musynfit`, except for IO set 5. Hence, IO selection based on this D-scale would term the nine IO sets nonviable (implying *all* 45 candidate IO sets are nonviable), which is incorrect.

For 1st and higher order D-scales, the results are significantly better, in the sense that none of the nine IO sets would unjustly be rejected during IO selection. It is remarkable, that for IO sets 3–7 and 9 the optimal $\mathcal{H}_\infty$ norms are (approximately) the same for 1st–5th order

Table 5.4: RP-based IO selection results; excluding y-noise and u-weights

D-scale order	Number of *viable* IO sets	*Nonviable* IO sets	CPU time [s]
0	0	all	160
1	28	y_1/u_2, y_1/u_1u_2, and 15 IO sets with single u_1	200
2	28	,,	238
3	28	,,	279
4	28	,,	348
5	28	,,	408

D-scales. In addition, the $\mathcal{H}_\infty$ norms for IO sets 3–5, 7, and 9 are (almost) equal to their $\|M\|_{\bar{\mu}}$ values, which are in turn equal to $\|M^\star\|_{\bar{\mu}}$ for the overall IO set 1. So, even though the D-scales (and hence their approximations $\hat{D}_z$, $\hat{D}_w$) for the overall IO set considerably differ from the D-scales for IO sets 3–5, 7, and 9 (Fig. 5.2), good estimates for $\|M\|_{\bar{\mu}}$ result; also see the final remark in Section 5.1. However, for IO sets 2 and 8 there is a "gap" between the optimal $\mathcal{H}_\infty$ norms and $\|M\|_{\bar{\mu}}$. Note, that for IO set 2 this gap increases for higher order D-scales, while for IO set 8 it decreases. Apparently (and counterintuitively), high order D-scales for the overall IO set do not guarantee a better match of the optimal $\mathcal{H}_\infty$ norm and $\|M\|_{\bar{\mu}}$ for the other IO sets. This indicates that a suitable choice of the D-scale order to be used in IO selection might not be straightforward.

If `musynflp` is used instead of `musynfit` (no results depicted), it is observed that for 1st order D-scales the gaps between the $\|M\|_{\hat{\mu}}$ values and the optimal $\mathcal{H}_\infty$ norms are (considerably) larger; IO set 8 would even incorrectly be rejected during IO selection. For 2nd–4th order D-scales, the results are qualitatively comparable with the results for `musynfit`. However, `musynflp` fails to return 5th or higher order rational D-scales.

For the purpose of IO selection, all 45 candidate IO sets are checked for viability with respect to RP, *i.e.*, it is checked if an admissible K exists which achieves $\|M(G,K)\|_{\hat{\mu}} := \|\hat{D}_z M(G,K)\hat{D}_w^{-1}\|_\infty < 1$. This is done via the six viability conditions in Section 3.1. For D-scale orders 0–5 (`musynfit`), Table 5.4 shows the results.

As stated before, IO selection based on 0th order D-scales eliminates all 45 IO sets as candidates. For D-scales of 1st and higher order, always the same 28 IO sets are termed viable. As predicted from Table 5.1, all 15 candidate IO sets employing only the front actuator u_1 and the three IO sets employing only the front suspension deflection measurement y_1 are nonviable. So, no other IO sets are termed nonviable than could be predicted from Table 5.1. The 1×1 IO sets y_2/u_2, y_3/u_2, and y_4/u_2 are the lowest-dimensional viable IO sets, which are preferable in the sense of the IO selection goal stated in the Introduction. Performing D-K iterations for these IO sets, it appears that y_2/u_2 and y_4/u_2 are equally best ($\|M\|_{\bar{\mu}} = 0.76$, like for y_2/u_1u_2, y_4/u_1u_2), while y_3/u_2 is worst ($\|M\|_{\bar{\mu}} = 0.82$, like for y_3/u_1u_2).

Unfortunately, IO selection based on higher order D-scales requires more computation time, because the order of the original G is increased with twice the D-scale order. This in turn yields higher order Hamiltonians and more complex viability conditions. For the case where

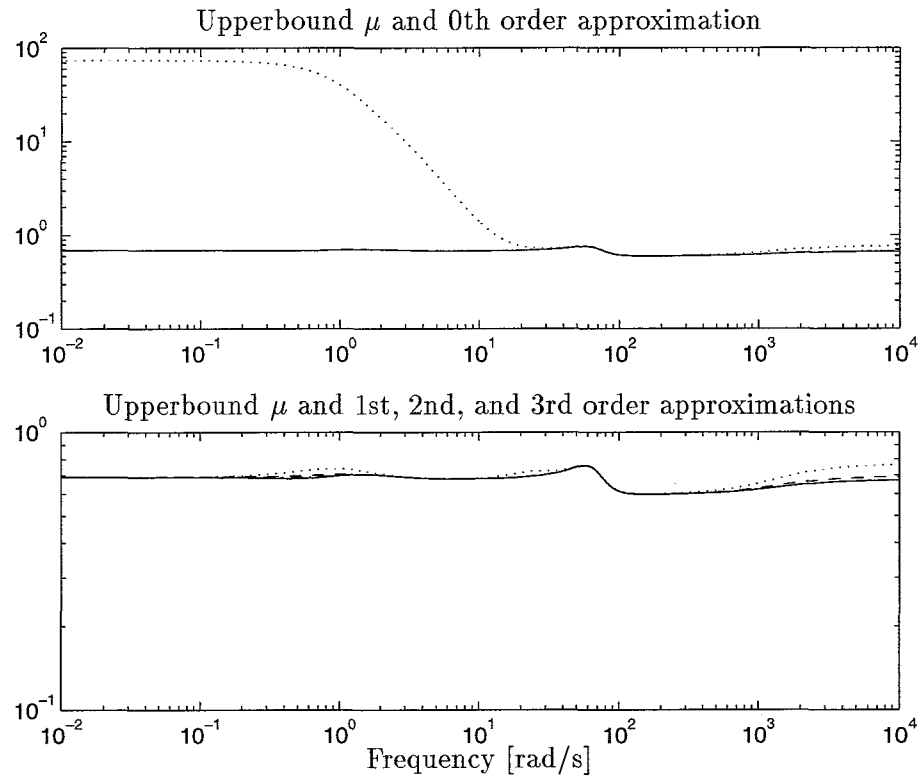

Figure 5.5: The frequency-dependent upperbound of μ for the overall IO set and some approximations using rational D-scales (`musynfit`) in the case with y-noise and u-weights: *upper plot:* (–) μ upperbound and approximation via 0th order (··) D-scale; *lower plot:* (–) μ upperbound and approximation via 1st order (··), 2nd order (- -), and (–·) 3rd order D-scale.

all six viability conditions are checked, Table 5.4 compares the CPU times on a SUN workstation. Obviously, for reasons of efficiency, low order D-scales are preferred; other ways to improve efficiency are discussed in the final chapter. For the particular problem considered here, it appeared from Table 5.3 that there is no need to use 2nd or higher order D-scales. A "guideline" for choosing appropriate D-scale orders for IO selection is highly desirable, but currently lacking. This certainly merits further investigation.

Next, IO selection including input weights and measurement noise is studied. In Section 3.1, it was conjectured that the IO selection will now be more "conservative."

In the presence of y-noise and u-weights, the overall IO set achieves $\|M\|_{\bar{\mu}} = 0.76$. Comparing Fig. 5.5 with Fig. 5.3, it is concluded that a very good approximation of the μ upperbound is already obtained with 2nd and 3rd order D-scales. Also note from Table 5.2, that the corresponding $\|M^\star\|_{\bar{\mu}}$ value is already approximately equal to $\|M^\star\|_{\bar{\mu}}$ for a 1st order D-scale.

Table 5.5 is generated as an equivalent of Table 5.3. Though the gap between $\|M\|_{\bar{\mu}}$ and the optimal $\mathcal{H}_\infty$ norms for 0th order D-scales is now smaller than in the case without y-noise and u-weights (at least with `musynfit`), during IO selection the IO sets 4, 5, 7, and 8 would

Table 5.5: Influence of the rational D-scale order (`musynfit`) on the optimal $\mathcal{H}_\infty$ norm of the scaled, generalized plant for some typical IO sets; *including* y-noise and u-weights.

IO set	Outputs	Inputs	$\|M\|_{\bar{\mu}}$	$\min_{K\in\mathcal{K}_A} \|\hat{D}_z M(G,K)\hat{D}_w^{-1}\|_\infty$							
				D-scale orders							
				×	0		1	2	3	4	5
					`musynflp`	`musynfit`					
1	$y_1\ y_2\ y_3\ y_4$	$u_1\ u_2$	0.76	189.96	3.38	0.83	0.76	0.76	0.75	0.75	0.75
2	$y_1\ y_2\ y_3\ y_4$	u_1	1.06	190.17	12.40	2.32	1.06	1.07	1.08	1.07	1.07
3	$y_1\ y_2\ y_3\ y_4$	u_2	0.76	189.96	3.58	0.93	0.76	0.76	0.75	0.76	0.75
4	$y_1\ y_2$	$u_1\ u_2$	0.77	435.63	5.66	1.02	0.77	0.77	0.77	0.76	0.77
5	$y_3\ y_4$	$u_1\ u_2$	0.76	207.50	3.38	1.70	0.76	0.76	0.76	0.76	0.76
6	y_1	$u_1\ u_2$	1.01	972.46	12.48	1.53	1.16	1.13	1.07	1.10	1.10
7	y_2	$u_1\ u_2$	0.77	436.08	5.66	1.02	0.77	0.77	0.77	0.77	0.77
8	y_3	$u_1\ u_2$	0.83	946.19	12.16	1.73	1.18	1.13	1.06	1.10	1.11
9	y_4	$u_1\ u_2$	0.77	288.35	3.70	1.70	0.76	0.76	0.76	0.76	0.76

still incorrectly be rejected for constant D-scales computed with `musynfit`, while *all* IO sets would be rejected for constant D-scales obtained with `musynflp`. For 1st and higher order D-scales (`musynfit`), the optimal $\mathcal{H}_\infty$ norms and the $\|M\|_{\bar{\mu}}$ values almost perfectly match for IO sets 1–5, 7, and 9. If `musynflp` is used to generate dynamic D-scales, the same qualitative conclusions are drawn for 1st–4th order D-scales. However, for a 5th order D-scale all IO sets are again rejected, which is most likely due to ill-conditioning of the extended generalized plants.

In the case *without* y-noise and u-weights, it is expected that the optimal $\mathcal{H}_\infty$ norms are closer to the $\|M\|_{\bar{\mu}}$ values than in the case *with* y-noise and u-weights (see Section 3.1). This conjecture is based on the following reasoning.

Obviously, μ-synthesis aimed at RP for the overall IO set is not "hindered" by y-noise and u-weights if these are absent or very small. Also, the influence in determining the D-scale estimates $\hat{D}_z$ and $\hat{D}_w$ for the overall IO set's optimal closed-loop will be absent or negligible. So, for very small y-noises and u-weights, the exogenous variables in w and the controlled variables in z are roughly "the same" if particular input weights or output noises are eliminated. As a consequence, skipping identity diagonal entries in $\hat{D}_z$ and $\hat{D}_w$ corresponding to non-considered inputs and outputs will not introduce extra conservativeness in the estimates for $\|M\|_{\bar{\mu}}$. Note, that these estimates for IO sets 3–5, 7, and 9 in Table 5.3 are very good (despite the relatively large difference between their optimal D-scales and those for the overall IO set (Fig. 5.2), as already remarked). The $\|M\|_{\bar{\mu}}$ estimates for the same IO sets in Table 5.5 are also very good. Apparently, the effect of y-noise and u-weights in the RP design is relatively small.

For IO sets with an optimal closed-loop M which considerably differs from $M^\star$ for the overall

IO set, the rational D-scales $\hat{D}_z$ and $\hat{D}_w$ employed in an optimal $\mathcal{H}_\infty$ design may result in an inaccurate estimate for $\|M\|_{\bar{\mu}}$, see IO set 8 ($\Omega = 2.93$) in Table 5.3. In case of y-noise and u-weights, this effect is expected to be even more serious, since μ-synthesis for the overall IO set including all y-noises and u-weights in fact accounts for *additional* objectives. The resulting $\hat{D}_z$ and $\hat{D}_w$ will therefore be less appropriate to arrive at a reliable estimate for the achievable $\|M\|_{\bar{\mu}}$'s. This conjecture is supported by the results for IO sets 6 ($\Omega = 1.70$) and 8 ($\Omega = 4.51$) in Table 5.5: the gaps between the optimal $\mathcal{H}_\infty$ norms and the $\|M\|_{\bar{\mu}}$ values are relatively large and much larger than in the case without y-noise (and u-weights, but this is not important since the inputs are the same as for the overall IO set) in Table 5.3. Note, that IO set 8 will even be rejected in the IO selection. However, contrary to the expectations, the optimal $\mathcal{H}_\infty$ norms for IO set 2 ($\Omega = 0.65$) are even *closer* to $\|M\|_{\bar{\mu}}$ than in the case without u-weights (and y-noise).

Performing IO selection for the case with y-noise and u-weights, 18 IO sets are termed viable for 0th order D-scale approximations resulting from `musynfit`, while *no* IO sets are viable for 0th order D-scales obtained with `musynflp`. For 1st–5th order D-scales (`musynfit`), 26 IO sets are termed *viable*. Apart from the 17 nonviable IO sets mentioned in Table 5.4, the two IO sets y_3/u_2 and y_3/u_1u_2 are rejected. According to Table 5.5 however, y_3/u_1u_2 has an RP level of 0.83, while D-K iteration for y_3/u_2 shows that the same RP level of 0.83 can be achieved. Hence, these two IO sets are *incorrectly* rejected by the IO selection approach. The lowest-dimensional, viable IO sets are y_2/u_2 ($\|M\|_{\bar{\mu}} = 0.77$), y_4/u_2 ($\|M\|_{\bar{\mu}} = 0.77$), and the rejected one y_3/u_2.

5.3 Input Output Selection with Linear Matrix Inequalities

This section illustrates the IO selection for the method based on Linear Matrix Inequalities (LMIs) discussed in Section 3.2. Emphasis will be on the case *including* y-noise and u-weights, since these will be present in a natural control problem formulation. Moreover, contrary to the method based on D-scale estimates, there is no reason to expect that the IO selection results will be less reliable than in the case without y-noise and u-weights.

Both the input selection LMI (A.13) and the output selection LMI (A.4) are *strict* inequalities. Moreover, d must be strictly larger than zero, see (2.7). Since LMITOOL relies on *nonstrict* inequalities, a small positive parameter ξ is introduced to replace inequalities of the form "$\Sigma > 0$" by "$\Sigma - \xi I \geq 0$." Parameter $\xi_1 = 10^{-6}$ is used to account for the strictly positive D-scales (so, $s - \xi_1^2 \geq 0$ and $-t + 1/\xi_1^2 \geq 0$), while $\xi_2 = 10^{-10}$ accounts for the negative-definiteness of the left-hand-sides of the LMIs.

To start with, condition (3.11) is studied to eliminate nonviable input sets among the candidates u_1, u_2, and u_1u_2. The same frequency grid is used as in the μ-synthesis, *i.e.*, 100 frequencies logarithmically spaced between 10^{-1} and 10^3 rad/s. The input selection LMI is checked at each frequency, starting with $\omega = 10^{-1}$ and working upwards to $\omega = 10^3$. For the purpose of efficiency, checking (3.11) for a particular input set could be stopped as soon as an "infeasible frequency" is encountered, *i.e.*, a frequency for which the input set is nonviable.

Table 5.6: Input selection results including u-weights

γ	Nonviable input sets	Infeasible frequencies [rad/s]	CPU time [s]
1.06	–	–	155
1.05	u_1	12.62, 13.85	155
1.00	u_1	11.50, ..., 16.68	156
0.75	u_1	7.92, ..., 55.91	179
0.74	u_1, u_2, u_1u_2	7.92, ..., 55.91 (u_1), 55.91 (u_2, u_1u_2)	179

However, to better interpret the results the *whole* frequency range will be studied here.

To check the feasibility of the input selection LMI with LMITOOL, an initial estimate d_0 for d (in fact, for t) must be specified. The computation time is considerably reduced if d_0 is feasible. In order to supply a good initial estimate to the LMI-solver, the following is done: if the LMI is feasible for ω_i, the corresponding d is used as d_0 for the next frequency ω_{i+1}; if the LMI is infeasible, d_0 corresponding to the latest, feasible d is used; for ω_1, d_0 is fixed at one.

The nonviable input sets for various RP levels γ are depicted in Table 5.6. Also the CPU times are listed, as well as the infeasible frequencies in the investigated grid. Note, that first input u_1 is eliminated for a decreasing γ. This is also expected, since with all four sensors included $\|M\|_{\bar{\mu}} = 1.06$ for u_1 and $\|M\|_{\bar{\mu}} = 0.76$ for u_2 and u_1u_2, see Table 5.1. Moreover, the infeasible frequencies for u_1 correspond to the frequency range where $\mu_{\mathbf{\Delta}}(M)$ for the optimal closed-loop with $y_1y_2y_3y_4/u_1$ is largest. In analogy, the infeasible frequency for u_2 and u_1u_2 with $\gamma = 0.74$ is close to the frequency $\omega = \sqrt{(k_{tr}/m_{ar})} = 57.74$ where $\mu_{\mathbf{\Delta}}(M)$ peaks for $y_1y_2y_3y_4/u_2$ and $y_1y_2y_3y_4/u_1u_2$.

Also observe from Table 5.6, that the input sets are first eliminated for γ values which are approximately the same as the best achievable $\|M\|_{\bar{\mu}}$ values with all four measurements. Apparently, the conservatism introduced by dropping the stabilizing property of K and neglecting the output selection LMI is negligible for the particular problem studied here. In the "absence" of u-weights, the same results as in Table 5.6 are obtained, except that the infeasible frequency range for u_1 with $\gamma = 1.00$ is somewhat smaller: 12.62, ..., 16.68 rad/s. Finally, it is observed that the CPU time tends to increase for decreasing γ values, because for a smaller γ an iterative search for a feasible d must be performed more frequently.

Next, the output selection condition (3.10) is checked for the same frequency range and grid as the input selection condition. Unfortunately, the output selection is hindered by numerical problems. For $\xi_1 = 10^{-6}$, $\xi_2 = 10^{-10}$ and $\gamma = 1.00$, the output selection LMI may be called feasible by the LMI-solver, though this is contradicted by substituting the corresponding d (in fact, s) in the LMI: *positive* eigenvalues with order of magnitude 10^{-7} occur in the LMI's left-hand-side, which must be negative-definite. It is expected, that this phenomenon is reduced by using a larger ξ_2, in this way imposing a stronger requirement for negative-definiteness. However, for $\xi_2 = 10^{-6}$ the same problem still occurs, while for $\xi_2 = 10^{-5}$ only the output sets including y_4 are accepted; this is obviously incorrect according to the μ-synthesis results in Table 5.1. If ξ_1 is manipulated while holding ξ_2 fixed at 10^{-10}, similar problems occur: with

Table 5.7: Output selection results including y-noise

γ	New nonviable output sets	Infeasible frequencies [rad/s]	CPU time [s]
1.00	–	–	814
0.24	y_2	8.70, 9.55	965
0.19	y_4, y_2y_4	8.70, 9.55	1016
0.09	y_1, y_1y_2	55.91, 61.36	1121
0.08	$y_1y_4, y_1y_2y_4$	50.94,..., 73.91	1124
0.04	y_3, y_2y_3, y_3y_4, $y_2y_3y_4$,	46.42,..., 97.70	1150
	y_1y_3, $y_1y_2y_3$,	55.91,..., 97.70	
	$y_1y_3y_4$, $y_1y_2y_3y_4$	61.36,..., 97.70	

$\gamma = 1.00$, $\xi_1 = 10^{-2}$, all output sets are termed nonviable, while with $\xi_1 = 10^{-3}$ all output sets are termed viable, but small positive eigenvalues may occur.

It is now decided to perform output selection with $\xi_1 = 10^{-6}$ and $\xi_2 = 10^{-10}$, bearing in mind that the negative-definiteness requirement on the output selection LMI might be "slightly" violated. With four candidate measurements, there are 15 candidate output sets. The results are depicted in Table 5.7, which has a somewhat different set-up than Table 5.6. For various γ values, the table shows the output sets which are for the first time eliminated for that particular value, reducing γ with steps 0.01. The investigated frequencies for which the associated output selection LMIs are infeasible are also printed.

The most striking observation from Table 5.7 is, that the γ values for which an output set is first eliminated are significantly smaller than the best achievable $\|M\|_{\bar{\mu}}$ values for the corresponding output sets using u_1u_2 (this observation can of course only be done for output sets subjected to μ-synthesis, see Table 5.1). Under the assumption that the numerical errors do not play a crucial role, the reason for this is twofold. First, the output selection condition (3.10) does not require K to be stabilizing. As a consequence, a larger class of controllers is allowed than during μ-synthesis, which is aimed at designing stabilizing controllers. Second, if the output selection is *only* based on (3.10) it is implicitly assumed that all variables z can be controlled independently. For this it is necessary that $n_u \geq n_z$, but here $n_z = 7 + n_u$. It is currently unclear why these two sources of ineffectiveness play such a significant role in the output selection for the investigated problem, where they did not for the input selection.

Studying the μ-synthesis results in Table 5.1, it is expected that during output selection y_1 is first eliminated for decreasing γ, followed by y_3. However, Table 5.7 shows that the rear measurements y_2 and y_4 are first rejected, while output sets including the front acceleration measurement y_3 are eliminated last, *i.e.*, for $\gamma \leq 0.04$. Furthermore, it is observed that the frequency ranges where the "typical" output sets y_1, y_2, y_3, y_4, y_1y_2, y_3y_4, and $y_1y_2y_3y_4$ first drop out do in general *not* correspond to the frequency ranges where $\mu_{\mathbf{\Delta}}(M)$ for the corresponding optimal closed-loop with u_1u_2 is largest. For $\gamma \leq 0.04$, all candidate output sets are eliminated. In the "absence" of y-noise, all output sets are viable for $\gamma \geq 0.01$, except y_2 (nonviable for $\gamma \leq 0.23$) and y_4 (nonviable for $\gamma \leq 0.01$).

In the considered problem, the only uncertainty is the semitrailer mass, so Δ_u is a 1×1 full

block. In addition, Δ_p is a full block. Thanks to this special structure of Δ, a *combined* input and output selection (IO selection) is easily performed, see Section 3.2. Only the input and output sets which passed the individual LMIs for $\gamma = 1.00$ are considered, see Tables 5.6 and 5.7. The implementation of the IO selection is detailed next.

Fundamentally, it must be checked if the intervals for $s = d^2$ in (3.14) and $t = 1/s = 1/d^2$ in (3.15) intersect. For this purpose, the IO selection is split up into two optimization parts (1, 2) and a feasibility part (3):

1. For all considered input sets and frequencies, t is *minimized* subject to feasibility of the input selection condition (3.11); this yields the value $\underline{t}$. Note that $\underline{t}$ is allowed to be zero, since possibly $d \Rightarrow \infty$.
2. For all considered input sets and frequencies, t is *maximized* subject to feasibility of the input selection condition (3.11); this yields the value $\bar{t}$. Since $d \geq \xi_1$, $\bar{t} \leq 1/\xi_1^2$ is required in the maximization (strictly speaking, $\underline{t} \leq 1/\xi_1^2$ is also required in the minimization).
3. Given $\underline{t}$ and $\bar{t}$ for a particular input set and frequency, s for that same input set and frequency is restricted according to $1/\bar{t} \leq s \leq 1/\underline{t}$. This is imposed as an additional requirement on s in checking the *feasibility* of the output selection condition (3.10). If $\underline{t}$ is below a small number κ, say $\kappa = 10^{-10}$, an upperbound on s is not imposed. If the output selection LMI is feasible under the additional restrictions for s, the investigated IO set is viable for the considered frequency and RP level γ.

With respect to this implementation, the following additional remarks are made. First, the search for $\underline{t}$ and $\bar{t}$ is useless if the input selection LMI is nonfeasible. Therefore, IO selection is only performed for γ values for which this LMI is feasible, see Table 5.6. Second, in contrast with the above, part 1 and 2 of the IO selection could be performed for the output selection condition and part 3 for the input selection condition. This is not done for the following reasons, the second and third of which are tied to the active suspension control problem studied here:

- Under the requirement $d \geq \xi_1$, the following applies for s and t: $\xi_1^2 \leq s \leq \infty$, $0 \leq t \leq 1/\xi_1^2$. Since $\bar{t}$ is bounded and $\bar{s}$ unbounded, the search for $\bar{t}$ will stop in a finite number of steps, while the search for $\bar{s}$ may continue (until the prescribed maximum number of iterations is exceeded).
- From an efficiency point of view, a feasibility problem is preferred to an optimization problem. Since the number of candidates is less for the input sets than for the output sets, the input selection LMI is subjected to the optimizations.
- The results for the input selection LMI (Table 5.6) are better than for the output selection LMI (Table 5.7), in the sense that they better match with the results from μ-synthesis aimed at designing internally stabilizing controllers. For this reason, it is conjectured that $\underline{t}$ and $\bar{t}$ provide a better estimate for the "viable D-scale range" with stabilizing controllers than $\underline{s}$ and $\bar{s}$ would do.

Performing the IO selection for the 30 candidate IO sets left (recall that 15 candidates based on the single u_1 did not pass the input selection for $\gamma = 1.00$), *all* 30 IO sets remain viable for $\gamma \in [0.75,\ 1.00]$ with the same frequency grid as used before. Hence, the combination of the input and output selection LMIs is not able to eliminate extra IO sets. Note from Table 5.1, that for $\gamma = 0.75$ all 30 IO sets should be termed nonviable if only stabilizing controllers were considered. The fact that all 30 IO sets pass is therefore due to dropping the stabilizing property of the controller. However, the numerical problems with the output selection LMI may also affect the outcome considerably. Based on the goal of IO selection as stated in the Introduction, the IO sets y_1/u_2 ($\|M\|_{\bar{\mu}} = 1.01$), y_2/u_2 ($\|M\|_{\bar{\mu}} = 0.77$), y_3/u_2 ($\|M\|_{\bar{\mu}} = 0.83$), and y_4/u_2 ($\|M\|_{\bar{\mu}} = 0.77$) are indicated as the lowest-dimensional IO sets achieving an RP level $\gamma = 1.00$, but μ-synthesis shows that this is incorrect for y_1/u_2.

5.4 Comparison of Input Output Selection Results

The results with and efficiency of the two RP based IO selection methods applied in the previous sections are shortly compared. For a further discussion on these and various other issues, see Chapter 6. The method based on D-scale estimates will be abbreviated "DSE method" and the one employing linear matrix inequalities "LMI method."

In the case of u-weights and y-noise and a desired RP level $\gamma = 1.00$, the DSE method with 1st or higher order D-scale estimates accepts 26 IO sets and the LMI method 30. Due to its sufficiency, the DSE approach incorrectly rejects IO sets y_3/u_2, y_3/u_1u_2 ($\|M\|_{\bar{\mu}} = 0.83$), while due to its necessity the LMI approach incorrectly accepts IO sets y_1/u_2, y_1/u_1u_2 ($\|M\|_{\bar{\mu}} = 1.01$), even for all $\gamma \in [0.75,\ 1.00]$.

In the current implementation, the DSE method checks the six viability conditions of Section 3.1 for each candidate IO set until one condition fails. Depending on the D-scale order, the CPU times when *all six* conditions are checked for each of the 45 IO sets are listed in Table 5.4. In case of the LMI method, the CPU time not only depends on the (number of) investigated frequencies, but also on the specified γ. For checking the *combined* LMIs for the 45 candidates at one frequency, a typical CPU time is 40 seconds. So, an IO selection with the LMI method based on only five frequencies would take approximately as much time as the DSE method with 1st order D-scales. It is emphasized, that this only applies if the LMIs are checked for *all five* frequencies. The efficiency of the LMI method is improved if for a given IO set and frequency grid the computations are stopped as soon as an infeasible frequency is encountered. Chapter 7 provides an extensive discussion on how to further improve efficiency for both IO selection methods.

Chapter 6

Discussion

Two approaches for IO selection based on robust performance have been proposed and applied to a practical example. This chapter assesses these methods, using the list of desirable properties proposed in [47] as a guideline. For the method based on D-scale estimates, there is quite some overlap with the Discussion in [45, Chapter 6].

1. Efficiency: *Efficiency is related to the amount of analytical and computational effort inherent in the IO selection.*

The *analytical* effort for both methods mainly consists of (uncertainty) modeling and specifying appropriate shaping and weighting filters. In addition, the method based on D-scale estimates (DSE method) requires specifying a suitable frequency grid to be used in the μ-synthesis for the overall IO set. Moreover, a sensible choice of the order of the rational D-scale estimate must be made. For the method employing Linear Matrix Inequalities (LMI method), a representative but not too dense frequency grid must be chosen.

The *computational* effort for both methods could be reduced significantly, see Chapter 7. From Section 5.4 it is concluded, that with the current implementations and for the active suspension example, the DSE method is considerably more efficient than the LMI method. Currently, for each candidate IO set the DSE method checks six conditions (until one fails) for existence of a stabilizing controller satisfying an $\mathcal{H}_\infty$ performance specification on a scaled plant. The computation time with this method is strongly affected by the order of the D-scale estimates. The LMI method is split up into two or three phases: input selection, output selection, and combined input and output selection if Δ consists of two full blocks. In case of input or output selection, a feasibility problem is solved for the associated LMI at each considered frequency, until an "infeasible frequency" occurs. In case of three-phase-IO selection, this is followed by two optimizations for each viable input (or output) set and a feasibility check for each viable output (or input) set. For this purpose, `lmisolver` from [9] can be used.

2. Robust Performance: *The control system must remain stable and achieve the performance specifications in the presence of uncertainties.*

Both methods account for RP against structured uncertainties Δ consisting of full complex, not necessarily square, diagonal blocks. In [35], an extension is made to repeated complex blocks for the LMI method. While that method is based on a necessary condition for existence of a stabilizing controller achieving RP, the DSE method is based on a sufficient condition, also see the Effectiveness property below. The two IO selection methods require the performance and uncertainty to be characterized via the $\mathcal{H}_\infty$ norm, which is obviously restrictive if other norms are more appropriate.

3. Robust Stability: *The control system must remain stable in the presence of uncertainties.*

Essentially, the RP problem is an RS problem with an additional block Δ_p (see also Section 2.2) and hence the same remarks apply as for RP.

4. Nominal Performance: *The control system must achieve the performance specifications in the absence of uncertainties.*

In case of NP, Δ reduces to an unstructured complex block Δ_p. Consequently, for the DSE method the D-scales are identity and IO selection boils down to checking the existence of a stabilizing K achieving $\|M\|_\infty < \gamma$ instead of $\|M\|_{\bar{\mu}} < \gamma$. The IO selection is then again based on a necessary and sufficient condition, like in [45]. In analogy, X_z and X_w in the LMI method become identity and the IO selection simplifies to checking properties of the generalized plant. However, the resulting conditions do still not require the controller to be stabilizing. Hence, in case of NP the ineffective "LMI method" is better replaced by the more effective "DSE method."

5. Controller Independence: *An IO selection method must provide a way to eliminate IO sets for which any controller meeting the control objectives does not exist.*

Both the DSE and LMI method check for the existence of a linear, time-invariant, finite-dimensional, and proper controller meeting a desired RP measure. In contrast with the DSE method, the LMI method does not require the controller to be internally stabilizing.

If for a given IO set all six viability conditions in the DSE method are met, the controller is "almost" obtained: only some straightforward algebraic operations involving the Riccati equation solutions X_∞ and Y_∞ must be performed to synthesize K. For an IO set passing the LMI method, the obtained d might provide a useful initial guess for the D-scales to be used in D-K iteration, possibly reducing the number of iterations.

6. Effectiveness: *An IO selection method must be able to eliminate nonviable candidates and maintain viable ones.*

Since the DSE method is based on *sufficiency*, IO sets may incorrectly be rejected as illustrated by the example. This conservatism is due to various sources. First, IO selection focuses on the μ-upperbound, since in general the exact μ cannot be computed efficiently:

$\|M^\star\|_{\bar{\mu}} \geq \|M^\star\|_\mu$, with $M^\star$ the overall IO set's optimal closed-loop. Fortunately, the upper-bound is usually tight. Second, due to finite order of the D-scale estimates the approximation of the true D-scales might be crude: $\|\hat{D}_z M^\star \hat{D}_w^{-1}\|_\infty \geq \|M^\star\|_{\bar{\mu}}$. Recall, that from an efficiency viewpoint low order D-scale estimates are preferred. For this reason, a guideline for choosing efficient and effective D-scale orders is highly desirable. Third, the D-scale estimate resulting from $M^\star$ might be worse for other IO sets, see inequality (3.4). One reason is, that compared to the other IO sets the D-scale estimate from $M^\star$ accounts for *additional* control objectives if y-noise and u-weights are included.

Assuming that the μ-upperbound is tight [22], the LMI method is completely based on *necessity* and nonviable IO sets may be accepted. This ineffectiveness arises from the following sources. First, the requirement that K must be stabilizing is dropped. Second, critical frequencies may be overlooked in the specified frequency grid. An indication for a suitable grid is provided from a μ-synthesis with the overall IO set (at least, if all critical frequencies are present in the grid for μ-synthesis). However, critical frequencies for stabilizing controllers may not be critical with not-necessarily-stabilizing controllers. A third source of ineffectiveness is the inability to jointly check the LMIs for problems with Δ consisting of more than two blocks. To partially resolve this shortcoming, all possible combinations of two full blocks could be studied. Note however, that an IO set which passes all possibilities may not pass the IO selection for the original multi-block Δ.

7. Quantitative Nature: *The IO selection must be based on quantitative measures to clearly distinguish between the candidate IO sets.*

In both the DSE and LMI method, design filters quantitatively account for performance specifications and uncertainty characterizations. As an "extra" design parameter, γ is used to prescribe the desired RP level.

8. General Applicability: *An IO selection method should be applicable to a large class of control problems.*

Both methods are restricted to linear, time-invariant, finite-dimensional, and proper systems. In addition, the system must satisfy the standard $\mathcal{H}_\infty$ assumptions. Although this is not explicitly remarked for the LMI method in [22], assumptions 5 and 6 are necessary to derive the IO selection conditions and the other four assumptions are also appropriate for a physically meaningful control problem formulation. The (fictitious) uncertainties must be stable and bounded by the $\mathcal{H}_\infty$ norm.

Three frequently encountered generality restrictions in IO selection (see Introduction) are resolved by both the DSE and LMI method, *i.e.*, the IO sets are allowed to be nonsquare, y and z are treated separately (no performance specifications are imposed on y), and the method is applicable in any frequency range of special interest.

9. Applicability to Nonlinear Systems: *Desirably, the IO selection method can be applied to, or can be generalized to be applied to nonlinear systems.*

Since the $\mathcal{H}_\infty$ concept has been extended to nonlinear systems, there might be some prospects

for generalization of the DSE method to nonlinear systems with *unstructured* uncertainties, involving identity D-scales. Chapter 8 addresses this issue in detail. In case of structured Δ, a μ-synthesis for the overall IO set must be performed, but this is unsolved for nonlinear systems. Therefore, it is unlikely that the general DSE method and LMI method can be extended to nonlinear systems in the short term.

Further research must reveal if the DSE and LMI methods can be applied successfully to *linearizations* of nonlinear systems. It must be investigated, if nonlinearities due to deviations from a nominal operating point can be accounted for via the uncertainty block Δ, see, *e.g.*, [3, Section 5.5.5]. If various "operating points" play a role, the DSE and LMI methods could be applied to the corresponding linearizations in succession. It is emphasized, that such an approach may yield incorrect results, since crucial features of the nonlinear system can be lost due to linearization. For instance, it is well-known that a linearized description can be uncontrollable, while the original nonlinear system is controllable [32, Chapter 3]. On the other hand, [21,41] show that existence of an $\mathcal{H}_\infty$ controller for the linearized model implies that there also exists a nonlinear $\mathcal{H}_\infty$ controller *locally* solving the original nonlinear problem.

10. Control System Complexity: *During IO selection, it must be possible to impose the allowable control system complexity.*

Trivially, both IO selection methods are able to limit the maximum number of actuators and sensors by prescription. For the DSE method, the controller order and design effort as other complexity aspects can be addressed as well. The maximally required controller order for a viable IO set is equal to the order of the generalized plant including the D-scale estimates. So, by limiting the D-scale order it can be checked if there are admissible controllers with a prescribed order ((stronger) restrictions on the controller order could also be taken care of after the controller design, by applying model reduction techniques, see, *e.g.*, [59, Chapter 19]). The controller design effort is equal to the effort of designing a sub-optimal $\mathcal{H}_\infty$ controller via the Riccati equation approach. For the LMI method, there is no clear relation between required controller order or design effort and the IO selection.

For both methods, no prospects are seen to automatically account for complexity issues such as hardware and operating costs, reliability and maintainability, and implementation effort. Instead, these considerations could be done beforehand when defining the candidate IO sets, or afterwards when evaluating accepted IO sets.

11. Directness: *Desirably, the IO selection directly indicates the favorable IO set(s).*

The investigated IO selection methods are both indirect, since all relevant candidate IO sets are checked for viability. Both procedures are also iterative if accepted IO sets are subjected to other requirements, such as smaller γ values.

12. Solid Theoretical Foundation: *The theory behind an IO selection method must be well-founded and a successful application should prove its practical relevance.*

The theoretical foundation of the DSE method is rather weak, in the sense that it is currently unclear how to choose the D-scale order to "work well" for all IO sets. As a result, the gap be-

tween the resulting sufficient condition for an IO set to be viable ($\min_K \|\hat{D}_z M(G,K)\hat{D}_w^{-1}\|_\infty < \gamma$) and the necessary and sufficient condition ($\min_K \|M(G,K)\|_\mu < \gamma$) may be large. For a bad D-scale estimate, it is even possible that $\min_K \|\hat{D}_z M(G,K)\hat{D}_w^{-1}\|_\infty > \min_K \|M(G,K)\|_\infty$, see IO set 5 in Table 5.3 with the 0th order D-scale estimate from `musynfit`. The LMI method is based on a stronger theoretical foundation. Unfortunately, there is currently no method to solve the general RP problem with multi-block uncertainty.

In the absence of y-noise and u-weights, the DSE method was successfully applied in the active suspension problem. However, two IO sets were incorrectly eliminated in the presence of y-noise and u-weights. It appeared, that in general the conservatism is larger for IO sets with a larger difference between their optimal $\|M\|_{\bar{\mu}}$ and $\|M^\star\|_{\bar{\mu}}$ for the overall IO set. It is unclear, if the same would be concluded from other applications. For the LMI method, the results with the input selection LMI could be interpreted and are consistent with the results from μ-synthesis. On the other hand, the results with the output selection LMI are counterintuitive and conflict with μ-synthesis; numerical problems might have played a critical role here. The combined input and output selection suffers from the shortcoming that it accepts too many IO sets, which is mainly due to the output selection part. In [22], the LMI method was used for sensor selection in a distillation column. Although that application was qualified successful, it is emphasized that only steady-state was considered.

13. Practical Applicability: *The implementation and application of the method must be straightforward.*

Both IO selection procedures have been implemented in MATLAB. For the DSE method, algorithms available in the μ-Toolbox [1] are employed: `mu` to perform μ-analysis and to obtain frequency-dependent D-scales, followed by `musynfit` or `musynflp` to derive rational D-scale estimates. From the active suspension application it became clear, that `musynfit` delivers incorrect constant D-scales. However, for dynamic D-scales `musynfit` gives better results than `musynflp`. Once the scaled generalized plant is generated, existing programs for the IO selection method in [45] are used; see Chapter 6 of [45] for a detailed discussion on the implementation aspects. The LMI method relies on `lmisolver` from LMITOOL [9], which calls `sp` from [53] to solve a standard optimization problem. The active suspension application illustrated that the LMI method is not free of numerical problems.

With the provisional MATLAB programs (which are available from the author), RP based IO selection is straightforward. It is emphasized however, that besides supplying the system model $\bar{G}$ and the filters V and W, the designer must be aware of potential numerical problems, *e.g.*, in D-K iteration, in D-scale approximation, and in solving the LMIs.

Chapter 7

Further Research on IO Selection for Linear Systems

This chapter discusses some topics related to the improvement and generalizations of the two IO selection methods, as well as one potential alternative approach.

1. Improvement of Efficiency: *It must be studied how the efficiency of the current implementations of the DSE and LMI methods can be improved.*

Due to the combinatorial nature of the problem, an IO selection must be performed as efficiently as possible. To illustrate this, in case of 10 candidate actuators and sensors there are 1,0467,529 candidate IO sets and computation time becomes a major issue. Three possible ways to improve efficiency are discussed below, the first of which applies to both the DSE and LMI method.

I. *Branch-and-Bound Procedure (DSE & LMI):* In the current implementations of the DSE and LMI method, *all* candidate IO sets are checked. Obviously, IO sets made up of sensors and actuators from a larger but nonviable IO set are also nonviable, since control will never become better by eliminating sensors or actuators. For instance, if IO set y_1y_2/u_1u_2 is nonviable, the eight subsets associated with it are also nonviable. So, efficiency is improved if, starting with the overall IO set, only those lower-dimensional IO sets are further studied which are subsets of viable, higher-dimensional IO sets ("subset approach").

Based on the IO selection goal of finding the lowest-dimensional IO set achieving RP, the following (complementary) approach would also improve efficiency: start with the 1×1 IO sets and work upwards to higher-dimensional supersets ("superset approach"). Obviously, IO sets incorporating actuators and sensors from a smaller and viable IO set are also viable. The IO selection can be stopped as soon as a viable $m \times n$ IO set is detected. Note, that in this way other $m \times n$ viable IO sets can be overlooked, which might be preferable with respect to additional complexity aspects such as costs. Therefore, it is advisable to check the other $m \times n$ IO sets as well.

II. *Splitting up IO Selection (DSE):* Like in the LMI method, it is conjectured that in the DSE method the IO selection can be split into the following three phases: 1) input selection, 2) output selection, and 3) IO selection for the candidate IO sets made up of inputs and outputs passing phase 1 and 2. Recall from Section 3.1, that the DSE method involves checking six viability conditions. Assume $D_{11} = 0$ (eventually of the scaled plant), so the first viability condition is met for each IO set. It is *conjectured* that the requirements on H_X and X_∞ (viability conditions 2 and 4) are independent of the output set, while the requirements on H_Y and Y_∞ (viability conditions 3 and 5) are independent of the input set. If this is true and if $D_{11} = 0$, phase 1 requires checking H_X and X_∞, phase 2 requires checking H_Y and Y_∞, and phase 3 requires checking viability condition 5, *i.e.*, $\rho(X_\infty Y_\infty) < \gamma^2$.

The preference for the three-phase-approach is illustrated by the active suspension example. Suppose that $D_{11} = 0$ (as for the NP problem in [45, Chapter 4]) and that all 45 candidate IO sets are viable. In the current implementation, $45 \times 5 = 225$ tests are performed, whereas in the three-phase IO selection 3×2 tests would be performed in phase 1, 15×2 tests in phase 2, and 45×1 tests in phase 3, yielding a total number of 81 tests.

It is currently unclear if this implementation of the DSE method is possible, because it may be ruined by the following two effects:

1. The influence of the output set via y-noise in H_X, X_∞ and the influence of the input set via u-weights in H_Y, Y_∞. In Appendix D, the effect of y-noise and u-weights in the generalized plant's state-space description is explicitly documented.
2. The scalings of u and y together with the unitary transformations on w and z, which are needed to rewrite D_{12} and D_{21} in the appropriate form, see Appendix D.

III. *LMIs instead of Riccati Equations (DSE):* In [19,20], a necessary and sufficient condition for existence of a stabilizing controller achieving $\|M\|_\infty < 1$ is given in the form of an LMI feasibility condition. Realizing that $\|M\|_\infty < \gamma \Leftrightarrow \|\frac{1}{\gamma}M\|_\infty < 1$ and scaling C_1, D_{11}, and D_{12} in (3.5) with γ, the following provides a useful notion for IO selection:

There exists an internally stabilizing controller such that $\|M\|_\infty < \gamma$ *if and only if there exist* $X \in \mathbb{R}^{n_x \times n_x}$, $X = X^T \geq 0$ *and* $Y \in \mathbb{R}^{n_x \times n_x}$, $Y = Y^T \geq 0$ *for which:*

$$\begin{bmatrix} B_2 \\ \frac{1}{\gamma}D_{12} \end{bmatrix}_\perp \begin{bmatrix} AX + XA^T + B_1B_1^T & \frac{1}{\gamma}XC_1^T + \frac{1}{\gamma}B_1D_{11}^T \\ \frac{1}{\gamma}C_1X + \frac{1}{\gamma}D_{11}B_1^T & \frac{1}{\gamma^2}D_{11}D_{11}^T - I_{n_z} \end{bmatrix} \begin{bmatrix} B_2 \\ \frac{1}{\gamma}D_{12} \end{bmatrix}_\perp^T < 0 \qquad (7.1)$$

$$\begin{bmatrix} C_2^T \\ D_{21}^T \end{bmatrix}_\perp \begin{bmatrix} YA + A^TY + \frac{1}{\gamma^2}C_1^TC_1 & YB_1 + \frac{1}{\gamma^2}C_1^TD_{11} \\ B_1^TY + \frac{1}{\gamma^2}D_{11}^TC_1 & \frac{1}{\gamma^2}D_{11}^TD_{11} - I_{n_w} \end{bmatrix} \begin{bmatrix} C_2^T \\ D_{21}^T \end{bmatrix}_\perp^T < 0 \qquad (7.2)$$

$$\begin{bmatrix} X & I_{n_x} \\ I_{n_x} & Y \end{bmatrix} \geq 0, \qquad (7.3)$$

with the matrices A, $B_1, \ldots, D_{21}$ related to the generalized plant's state-space representation (3.5), possibly extended with rational D-scale estimates. It is emphasized, that these

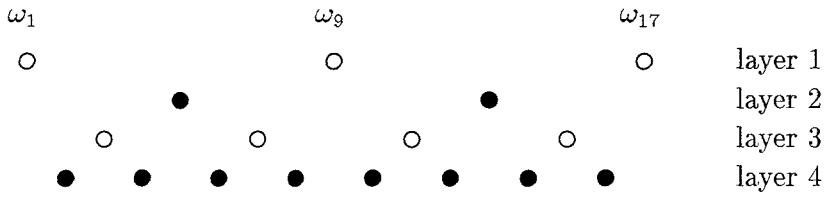

Figure 7.1: Effective frequency grid policy; $N = 4 \Rightarrow n = 17$

LMI existence conditions are derived *without* any assumptions on these matrices. In IO selection, an IO set is termed viable if the corresponding LMIs (7.1)–(7.3) are feasible. In future research, it must be investigated if the efficiency of the DSE method is improved by using these three LMI feasibility conditions instead of the six viability conditions arising in the Riccati equation formulation.

IV. *Effective Frequency Grid (LMI):* Assume that for the LMI method an interesting frequency range and grid $\omega_1, \ldots, \omega_n$ have been chosen. In the current implementation, the LMIs are checked for consecutive frequencies ω_1, $\omega_2, \ldots, \omega_n$ until an "infeasible frequency" occurs. Suppose that ω_i is feasible. If ω_{i+1} is close to ω_i, this frequency is likely to be feasible as well, since the system dynamics is approximately the same. For this reason, it is expected that efficiency can be improved by working through the frequency grid with a policy aimed at raising the chance of early encountering an infeasible frequency. With n frequencies given by $n = 2 + \sum_{i=1}^{N-1} 2^{i-1}$ where N is the number of "layers," see Fig. 7.1, a potential scheme is to check feasibility as follows: 1) ω_1, $\omega_{\frac{n+1}{2}}$, ω_n, 2) $\omega_{\frac{n+3}{4}}$, $\omega_{\frac{3n+1}{4}}$, 3) $\omega_{\frac{n+7}{8}}$, $\omega_{\frac{3n+5}{8}}$, $\omega_{\frac{5n+3}{8}}$, $\omega_{\frac{7n+1}{8}}$, *etc*; stop if an infeasible frequency is encountered.

2. Extension to Real and Repeated Perturbations: *It must be studied if the methods can be used for repeated complex uncertainty blocks, as well as repeated or full real blocks.*

In this report, Δ was restricted to consist of full complex individual blocks, but also other block types are important, as already mentioned in Section 2.1. Possible generalizations of the DSE and LMI method in this direction are considered next.

First, *repeated complex* blocks could be added to the full complex blocks in Δ, *i.e.*:

$$\boldsymbol{\Delta} = \left\{ \mathrm{diag}(\delta_1 I_{r_1}, \ldots, \delta_k I_{r_k}, \Delta_1, \ldots, \Delta_l) : \ \delta_i \in \mathbb{C}, \ \Delta_j \in \mathbb{C}^{m_j \times n_j} \right\},$$

with D-scale sets:

$$\begin{aligned} \boldsymbol{D_z} &= \left\{ \mathrm{diag}(D_1, \ldots, D_k, d_1 I_{m_1}, \ldots, d_l I_{m_l}) : D_i \in \mathbb{C}^{r_i \times r_i}, \ D_i = D_i^* > 0; \ d_j \in \mathbb{R}^+ \right\}, \\ \boldsymbol{D_w} &= \left\{ \mathrm{diag}(D_1, \ldots, D_k, d_1 I_{n_1}, \ldots, d_l I_{n_l}) : D_i \in \mathbb{C}^{r_i \times r_i}, \ D_i = D_i^* > 0; \ d_j \in \mathbb{R}^+ \right\}. \end{aligned}$$

So, each repeated uncertainty $\delta_i I_{r_i}$ is accompanied by a positive-definite scaling matrix D_i. In the DSE method, the D-K iteration for the overall IO set should account for repeated complex blocks. Although this is possible in the μ-analysis part, the current version of the μ-Toolbox [1] does not allow rational approximation of D-scales for repeated uncertainties. As an alternative, during D-K iteration each repeated block could be replaced by the appropriate number of independent scalar blocks. For the resulting optimal closed-loop, a μ-analysis

accounting for repeated blocks must be performed to verify the μ-upperbound. The derivation of the LMI method in [22] already accounts for repeated complex blocks, which was employed by the active suspension example in [35].

Second, full real and repeated real blocks may be important in practice, see the truck uncertainty model in Section 4.3. Although (to our knowledge) *full real* blocks have not been treated in literature and can neither be handled with the μ-Toolbox, *repeated real* blocks have been paid attention to. In [54], the D-K iteration is modified to account for full and repeated complex blocks and repeated real blocks. For this purpose, an extra "G-scaling" is invoked. Like in the D-K iteration described in Section 2.3, the frequency-dependent D- and G-scalings are fit with real-rational approximations and the generalized plant is augmented with them. So, it is again possible to perform an approximate μ-synthesis by alternate μ-analysis for mixed real/complex blocks, approximation of scalings, and $\mathcal{H}_\infty$ design for an extended plant. Unfortunately, with the current μ-Toolbox it is neither possible to approximate G-scales due to real repeated blocks, nor to approximate D-scales due to real or complex repeated blocks, as mentioned before. In [40], an alternative μ-synthesis for mixed uncertainties is highlighted, which is claimed to be simpler and more reliable than the approach in [54]. Again, $\mathcal{H}_\infty$ design for a scaled plant is involved.

Based on the above, extension of the DSE method to deal with complex and real uncertainties is straightforward, once the problems with the approximations of the scalings are solved. However, no prospects are seen for generalization of the LMI method.

3. An Alternative Sufficiency-Based IO Selection for RP: *It must be studied if employing constant D-scales instead of frequency-dependent ones can be useful for IO selection.*

A major disadvantage of the LMI method is the need to check feasibility for possibly many frequencies, leading to large computation times. Moreover, effectiveness is endangered if critical frequencies are absent in the specified grid. Both problems are avoided if the so-called State-Space UpperBound (SSUB, [33, Section 10.3]) for μ is used instead of the Frequency Domain UpperBound (FDUB, see (2.18)), which has been the focus throughout this report. In fact, the SSUB and the FDUB are the same in case of *constant* D-scales in the frequency domain:

$$\text{SSUB} \equiv \inf_{d \in \boldsymbol{d}} \sup_{\omega} \bar{\sigma}\{D_z M(j\omega) D_w^{-1}\}. \tag{7.4}$$

The RP specification SSUB $< \gamma$ is much stronger than the RP specification FDUB $< \gamma$, since for the SSUB the *same* D-scale must work for all frequencies. If the RP specification on the SSUB is satisfied, then RP also holds for arbitrarily fast time-varying uncertainties and cone bounded nonlinear uncertainties [33, Section 10.2]. So, if the uncertainties are better modeled as linear and time-invariant, the SSUB is conservative and the "common" FDUB is more appropriate.

In the full information case (both x and w are measured) and with square diagonal blocks in Δ, the following condition is derived in [34], which might serve as an alternative for the input selection condition (3.11):

There exists a stabilizing, static, full information controller K achieving SSUB < 1 if and only if there exists a Z such that:

$$\begin{bmatrix} B_2 \\ D_{12} \end{bmatrix}_\perp^T \left(\begin{bmatrix} A & B_1 \\ C_1 & D_{11} \end{bmatrix} Z \begin{bmatrix} A & B_1 \\ C_1 & D_{11} \end{bmatrix}^T - Z \right) \begin{bmatrix} B_2 \\ D_{12} \end{bmatrix}_\perp < 0. \tag{7.5}$$

In this condition, Z not only involves D-scales, but a positive definite state-coordinate scaling as well. The matrices A, B_1, B_2, C_1, D_{11}, D_{12} are discrete time versions of those in (3.5). It is conjectured, that an analogous condition can be derived for the full control case (where K has direct access to the states x and the controlled variables z), which might be a useful alternative for the output selection condition (3.10).

Note that (7.5) depends on state-space matrices, whereas input selection condition (3.11) depends on frequency-dependent TFMs. So, if (7.5) is used for input selection there is no need to specify a suitable frequency grid and each candidate input set need only be checked once. The same advantages apply for the output selection equivalent of (7.5). Unfortunately, IO selection based on the SSUB may give conservative results, since it accounts for a large class of uncertainties. Moreover, the *combination* of (7.5) and its output selection complement would introduce additional conservativeness, since it would give a necessary and sufficient condition for existence of a *static* output feedback controller achieving SSUB < 1. Future research must reveal the usefulness of this sufficiency-based IO selection approach.

Chapter 8

Nonlinear $\mathcal{H}_\infty$ Control and Input Output Selection

This final chapter tries to give an answer to the following specific question: are there prospects for an IO selection procedure for *nonlinear* control systems based on the $\mathcal{H}_\infty$ concept, without the need for linearization? The findings of a mini literature search on $\mathcal{H}_\infty$ control for nonlinear systems are described. A representative paper on this subject is [15]. Emphasis will be on the controller existence conditions ("viability conditions"), since such conditions could lay the foundations for an IO selection method for nonlinear systems. The actual computation of the controllers is a difficult problem and finding an exact solution is often impossible. Instead, approximation techniques are used, see, *e.g.*, [18,49] and [31, Chapter 9]. To start this chapter, some definitions are made and the goal of nonlinear $\mathcal{H}_\infty$ control is formulated, followed by a survey of controller existence conditions for three classes of nonlinear systems, characterized by an increasing degree of generality.

8.1 Some Definitions and Notations

In this section, some commonly encountered definitions and notations are listed:

- A function is said to be of class C^k if it is continuously differentiable k times [26]. So, C^0 stands for the class of continuous functions. A function is smooth, if $k = \infty$ [17].
- The notation $\|x(t)\|$ is used to express the Euclidean norm of the vector x at time t: $\|x(t)\| := \sqrt{x^T(t)x(t)}$.
- For $x \in \mathbb{R}^n$, a function $V(x) : \mathbb{R}^n \to [0, \infty)$ is *globally* positive-definite if $V(x) = 0$ implies that $x = 0$ and $\lim_{x\to\infty} V(x) = \infty$; with $\boldsymbol{B}_r := \{x \in \mathbb{R}^n \mid \|x\| < r\}$, $V(x)$ is *locally* positive-definite if there exists $r > 0$ such that for $x \in \boldsymbol{B}_r$, $V(x) = 0 \Rightarrow x = 0$ [26].

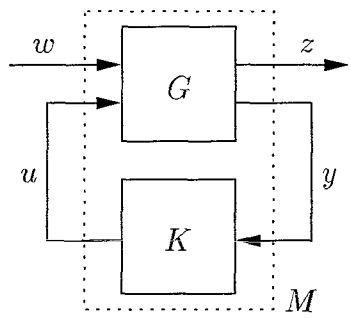

Figure 8.1: Standard control system set-up

- Consider the general nonlinear system $\dot{x} = f(x, w, u)$, $z = g(x, u)$. This system is called detectable if for $w = 0$ and for any bounded $x(t)$ for which $g(x(t), u(t)) = 0 \; \forall \; t$ this implies that $\lim_{t\to\infty} x(t) = 0$ [18].
- The notation V_x is used to denote the row vector $[\partial V/\partial x_1, \ldots, \partial V/\partial x_n]$.
- The Hessian matrix of a function $F(x_1, \ldots, x_n) : \mathbb{R}^n \to \mathbb{R}$ can be interpreted as the "second-derivative-matrix" of F, whose entries are given by $\partial^2 F/\partial x_i \partial x_j$.
- The notation $x(t) \in \mathcal{L}_2[0, T]$ expresses that $(\int_0^T \|x(t)\|^2 \mathrm{d}t < \infty)$, *i.e.*, that the energy of the signal $x(t)$ is bounded in the interval $[0, T]$.

8.2 Nonlinear $\mathcal{H}_\infty$ Control Problem Formulation

The set-up for nonlinear control systems in Fig. 8.1 is similar to that for linear systems with the same meaning of the variables as in Fig. 2.3. The goals in nonlinear $\mathcal{H}_\infty$ control are 1) to achieve closed-loop stability with $w = 0$ and 2) to achieve a prescribed performance level. The performance is expressed in terms of the $\mathcal{L}_2$ gain of the closed-loop, see, *e.g.*, [29,49]:

Definition of $\mathcal{L}_2$ gain: *The closed-loop system M with zero initial state is said to have $\mathcal{L}_2$ gain less than or equal to γ for some $\gamma > 0$ if*

$$\int_0^T \|z(t)\|^2 dt \leq \gamma^2 \int_0^T \|w(t)\|^2 dt \tag{8.1}$$

for all $T \geq 0$ and for all $w(t) \in \mathcal{L}_2[0, T]$.

Note, that (8.1) expresses the difference between the energy supply and the energy outflow, with γ a measure for the energy gain. The commonly used but incorrect terminology "nonlinear $\mathcal{H}_\infty$ control" is due to the fact that the $\mathcal{H}_\infty$ norm of a *linear* system equals its $\mathcal{L}_2$ induced norm. In [50], it is remarked that the above definition is slightly different from the one in the linear $\mathcal{H}_\infty$ case, where (8.1) is considered only for $T = \infty$, together with the requirement that the closed-loop is asymptotically stable. It is stated in [50], that for the linear case this *implies* that (8.1) holds for arbitrary $T \geq 0$. It is also remarked, that in the nonlinear case stability is often implied by the finite $\mathcal{L}_2$ gain condition.

The studied literature on nonlinear $\mathcal{H}_\infty$ control deals with various descriptions of the nonlinear plant G and the controller K, differing in structural restrictions. Three distinct descriptions will be considered here, starting with the most restrictive one.

8.3 Nonlinear Systems with State-Dependent Coefficient Matrices

The following nonlinear time-invariant plant G (x evolves on $\boldsymbol{X}$) and controller K (x_k evolves on $\boldsymbol{X}_k$) are considered in [24,29]:

$$G: \quad \begin{cases} \dot{x} = A(x)x + B_1(x)w + B_2(x)u \\ z = C_1(x)x + D_{11}(x)w + D_{12}(x)u \\ y = C_2(x)x + D_{21}(x)w + D_{22}(x)u, \end{cases} \tag{8.2}$$

$$K: \quad \begin{cases} \dot{x}_k = A_k(x_k)x_k + B_k(x_k)y \\ u = C_k(x_k)x_k + D_k(x_k)y. \end{cases} \tag{8.3}$$

(compare (8.2) with the linear plant in (3.5)). The closed-loop M is written as:

$$M: \quad \begin{cases} \dot{x}_m = A_m(x_m)x_m + B_m(x_m)w \\ z = C_m(x_m)x_m + D_m(x_m)w, \end{cases} \tag{8.4}$$

with $x_m = \binom{x}{x_k}$, $\boldsymbol{X}_m = \boldsymbol{X} \times \boldsymbol{X}_k$. The following is assumed on G: all involved matrix functions are C^0; $\boldsymbol{X}$ and $\boldsymbol{X}_k$ are convex subsets and include the origin; the initial states are $x(0) = 0$ and $x_k(0) = 0$; $n_x + n_w \geq n_y$, $n_x + n_z \geq n_u$, which is guaranteed if y-noise and u-weights are incorporated. Four additional assumptions are made. While the first three assumptions are made for technical reasons, the fourth assumption guarantees well-posedness of the closed-loop [29]:

1. $\text{rank}\left(M(x) := \begin{bmatrix} B_2(x) \\ D_{12}(x) \end{bmatrix}\right) = n_u$ for all $x \in \boldsymbol{X}$,
2. $\text{rank}\left(N(x) := \begin{bmatrix} C_2(x) & D_{21}(x) \end{bmatrix}\right) = n_y$ for all $x \in \boldsymbol{X}$,
3. $D_{11}(x)D_{11}^T(x) < I$ for all $x \in \boldsymbol{X}$,
4. $I - D_k(x_k)D_{22}(x)$ is invertible for all $x_m \in \boldsymbol{X}_m$.

In [24,29], the focus is on $\gamma = 1$ and so-called "strong" $\mathcal{H}_\infty$ performance, which will not be defined here. The necessary conditions for existence of a controller solving this problem are characterized in terms of three NonLinear Matrix Inequalities (NLMIs) [29]:

Consider the system (8.2), satisfying the above assumptions. There is a solution to the $\mathcal{H}_\infty$ control problem with $\gamma = 1$ only if there exist C^0 positive-definite matrix-valued func-

tions Y and Z, such that for all $x \in \boldsymbol{X} \subset \mathbb{R}^{n_x}$:

$$M_\perp^T(x) \begin{bmatrix} A(x)Y(x) + Y(x)A^T(x) + B_1(x)B_1^T(x) & Y(x)C_1^T(x) + B_1(x)D_{11}^T(x) \\ C_1(x)Y(x) + D_{11}(x)B_1^T(x) & D_{11}(x)D_{11}^T(x) - I_{n_z} \end{bmatrix} M_\perp(x) < 0 \tag{8.5}$$

$$N_\perp^T(x) \begin{bmatrix} Z(x)A(x) + A^T(x)Z(x) + C_1^T(x)C_1(x) & Z(x)B_1(x) + C_1^T(x)D_{11}(x) \\ B_1^T(x)Z(x) + D_{11}^T(x)C_1(x) & D_{11}^T(x)D_{11}(x) - I_{n_w} \end{bmatrix} N_\perp(x) < 0 \tag{8.6}$$

$$\begin{bmatrix} Y(x) & I_{n_x} \\ I_{n_x} & Z(x) \end{bmatrix} \geq 0, \tag{8.7}$$

with $M(x)$ and $N(x)$ as defined in assumptions 1 and 2. Note the similarity between these NLMIs and the LMIs (7.1)–(7.3); conditions (8.5)–(8.7) are actually state-dependent LMIs. Though a separation structure is not assumed for K, the NLMIs (8.5) and (8.6) are closely related to state-feedback and observer design problems respectively.

In [29], it is claimed that all couples $Y(x), Z(x)$ satisfying the three NLMIs form a convex set. Therefore, the NLMIs provide a convex characterization to the solvability of the nonlinear (strong) $\mathcal{H}_\infty$ control problem. However, it is emphasized that meeting the NLMIs is in general not sufficient, since an additional condition must be met. More specific, it is also required, that there exists a positive-definite Lyapunov function $V(x_m)$ such that $V_{x_m}(x_m) = 2x_m^T P(x_m)$, with $P(x_m) = P^T(x_m) > 0$ satisfying:

$$\begin{bmatrix} A_m^T(x_m)P(x_m) + P(x_m)A_m(x_m) & P(x_m)B_m(x_m) & C_m^T(x_m) \\ B_m^T(x_m)P(x_m) & -I & D_m^T(x_m) \\ C_m(x_m) & D_m(x_m) & -I \end{bmatrix} < 0. \tag{8.8}$$

Note, that this NLMI depends on closed-loop matrices, the computational implications of which are unclear at the moment. For instance, the existence of $P(x_m)$ meeting (8.8) is guaranteed if (8.5)–(8.7) hold, but it is unclear how to construct $P(x_m)$ and how to exploit $Y(x)$ and $Z(x)$ for this purpose. For a given $P(x_m)$ satisfying (8.8), [29] describes a method to check the existence of a Lyapunov function $V(x_m)$. If the $\mathcal{H}_\infty$ problem is considered only *locally* ($x \in \boldsymbol{B}_r$), it is proven in [29], that the NLMIs (8.5)–(8.7) provide a necessary *and* sufficient condition, as in the linear case.

In the context of IO selection, the NLMIs (8.5)–(8.7) would be useful if their solvability were "easily" checked. Unfortunately, it is unclear how this should be achieved in general. In this respect, it is remarked in [28, Section 2.3] that point-wise (*i.e.*, for all interesting x) feasibility of the NLMIs is too strong. In [29], an efficient but potentially conservative alternative approach is proposed. This is illustrated by the NLMI (8.8), with the matrix functions $A_m(x), \ldots, D_m(x)$ continuous on $\boldsymbol{X}_m$ and in a convex set:

$$[A_m(x), B_m(x), C_m(x), D_m(x)] \in \text{Co}\,\{[A_{m_i}, B_{m_i}, C_{m_i}, D_{m_i}]|_{i\in\{1,2,\ldots,l\}}\} \;\forall\; x \in \boldsymbol{X}_m,$$

for some l, where "Co" stands for the convex hull. If there is a *constant* P such that

$$\begin{bmatrix} A_{m_i}^T P + P A_{m_i} & P B_{m_i} & C_{m_i}^T \\ B_{m_i}^T P & -I & D_{m_i}^T \\ C_{m_i} & D_{m_i} & -I \end{bmatrix} < 0 \;\forall\; i \in \{1, 2, \ldots, l\}, \tag{8.9}$$

then the constant P also satisfies (8.8) for all $x \in \boldsymbol{X}_m$. Note, that (8.9) represents a *set* of LMI feasibility conditions, which could efficiently be solved with, *e.g.*, LMITOOL [9]. It is mentioned in [29], that this treatment suggests a tractable approach to get *local* solutions, but that it may lead to conservative results if the prescribed convex hull is too large (as illustrated by an example in [28, Section 6.3]). So, for IO selection, viable IO sets may incorrectly be rejected.

In [27,28], robust performance and structured nonlinear uncertainty blocks are considered. Like in the linear case, scalings are involved to (partially) account for a structured Δ block. The aim is to achieve closed-loop stability and bounded $\mathcal{L}_2$ gain of the scaled closed-loop $D_z M D_w^{-1}$, with D_z and D_w real invertible matrices as in (2.5) and (2.6). For the state-feedback case, [27,28] derive a condition for controller existence expressed in an NLMI, which is very much alike (8.5) and which involves $Y(x)$ and the "D-scales" as free variables. Due to the restriction to static D-scales, this condition may be arbitrarily conservative. In the same way, the NLMIs (8.5)–(8.7) associated with the output feedback case can be modified to include D-scales.

8.4 Input Affine Nonlinear Systems

In the majority of the studied papers on nonlinear $\mathcal{H}_\infty$ control, the plant G is restricted to be affine in the exogenous inputs w and the manipulated inputs u, while the controller K is affine in the measured outputs y [25]:

$$G: \quad \begin{cases} \dot{x} = a(x) + B_1(x)w + B_2(x)u \\ z = c_1(x) + D_{12}(x)u \\ y = c_2(x) + D_{21}(x)w, \end{cases} \tag{8.10}$$

$$K: \quad \begin{cases} \dot{x}_k = a_k(x_k) + B_k(x_k)y \\ u = c_k(x_k) + D_k(x_k)y, \end{cases} \tag{8.11}$$

where all mappings $a, \ldots, D_k \in C^2$ (sometimes different smoothness properties are required) and $a(0) = 0$, $a_k(0) = 0$, $c_1(0) = 0$, $c_2(0) = 0$, $c_k = 0$. Further, the initial states $x(0)$ and $x_k(0)$ are zero. Note, that "$D_{11}(x)$" and "$D_{22}(x)$" are fixed at zero, as often seen for D_{11} and D_{22} in linear $\mathcal{H}_\infty$ control [7]; mostly, $D_k(x_k)$ is also fixed at zero. It is remarked in [28], that in many cases system (8.10) can (nonuniquely) be rewritten in the form (8.2).

The following assumptions on (8.10) are made in addition:

1. $D_{12}^T(x) \begin{bmatrix} c_1(x) & D_{12}(x) \end{bmatrix} = \begin{bmatrix} 0 & I \end{bmatrix}$,
2. $\begin{bmatrix} B_1(x) \\ D_{21}(x) \end{bmatrix} D_{21}^T(x) = \begin{bmatrix} 0 \\ I \end{bmatrix}$,
3. the pair $\{c_1(x), a(x)\}$ is detectable.

As in the linear case [7], the first two assumptions are introduced to simplify algebra, but they can be relaxed, see, *e.g.*, [15] and [31, Chapter 7]. According to [15], the detectability assumption corresponds to the fifth standard assumption in the linear case (see Section 3.1), implying that the TFM $G_{12}(j\omega)$ does not have $j\omega$-axis transmission zeros.

In [25] and its compressed form [26], the nonlinear $\mathcal{H}_\infty$ control problem is tackled by splitting it up into a full information problem (x and w are measured) and a full control problem (u has direct access to x and z), as it is done in the linear case of [7]. An additional assumption is made in [25] (remarkably not in [26]), namely the detectability of the pair $\{c_2(x), a(x)\}$. Before discussing the conditions for existence of an output feedback controller solving the $\mathcal{H}_\infty$ problem, the conditions for the full information and full control problems will be given.

Consider the Hamilton-Jacobi (HJ) inequality associated with the full information nonlinear $\mathcal{H}_\infty$ problem with $\gamma = 1$ [25]:

$$H_{FI} := V_x(x)a(x) + c_1^T(x)c_1(x) + \frac{1}{4}V_x(x)\{B_1(x)B_1^T(x) - B_2(x)B_2^T(x)\}V_x^T(x) \leq 0. \tag{8.12}$$

This control problem is solvable if there exists a C^3 positive-definite function $V(x)$, $V(0) = 0$ such that (8.12) holds. So, this sufficient condition could be useful for input selection in the full information case.

In analogy, consider the HJ inequality associated with the full control nonlinear $\mathcal{H}_\infty$ problem with $\gamma = 1$ [25]:

$$H_{FC} := U_x(x)a(x) + c_1^T(x)c_1(x) - c_2^T(x)c_2(x) + \frac{1}{4}U_x(x)B_1(x)B_1^T(x)U_x^T(x) \leq 0. \tag{8.13}$$

This control problem is solvable if there exists a C^3 positive-definite function $U(x)$, $U(0) = 0$ such that (8.13) holds *and* if there exists a C^2 function $L(x)$ such that $U_x(x)L(x) = -2c_2^T(x)$ holds. This sufficient condition could be useful for output selection in the full control case.

With some modifications and an additional requirement, (8.12) and (8.13) are combined to give a sufficient condition for the solvability of the original problem:

The output feedback nonlinear $\mathcal{H}_\infty$ control problem with $\gamma = 1$ is locally solvable if there is some positive-definite function $\psi(x)$, $\psi(0) = 0$ such that the following conditions hold:

1. *there exists a positive-definite $V(x)$, $V(0) = 0$ solving the HJ equality $H_{FI} + \psi(x) = 0$,*
2. *there exists a positive-definite $U(x)$, $U(0) = 0$ satisfying the HJ inequality $H_{FC} + \psi(x) \leq 0$ with $H_{FC} + \psi(x)$ having a nonsingular Hessian for $x = 0$,*
3. *$\{U(x) - V(x)\} \geq 0$ and $\{U_x(x) - V_x(x)\}L(x) = -2c_2^T(x)$ has a solution $L(x)$.*

In [2] and [50], closely related necessary conditions in the form of HJ inequalities are given. Essentially, the local solvability of the $\mathcal{H}_\infty$ problem requires positive-definite solutions to

a HJ equality associated with a "state-feedback-gain design" (condition 1) and a HJ inequality associated with an "observer-gain-design" (condition 2), together with the coupling condition 3. As in the linear case, the controllers have a separation structure. In fact, the HJ equality and inequality replace the Riccati equalities in the linear case [7]. In [25,26], it is shown that the solutions $V(x)$ and $L(x)$ parametrize the controllers which locally solve the $\mathcal{H}_\infty$ problem, but an expression for the validity region $\boldsymbol{B}_r$ is lacking. Unfortunately, in [25,26] no attention is paid to the (un)solvability of conditions 1–3 and to possible solution methods.

In [57], the same nonlinear $\mathcal{H}_\infty$ problem is treated, except that the plant is assumed to be smooth and that γ is not necessarily equal to one. The following sufficient condition for controller existence is proposed:

The output feedback nonlinear $\mathcal{H}_\infty$ control problem is locally solvable if:

1. *there exists a smooth positive-definite function $V(x)$, $V(0) = 0$ satisfying the nonstrict HJ inequality*

$$H_{FI} := V_x(x)a(x) + c_1^T(x)c_1(x) + \frac{1}{4}V_x(x)\{\frac{1}{\gamma^2}B_1(x)B_1^T(x) - B_2(x)B_2^T(x)\}V_x^T(x) \leq 0, \tag{8.14}$$

2. *there exists a smooth positive-definite function $Q(x)$, $Q(0) = 0$ satisfying the HJ strict inequality*

$$\begin{aligned} H_{OF} \;:=\; & Q_x(x)\{a(x) + \frac{1}{2\gamma^2}B_1(x)B_1^T(x)V_x^T(x)\} + \frac{1}{4}V_x(x)B_2(x)B_2^T(x)V_x^T(x) \\ & -\gamma^2 c_2^T(x)c_2(x) + \frac{1}{4\gamma^2}Q_x B_1(x)B_1^T(x)Q_x^T(x) < 0, \end{aligned} \tag{8.15}$$

and which is such that the Hessian of H_{OF} is nonsingular at $x = 0$.

Notice the resemblance between the HJ inequalities (8.12) and (8.14). Also note, that the solution to (8.14) is substituted in (8.15). So, the HJ inequalities are coupled, while (8.12) and (8.13) were only coupled via their solutions. Closely related conditions are derived in [15,16], where [18] replaces assumptions one and two by the less restrictive alternatives of $D_{12}^T(x)D_{12}(x)$ and $D_{21}^T(x)D_{21}(x)$ being nonsingular for each x.

In [15] and [17] (the first with less restrictive assumptions), different sufficient conditions for existence of an $\mathcal{H}_\infty$ controller are given; in a slightly different formulation, the same results can be found in [58]. Since the formulas are much more complicated than the ones discussed earlier in this section, they are omitted here. Checking controller existence again involves checking the solvability of two HJ (in)equalities. One major problem with the approach is, that the second HJ (in)equality has twice as many independent variables as the first one, which is not the case for the previously discussed approaches. Essentially, this problem is due to the presence of both the states of G and the same number of states in the controller K to be designed (K is structured as a copy of the plant dynamics, together with a correction term for the measurement estimation error). It is shown in [17], that under certain assumptions on the linearization of the system the sufficient conditions are *necessary* as well.

Especially for IO selection, it is important that the solvability of the controller existence conditions ("viability conditions" for IO selection) can be checked efficiently and effectively. In this context, the following observation from [17] is important: if there exists a controller solving the $\mathcal{H}_\infty$ problem for the *linearized version* of G (which can be checked via the viability conditions mentioned in Section 3.1) and if the resulting linear controller is either controllable or observable, then the nonlinear $\mathcal{H}_\infty$ control problem is locally solvable in a region $\boldsymbol{B}_r$ around the origin $(x, x_k) = (0, 0)$. See also [50], which shows that local solvability of the nonlinear *state-feedback* $\mathcal{H}_\infty$ control problem is implied by solvability of the linearized problem. In fact, checking the solvability of HJ equalities is replaced by checking the solvability of Riccati equations associated with the linearized plant. In analogy, it is conjectured that checking the local solvability of HJ inequalities can be done by checking the solvability of Riccati inequalities, which can be reformulated as LMI feasibility problems [4]. It is however unclear if the size of the validity region $\boldsymbol{B}_r$ is easily determined, or can be determined at all. Ideally, the IO selection would incorporate a specification for the size of $\boldsymbol{B}_r$.

Unfortunately, checking the solvability of the linearization only provides a *sufficient* condition for IO set viability: if the $\mathcal{H}_\infty$ problem for the linearized system is unsolvable, the original nonlinear $\mathcal{H}_\infty$ problem may still be solvable (as for the example in [18]). It is unclear if this conservatism can easily be reduced. A brute-force approach would be to solve the HJ (in)equalities. However, it is in general impossible to solve them exactly. Moreover, the polynomial approximation technique as discussed in [49], [31, Chapter 9] *assumes* the linearized problem to have a solution, but it is currently unclear if this is also a strict *requirement* for its application.

8.5 General Nonlinear Systems

This final section briefly discusses some results for rather general nonlinear systems. In [18] and [31, Sections 7.5, 7.6], the local $\mathcal{H}_\infty$ control problem is studied for the following nonlinear plant, defined in a neighborhood $\boldsymbol{B}_r$ of the origin:

$$G: \begin{cases} \dot{x} = f(x, w, u) \\ z = g(x, u) \\ y = h(x, w), \end{cases} \tag{8.16}$$

with $f(0,0,0) = 0$, $g(0,0) = 0$, and $h(0,0) = 0$. Notice that, as in (8.2), the exogenous input w and manipulated input u do not occur in the smooth mappings g and h respectively (f is also assumed smooth). Furthermore, it is assumed that the matrix $\partial g/\partial u|_{(0,0)}$ has full column rank, that $\partial h/\partial w|_{(0,0)}$ has full row rank, and that the system G possesses a detectability-like property. The controller is restricted to take the form:

$$K: \begin{cases} \dot{x}_k = f(x_k, w^*, u) + L(x_k)\{y - h(x_k, w^*)\} \\ u = c_k(x_k), \end{cases} \tag{8.17}$$

with w^* the worst-case exogenous input. Note, that the correction term is affine in the measurement estimation error [15], which is a possible limiting factor for this controller.

The approach for the general nonlinear system (8.16) in [18] is analogous to that for the input affine system (8.10) in [15]. Though the resulting sufficient conditions for controller existence have a similar interpretation, they appear in less transparent, *implicit* forms. As expected, the solution of the $\mathcal{H}_\infty$ control problem is related to the existence of solutions to a (coupled) pair of HJ inequalities, both of which depend on n_x independent variables. The inequalities are associated with a state-feedback-gain and an observer-gain design, together with some additional requirements. Unfortunately, it is currently unclear if the solvability of the HJ inequalities is easily checked and so if they offer prospects for IO selection. Maybe a similar approach as for the input affine systems can be used, *i.e.*, checking solvability for the linearized system.

Bibliography

[1] Gary J. Balas, John C. Doyle, Keith Glover, Andy Packard, and Roy Smith. *μ-Analysis and synthesis toolbox.* The MathWorks, Natick, MA, USA, 1991.

[2] Joseph A. Ball, J. William Helton, and Michael L. Walker. $\mathcal{H}_\infty$ control for nonlinear systems with output feedback. *IEEE Transactions on Automatic Control*, 38(4):546–559, April 1993.

[3] Okko H. Bosgra and Huibert Kwakernaak. Design methods for control systems. Lecture notes Dutch Graduate Network on Systems and Control, Spring term 1993-1994.

[4] Stephen Boyd, Venkataramanan Balakrishnan, Eric Feron, and Laurent El Ghaoui. Control system analysis and synthesis via linear matrix inequalities. In *Proc. of the 1993 American Control Conference*, volume 2, pages 2147–2154, San Francisco, CA, June 1993.

[5] Bram de Jager. Multiobjective suspension control problem. In *Proc. of the 34th IEEE Conference on Decision and Control*, volume 4, pages 3652–3657, New Orleans, Louisiana, December 1995.

[6] John C. Doyle. Analysis of feedback systems with structured uncertainty. In *IEE Proceedings, Part D*, volume 129, pages 242–250, November 1982.

[7] John C. Doyle, Keith Glover, Pramod P. Khargonekar, and Bruce A. Francis. State-space solutions to standard $\mathcal{H}_2$ and $\mathcal{H}_\infty$ control problems. *IEEE Transactions on Automatic Control*, 34(8):831–846, August 1989.

[8] John C. Doyle, Andrew K. Packard, Peter M. Young, Roy S. Smith, and Matthew P. Newlin. The structured singular value. NASA final report Technical Memorandum no. CIT-CDS 93-013, Control and Dynamical Systems, California Institute of Technology, Pasadena, CA, June 1993.

[9] Laurent El Ghaoui, Francois Delebecque, and Ramine Nikoukhah. *LMITOOL: A user-friendly interface for LMI optimization*, February 1995. Beta version.

[10] Bruce A. Francis. *A course in $\mathcal{H}_\infty$ control theory*, volume 88 of *Lecture Notes in Control and Information Sciences*. Springer-Verlag, New-York, 1987.

[11] James S. Freudenberg and Douglas P. Looze. Right half plane poles and zeros and design tradeoffs in feedback systems. *IEEE Transactions on Automatic Control*, AC-30(6):555–565, June 1985.

[12] Keith Glover and John C. Doyle. State-space formulae for all stabilizing controllers that satisfy an $\mathcal{H}_\infty$-norm bound and relations to risk sensitivity. *Systems & Control Letters*, 11:167–172, 1988.

[13] J. K. Hedrick and T. Butsuen. Invariant properties of automotive suspensions. In *Proc. IMechE, Int. Conf. on Advanced Suspensions*, pages 35–42, London, 1988. MEP.

[14] Rudolf Huisman. *A controller and observer for active suspensions with preview.* PhD thesis, Eindhoven University of Technology, 1994.

[15] Alberto Isidori. $\mathcal{H}_\infty$ control via measurement feedback for affine nonlinear systems. *Int. J. of Robust and Nonlinear Control*, 4(4):553–574, July-August 1994.

[16] Alberto Isidori. A necessary condition for nonlinear $\mathcal{H}_\infty$ control via measurement feedback. *Systems & Control Letters*, 23(3):169–177, September 1994.

[17] Alberto Isidori and Alessandro Astolfi. Disturbance attenuation and $\mathcal{H}_\infty$-control via measurement feedback in nonlinear systems. *IEEE Transactions on Automatic Control*, AC-37(9):1283–1293, September 1992.

[18] Alberto Isidori and Wei Kang. $\mathcal{H}_\infty$ control via measurement feedback for general nonlinear systems. *IEEE Transactions on Automatic Control*, AC-40(3):466–472, March 1995.

[19] T. Iwasaki and Robert E. Skelton. A complete solution to the general $\mathcal{H}_\infty$ control problem: LMI existence conditions and state space formulas. In *Proc. of the 1993 American Control Conference*, volume 1, pages 605–609, San Francisco, CA, June 1993.

[20] T. Iwasaki and Robert E. Skelton. All controllers for the general $\mathcal{H}_\infty$ control problem: LMI existence conditions and state space formula. *Automatica*, 30(8):1307–1317, August 1994.

[21] Michael C. Lai and John Hauser. Nonlinear $\mathcal{H}_\infty$ control via measurement feedback with guaranteed performance. In *Proc. of the 32nd Conf. on Decision and Control*, volume 2, pages 1644–1649, San Antonio, Texas, December 1993.

[22] Jay H. Lee, Richard Dean Braatz, Manfred Morari, and Andrew Packard. Screening tools for robust control structure selection. *Automatica*, 31(2):229–235, February 1995.

[23] J. A. Levitt and N. G. Zorka. The influence of tire damping in quarter car active suspension models. *J. of Dynamic Systems, Measurement, and Control*, 113:134–137, March 1991.

[24] Wei-Min Lu and John C. Doyle. $\mathcal{H}_\infty$ control of nonlinear systems: A convex characterization. Technical Report CDS 93-020, California Institute of Technology, Pasadena, CA, 1993.

[25] Wei-Min Lu and John C. Doyle. $\mathcal{H}_\infty$ control of nonlinear systems via output feedback: A class of controllers. In *Proc. of the 32nd Conference on Decision and Control*, volume 1, pages 166–171, San Antonio, Texas, December 1993.

[26] Wei-Min Lu and John C. Doyle. $\mathcal{H}_\infty$ control of nonlinear systems via output feedback: Controller parameterization. *IEEE Transactions on Automatic Control*, 39(12):2517–2521, December 1994.

[27] Wei-Min Lu and John C. Doyle. Robustness analysis and synthesis for uncertain nonlinear systems. In *Proc. of the 33rd Conf. on Decision and Control*, volume 1, pages 787–792, Lake Buena Vista, Florida, December 1994.

[28] Wei-Min Lu and John C. Doyle. A state space approach to robustness analysis and synthesis for nonlinear uncertain systems. Technical Report CDS 94-010, California Institute of Technology, Pasadena, CA, 1994.

[29] Wei-Min Lu and John C. Doyle. $\mathcal{H}_\infty$ control of nonlinear systems: A convex characterization. *IEEE Transactions on Automatic Control*, 40(9):1668–1675, September 1995.

[30] Jan M. Maciejowski. *Multivariable feedback design.* Addison-Wesley, Amsterdam, 1989.

[31] Jens Møller-Pedersen and Martin Pagh Petersen. Control of nonlinear plants - volume 1. Master's thesis, Mathematical Institute, University of Denmark, July 1995.

[32] Henk Nijmeijer and Arjan J. Van der Schaft. *Nonlinear dynamical control systems.* Springer-Verlag, New York, second edition, 1990.

[33] Andy Packard and John C. Doyle. The complex structured singular value. *Automatica*, 29(1):71–109, 1993.

[34] Andy Packard, Kemin Zhou, Pradeep Pandey, Jorn Leonhardson, and Gary Balas. Optimal, constant I/O similarity scaling for full-information and state-feedback control problems. *Systems & Control Letters*, 19:271–280, 1992.

[35] Patrick Philips. Selection of actuators and sensors based on robust performance. Master's thesis WFW 96.050, Fac. of Mechanical Engineering, Eindhoven University of Technology, May 1996.

[36] Kameshwar Poolla and Ashok Tikku. Robust performance against time-varying structured perturbations. *IEEE Transactions on Automatic Control*, 40(9):1589–1602, September 1995.

[37] Deborah E. Reeves. *A comprehensive approach to control configuration design for complex systems.* PhD thesis, Georgia Institute of Technology, 1991.

[38] Maarten Steinbuch, G. Schootstra, and S. G. Smit. μ-Synthesis of a flexible mechanical servo system. Technical Report Nat. Lab. technical note 144/90, Philips Research Laboratories Eindhoven, Eindhoven, 1990.

[39] Gilbert Strang. *Linear algebra and its applications.* Harcourt Brace Jovanovich, San Diego, third edition, 1988.

[40] Steen Tøffner-Clausen, Palle Andersen, Jakob Stoustrup, and Hans H. Niemann. A new approach to μ-synthesis for mixed perturbation sets. In *Proc. of the 3rd European Control Conference*, volume 1, pages 147–152, Rome, Italy, September 1995.

[41] H. D. Tuan and S. Hosoe. On linearization technique in robust nonlinear $\mathcal{H}_\infty$ control. *Systems & Control Letters*, 27(1):21–27, January 1996.

[42] Marc van de Wal. Control structure design for dynamic systems: A review. Technical Report WFW 94.084, Fac. of Mechanical Engineering, Eindhoven University of Technology, September 1994.

[43] Marc van de Wal. Control structure design for the 6 DOF tractor-semitrailer example: Application of the Matlab Control Configuration Design toolbox. Technical report WFW 95.124, Fac. of Mechanical Engineering, Eindhoven University of Technology, March 1995.

[44] Marc van de Wal. The pros and cons of some μ-based tools for control structure design. Technical Report WFW 95.125, Fac. of Mechanical Engineering, Eindhoven University of Technology, April 1995.

[45] Marc van de Wal. Input output selection based on nominal performance and robust stability against unstructured uncertainties: An active suspension application. Technical Report WFW 96.005, Fac. of Mechanical Engineering, Eindhoven University of Technology, January 1996.

[46] Marc van de Wal and Bram de Jager. Control structure design: A survey. In *Proc. of the 1995 American Control Conference*, volume 1, pages 225–229, Seattle, WA, June 1995.

[47] Marc van de Wal and Bram de Jager. A survey of methods for control structure design. unpublished, September 1995.

[48] Marc van de Wal and Bram de Jager. Selection of sensors and actuators for an active suspension control problem. In *Proc. of the 1996 IEEE International Conference on Control Applications*, Dearborn, Michigan, September 1996. submitted January 1996.

[49] Arjan J. van der Schaft. $\mathcal{L}_2$ gain analysis of nonlinear systems and nonlinear state feedback $\mathcal{H}_\infty$ control. *IEEE Transactions on Automatic Control*, 37(6):770–784, June 1992.

[50] Arjan J. van der Schaft. Nonlinear state space $\mathcal{H}_\infty$ control theory. In H. L. Trentelman and J. C. Willems, editors, *Essays on control: Perspectives in the theory and its applications*, pages 153–190. Birkhäuser, Boston, MA, 1993.

[51] Pieter J. M. van Groos. Robust control of a compact disc player. Master's thesis Nat. Lab. technical note 143/93, Philips Research Laboratories Eindhoven in co-operation with Dept. of Mechanical Engineering and Marine Technology, Delft University of Technology, 1993.

[52] Lieven Vandenberghe and Stephen Boyd. Semidefinite programming. submitted to SIAM Review, July 1994, with originial title *Positive definite programming*, November 1994.

[53] Lieven Vandenberghe and Stephen Boyd. *SP: Software for semidefinite programming*, November 1994. Beta version.

[54] Peter M. Young. Controller design with mixed uncertainties. In *Proc. of the 1994 American Control Conference*, pages 2333–2337, Baltimore, Maryland, June 1994.

[55] Peter M. Young, Matthew P. Newlin, and John C. Doyle. μ-Analysis with real parametric uncertainty. In *Proc. of the 30th Conference on Decision and Control*, volume 2, pages 1251–1256, Brighton, England, December 1991.

[56] Peter M. Young, Matthew P. Newlin, and John C. Doyle. Computing bounds for the mixed μ problem. *Int. J. of Robust and Nonlinear Control*, 5(6):573–590, October 1995.

[57] Chee-Fai Yung, Yung-Pin Lin, and Fang-Bo Yeh. A family of nonlinear $\mathcal{H}_\infty$-output feedback controllers. *IEEE Transactions on Automatic Control*, 41(2):232–236, February 1996.

[58] Chee-Fai Yung and Fang-Bo Yeh. Nonlinear $\mathcal{H}_\infty$ output feedback control problems. In *Proc. of the 32nd Conf. on Decision and Control*, volume 3, pages 2197–2198, San Antonio, Texas, December 1993.

[59] Kemin Zhou, John C. Doyle, and Keith Glover. *Robust and optimal control.* Prentice Hall, Upper Saddle River, NJ, 1996.

Appendix A

LMIs for IO Selection

This appendix provides the formulas for the LMIs replacing the IO selection conditions (3.10) and (3.11). As noted in Section 3.2, these convex conditions contain the complex matrices G_{11}, $\hat{G}_{12_\perp}$, and $\hat{G}_{21_\perp}$. For the MATLAB toolbox LMITOOL [9] to be applicable, (3.10) and (3.11) must be transformed into two LMIs which only involve real matrices.

First, the following equivalence is shown (3.16):

$$\Sigma_1 + j\Sigma_2 < 0 \Leftrightarrow \begin{bmatrix} \Sigma_1 & -\Sigma_2 \\ \Sigma_2 & \Sigma_1 \end{bmatrix} < 0,$$

with Σ_1 real and symmetric ($\Sigma_1 = \Sigma_1^T$) and Σ_2 real and skew-symmetric ($\Sigma_2 = -\Sigma_2^T$). Because $(\Sigma_1 + j\Sigma_2)^* = (\Sigma_1 + j\Sigma_2)$, the number $(x+jy)^*(\Sigma_1 + j\Sigma_2)(x+jy)$ is real for all complex vectors $x + jy$ with x and y real [39, Section 5.5]. Straightforward computation yields:

$$(x+jy)^*(\Sigma_1 + j\Sigma_2)(x+jy) < 0 \;\Leftrightarrow \tag{A.1}$$

$$x^T\Sigma_1 x + 2y^T\Sigma_2 x + y^T\Sigma_1 y + j(x^T\Sigma_2 x + y^T\Sigma_2 y) < 0. \tag{A.2}$$

Due to skew-symmetry of Σ_2, the imaginary part in (A.2) equals zero: the real number $u^T\Sigma_2 u$ equals $(u^T\Sigma_2 u)^T = -u^T\Sigma_2 u$, so it must be zero. Consequently, (A.2) can be rewritten as:

$$\begin{bmatrix} x^T & y^T \end{bmatrix} \begin{bmatrix} \Sigma_1 & -\Sigma_2 \\ \Sigma_2 & \Sigma_1 \end{bmatrix} \begin{bmatrix} x \\ y \end{bmatrix} < 0, \tag{A.3}$$

which shows the equivalence in (3.16).

Given this equivalence, the output selection condition (3.10)

$$\hat{G}_{21_\perp}\{G_{11}^* X_1 G_{11} - \gamma^2 X_2\}\hat{G}_{21_\perp}^* < 0 \;\forall\, \omega$$

is replaced by the LMI

$$\begin{bmatrix} \Sigma_1 & -\Sigma_2 \\ \Sigma_2 & \Sigma_1 \end{bmatrix} < 0, \tag{A.4}$$

with

$$\begin{aligned}\Sigma_1 &= (S_1+S_2)X_1(S_1+S_2)^T+(S_3-S_4)X_1(S_3-S_4)^T \\ &\quad -\gamma^2T_1X_2T_1^T-\gamma^2T_2X_2T_2^T, \qquad (A.5)\\ \Sigma_2 &= (S_1+S_2)X_1(S_3-S_4)^T+(-S_3+S_4)X_1(S_1+S_2)^T \\ &\quad +\gamma^2T_1X_2T_2^T-\gamma^2T_2X_2T_1^T, \qquad (A.6)\end{aligned}$$

and

$$\begin{aligned}S_1 &= \Re(\hat{G}_{21_\perp})\Re(G_{11}^T), \qquad (A.7)\\ S_2 &= \Im(\hat{G}_{21_\perp})\Im(G_{11}^T), \qquad (A.8)\\ S_3 &= \Re(\hat{G}_{21_\perp})\Im(G_{11}^T), \qquad (A.9)\\ S_4 &= \Im(\hat{G}_{21_\perp})\Re(G_{11}^T), \qquad (A.10)\\ T_1 &= \Re(\hat{G}_{21_\perp}), \qquad (A.11)\\ T_2 &= \Im(\hat{G}_{21_\perp}). \qquad (A.12)\end{aligned}$$

In analogy, the input selection condition (3.11)

$$\hat{G}_{12_\perp}^*\{G_{11}X_2^{-1}G_{11}^*-\gamma^2X_1^{-1}\}\hat{G}_{12_\perp}<0\ \forall\ \omega$$

is replaced by the LMI

$$\begin{bmatrix}\Sigma_3 & -\Sigma_4\\ \Sigma_4 & \Sigma_3\end{bmatrix}<0, \qquad (A.13)$$

with

$$\begin{aligned}\Sigma_3 &= (U_1+U_2)X_2^{-1}(U_1+U_2)^T+(U_3-U_4)X_2^{-1}(U_3-U_4)^T \\ &\quad -\gamma^2V_1X_1^{-1}V_1^T-\gamma^2V_2X_1^{-1}V_2^T, \qquad (A.14)\\ \Sigma_4 &= (U_1+U_2)X_2^{-1}(-U_3+U_4)^T+(U_3-U_4)X_2^{-1}(U_1+U_2)^T \\ &\quad -\gamma^2V_1X_1^{-1}V_2^T+\gamma^2V_2X_1^{-1}V_1^T, \qquad (A.15)\end{aligned}$$

and

$$\begin{aligned}U_1 &= \Re(\hat{G}_{12_\perp}^T)\Re(G_{11}), \qquad (A.16)\\ U_2 &= \Im(\hat{G}_{12_\perp}^T)\Im(G_{11}), \qquad (A.17)\\ U_3 &= \Re(\hat{G}_{12_\perp}^T)\Im(G_{11}), \qquad (A.18)\\ U_4 &= \Im(\hat{G}_{12_\perp}^T)\Re(G_{11}), \qquad (A.19)\\ V_1 &= \Re(\hat{G}_{12_\perp}^T), \qquad (A.20)\\ V_2 &= \Im(\hat{G}_{12_\perp}^T). \qquad (A.21)\end{aligned}$$

Appendix B

4 DOF Tractor-Semitrailer Model

In this appendix, the state-space description of the 4 DOF tractor-semitrailer model is given. Table B.1 lists the variables playing a role (see also Fig. 2.3), while Table B.2 lists the various physical parameters (see also Fig. B.1).

The equations of motion of the *nominal* tractor-semitrailer combination can be written as

$$M\ddot{s} + B\dot{s} + Ks = E_1\bar{v}^* + E_2\bar{w}^* + E_3u, \tag{B.1}$$

with $\bar{v}^*$ the road surface height and $\bar{w}^*$ the *derivative* of the road surface height (exogenous input): $\bar{w}^* = \dot{\bar{v}}^*$. The mass matrix M, the damping matrix B, and the stiffness matrix K are as follows:

$$M = \begin{bmatrix} m_{af} & 0 & 0 & 0 \\ 0 & m_{ar} & 0 & 0 \\ 0 & 0 & M_{ch} + M_t & cM_t \\ 0 & 0 & cM_t & J_{ch} + c^2M_t \end{bmatrix}, \tag{B.2}$$

$$B = \begin{bmatrix} b_{tf} + b_{sf} & 0 & -b_{sf} & ab_{sf} \\ 0 & b_{tr} + b_{sr} & -b_{sr} & -bb_{sr} \\ -b_{sf} & -b_{sr} & b_{sf} + b_{sr} & -ab_{sf} + bb_{sr} \\ ab_{sf} & -bb_{sr} & -ab_{sf} + bb_{sr} & a^2b_{sf} + b^2b_{sr} \end{bmatrix}, \tag{B.3}$$

$$K = \begin{bmatrix} k_{tf} + k_{sf} & 0 & -k_{sf} & ak_{sf} \\ 0 & k_{tr} + k_{sr} & -k_{sr} & -bk_{sr} \\ -k_{sf} & -k_{sr} & k_{sf} + k_{sr} & -ak_{sf} + bk_{sr} \\ ak_{sf} & -bk_{sr} & -ak_{sf} + bk_{sr} & a^2k_{sf} + b^2k_{sr} \end{bmatrix}. \tag{B.4}$$

These matrices are symmetric and positive definite. The distribution matrices E_1, E_2, and E_3 in (B.1) are as follows:

$$E_1 = \begin{bmatrix} k_{tf} & 0 \\ 0 & k_{tr} \\ 0 & 0 \\ 0 & 0 \end{bmatrix}, \; E_2 = \begin{bmatrix} b_{tf} & 0 \\ 0 & b_{tr} \\ 0 & 0 \\ 0 & 0 \end{bmatrix}, \; E_3 = \begin{bmatrix} 1 & 0 \\ 0 & 1 \\ -1 & -1 \\ a & -b \end{bmatrix}. \tag{B.5}$$

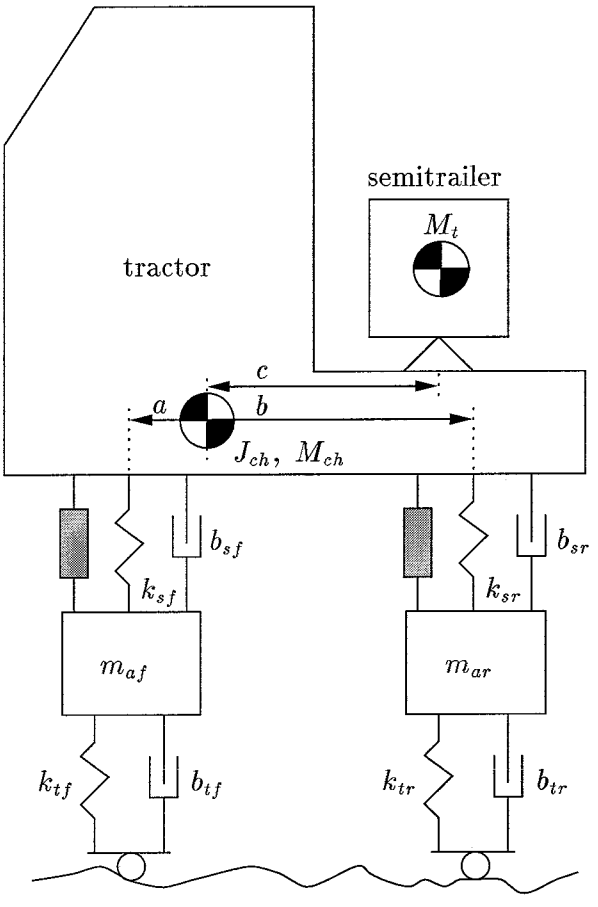

Figure B.1: 4 DOF tractor-semitrailer combination

Table B.1: List of variables

Symbol	Description
	Degrees-of-freedom s
$s_1,\ s_2$	displacements front and rear axle
s_3	displacement chassis center of mass
s_4	rotation around chassis center of mass
	Road surface heights $\bar{v}^*$
$\bar{v}_1^*,\ \bar{v}_2^*$	front and rear road heights
	Outputs $\bar{p}$ **from** Δ_u **and inputs** $\bar{q}$ **to** Δ_u
$\bar{p}_1/\bar{q}_1,\ \bar{p}_2/\bar{q}_2$	due to uncertain front and rear tire stiffnesses
$\bar{p}_3/\bar{q}_3,\ \bar{p}_4/\bar{q}_4$	due to uncertain front and rear tire dampings
$\bar{p}_5/\bar{q}_5,\ \bar{p}_6/\bar{q}_6$	due to uncertain front and rear suspension stiffnesses
$\bar{p}_7/\bar{q}_7,\ \bar{p}_8/\bar{q}_8$	due to uncertain front and rear suspension dampings
$\bar{p}_9/\bar{q}_9, \bar{p}_{10}/\bar{q}_{10}$	due to uncertain front and rear axle masses
$\bar{p}_{11}/\bar{q}_{11}$	due to uncertain chassis mass
$\bar{p}_{12}/\bar{q}_{12}$	due to uncertain chassis inertia
$\bar{p}_{13}/\bar{q}_{13}$	due to uncertain semitrailer effective mass
	Exogenous inputs $\bar{w}^*$
$\bar{w}_1^*,\ \bar{w}_2^*$	road height derivatives at front and rear
$\bar{w}_3^*, \ldots, \bar{w}_6^*$	measurement noises for $y_1, \ldots, y_4$
	Controlled variables $\bar{z}^*$
$\bar{z}_1^*$	vertical chassis acceleration at front
$\bar{z}_2^*$	rotational chassis acceleration
$\bar{z}_3^*,\ \bar{z}_4^*$	front and rear suspension deflections
$\bar{z}_5^*,\ \bar{z}_6^*$	front and rear tire deflections
$\bar{z}_7^*,\ \bar{z}_8^*$	controller outputs u_1 and u_2
	Inputs u
$u_1,\ u_2$	forces generated by front and rear actuators
	Outputs y
$y_1,\ y_2$	front and rear suspension deflections
$y_3,\ y_4$	front and rear chassis accelerations

Table B.2: List of model parameters

Parameter	Value	Unit	Description
	Spring coefficients		
k_{tf}	$2.5 \cdot 10^6$	N/m	front tire stiffness
k_{tr}	$5.0 \cdot 10^6$	N/m	rear tire stiffness
k_{sf}	$5.0 \cdot 10^5$	N/m	front suspension stiffness
k_{sr}	$5.0 \cdot 10^5$	N/m	rear suspension stiffness
	Damper coefficients		
b_{tf}	$1.0 \cdot 10^3$	Ns/m	front tire damping
b_{tr}	$1.7 \cdot 10^3$	Ns/m	rear tire damping
b_{sf}	$5.0 \cdot 10^4$	Ns/m	front suspension damping
b_{sr}	$5.0 \cdot 10^4$	Ns/m	rear suspension damping
	Masses and inertias		
m_{af}	$1.0 \cdot 10^3$	kg	front axle mass
m_{ar}	$1.5 \cdot 10^3$	kg	rear axle mass
J_{ch}	$1.1 \cdot 10^4$	$\mathrm{kg\,m^2}$	chassis inertia
M_{ch}	$7.0 \cdot 10^3$	kg	chassis mass
M_t	$6.5 \cdot 10^3$	kg	effective semitrailer mass
	Geometric parameters		
a	0.46	m	front chassis to COM chassis
b	3.04	m	rear chassis to COM chassis
c	2.44	m	kingpin to COM chassis

By stacking up the degrees-of-freedom s, their derivatives $\dot{s}$, and $\bar{v}^*$ in the state vector $\bar{x}$ and extracting additive parametric uncertainties ("$a' = a + \delta_a$"), the state-space description is derived. In order to illustrate the influence of the uncertainties, the inputs $\bar{q}$, $\bar{z}^*$ to and the outputs $\bar{p}$, $\bar{w}^*$ from the uncertainty block are considered separately:

$$\begin{aligned}
\dot{\bar{x}} &= \bar{A}\bar{x} + \begin{bmatrix} \bar{B}_{1_{\bar{p}}} & \bar{B}_{1_{\bar{w}^*}} \end{bmatrix} \begin{bmatrix} \bar{p} \\ \bar{w}^* \end{bmatrix} + \bar{B}_2 u \\
\begin{bmatrix} \bar{q} \\ \bar{z}^* \end{bmatrix} &= \begin{bmatrix} \bar{C}_{1_{\bar{q}}} \\ \bar{C}_{1_{\bar{z}^*}} \end{bmatrix} \bar{x} + \begin{bmatrix} \bar{D}_{11_{\bar{q}\bar{p}}} & \bar{D}_{11_{\bar{q}\bar{w}^*}} \\ \bar{D}_{11_{\bar{z}^*\bar{p}}} & \bar{D}_{11_{\bar{z}^*\bar{w}^*}} \end{bmatrix} \begin{bmatrix} \bar{p} \\ \bar{w}^* \end{bmatrix} + \begin{bmatrix} \bar{D}_{12_{\bar{q}}} \\ \bar{D}_{12_{\bar{z}^*}} \end{bmatrix} u \qquad \text{(B.6)} \\
y &= \bar{C}_2\bar{x} + \begin{bmatrix} \bar{D}_{21_{\bar{p}}} & \bar{D}_{21_{\bar{w}^*}} \end{bmatrix} \begin{bmatrix} \bar{p} \\ \bar{w}^* \end{bmatrix} + D_{22}u,
\end{aligned}$$

with:

$$\bar{A} = \begin{bmatrix} 0_{4\times4} & I_{4\times4} & 0_{4\times2} \\ -M^{-1}K & -M^{-1}B & M^{-1}E_1 \\ 0_{2\times4} & 0_{2\times4} & 0_{2\times2} \end{bmatrix},$$

$$\bar{B}_{1_{\bar{p}}}^T = \begin{bmatrix} & -1/m_{af} & 0 & 0 & 0 & \\ & 0 & -1/m_{ar} & 0 & 0 & \\ & -1/m_{af} & 0 & (J_{ch}+(ac+c^2)M_t)\psi & -((a+c)M_t+aM_{ch})\psi & \\ & 0 & -1/m_{ar} & (J_{ch}+(-bc+c^2)M_t)\psi & ((b-c)M_t+bM_{ch})\psi & \\ & -1/m_{af} & 0 & 0 & 0 & \\ & 0 & -1/m_{ar} & 0 & 0 & \\ 0_{13\times4} & -1/m_{af} & 0 & (J_{ch}+(ac+c^2)M_t)\psi & -((a+c)M_t+aM_{ch})\psi & 0_{13\times2} \\ & 0 & -1/m_{ar} & (J_{ch}+(-bc+c^2)M_t)\psi & ((b-c)M_t+bM_{ch})\psi & \\ & -1/m_{af} & 0 & 0 & 0 & \\ & 0 & -1/m_{ar} & 0 & 0 & \\ & 0 & 0 & -(J_{ch}+c^2M_t)\psi & cM_t\psi & \\ & 0 & 0 & cM_t\psi & -(M_{ch}+M_t)\psi & \\ & 0 & 0 & -J_{ch}\psi & -cM_{ch}\psi & \end{bmatrix},$$

$$\bar{B}_{1_{\bar{w}^*}} = \begin{bmatrix} 0_{4\times2} & \\ M^{-1}E_2 & 0_{10\times4} \\ I_{2\times2} & \end{bmatrix}, \quad \bar{B}_2 = \begin{bmatrix} 0_{4\times2} \\ M^{-1}E_3 \\ 0_{2\times2} \end{bmatrix},$$

$$\bar{C}_{1_{\bar{q}}} = \begin{bmatrix} 1 & 0 & 0 & 0 & & & -1 & 0 \\ 0 & 1 & 0 & 0 & & & 0 & -1 \\ 1 & 0 & -1 & a & 0_{4\times4} & & 0 & 0 \\ 0 & 1 & -1 & -b & & & 0 & 0 \\ & & & & 1 & 0 & 0 & 0 & & \\ & & & & 0 & 1 & 0 & 0 & & \\ & & 0_{4\times4} & & 1 & 0 & -1 & a & 0_{4\times2} & \\ & & & & 0 & 1 & -1 & -b & & \\ & & & & \{\bar{A}\}_{5-8:} & & & & & \\ & & & & \{\bar{A}\}_{7:}+c\{\bar{A}\}_{8:} & & & & & \end{bmatrix},$$

$$\bar{C}_{1_{z^*}} = \begin{bmatrix} & & & & \{\bar{A}\}_{7:}-a\{\bar{A}\}_{8:} & & & & & \\ & & & & \{\bar{A}\}_{8:} & & & & & \\ -1 & 0 & 1 & -a & 0 & 0 & 0 & 0 & 0 & 0 \\ 0 & -1 & 1 & b & 0 & 0 & 0 & 0 & 0 & 0 \\ 1 & 0 & 0 & 0 & 0 & 0 & 0 & 0 & -1 & 0 \\ 0 & 1 & 0 & 0 & 0 & 0 & 0 & 0 & 0 & -1 \\ & & & & 0_{2\times10} & & & & & \end{bmatrix},$$

$$\bar{D}_{11_{\bar{q}\bar{p}}} = \begin{bmatrix} 0_{8\times8} & & & 0_{8\times5} & & \\ & -1/m_{af} & 0 & 0 & 0 & 0 \\ & 0 & -1/m_{ar} & 0 & 0 & 0 \\ 0_{8\times8} & 0 & 0 & -(J_{ch}+c^2M_t)\psi & 0 & 0 \\ & 0 & 0 & 0 & -(M_{ch}+M_t)\psi & 0 \\ & 0 & 0 & 0 & 0 & -(J_{ch}+c^2M_{ch})\psi \end{bmatrix},$$

$$\bar{D}_{11_{\bar{q}\bar{w}^*}} = \begin{bmatrix} 0_{4\times2} & \\ -I_{2\times2} & 0_{8\times4} \\ 0_{2\times2} & \\ \{\bar{B}_{1_{\bar{w}^*}}\}_{5-8:} & \\ \{\bar{B}_{1_{\bar{w}^*}}\}_{7:}+c\{\bar{B}_{1_{\bar{w}^*}}\}_{8:} & \end{bmatrix},$$

$$\bar{D}^T_{11_{\bar{z}^*\bar{p}}} = \left[\begin{array}{ccc} 0 & 0 & \\ 0 & 0 & \\ (J_{ch}+(a^2+2ac+c^2)M_t+a^2M_{ch})\psi & -((a+c)M_t+aM_{ch})\psi & \\ (J_{ch}+(-ab+ac-bc+c^2)M_t-abM_{ch})\psi & ((b-c)M_t+bM_{ch})\psi & \\ 0 & 0 & \\ 0 & 0 & \\ (J_{ch}+(a^2+2ac+c^2)M_t+a^2M_{ch})\psi & -((a+c)M_t+aM_{ch})\psi & 0_{13\times 6} \\ (J_{ch}+(-ab+ac-bc+c^2)M_t-abM_{ch})\psi & ((b-c)M_t-bM_{ch})\psi & \\ 0 & 0 & \\ 0 & 0 & \\ -(J_{ch}+(ac+c^2)M_t)\psi & cM_t\psi & \\ ((a+c)M_t+aM_{ch})\psi & -(M_{ch}+M_t)\psi & \\ (-J_{ch}+acM_{ch})\psi & -cM_{ch}\psi & \end{array}\right],$$

$$\bar{D}_{11_{\bar{z}^*\bar{w}^*}} = \left[\begin{array}{cc} \{\bar{B}_{1_{\bar{w}^*}}\}_{7:}-a\{\bar{B}_{1_{\bar{w}^*}}\}_{8:} & \\ \{\bar{B}_{1_{\bar{w}^*}}\}_{8:} & 0_{8\times 4} \\ 0_{6\times 2} & \end{array}\right],$$

$$\bar{D}_{12_{\bar{q}}} = \left[\begin{array}{c} 0_{8\times 2} \\ \{\bar{B}_2\}_{5-8:} \\ \{\bar{B}_2\}_{7:}+c\{\bar{B}_2\}_{8:} \end{array}\right], \quad \bar{D}_{12_{z^*}} = \left[\begin{array}{c} \{\bar{B}_2\}_{7:}-a\{\bar{B}_2\}_{8:} \\ \{\bar{B}_2\}_{8:} \\ 0_{4\times 2} \\ I_{2\times 2} \end{array}\right],$$

$$\bar{C}_2 = \left[\begin{array}{ccccc} -1 & 0 & 1 & -a & \\ 0 & -1 & 1 & b & 0_{2\times 4} \\ \multicolumn{4}{c}{\{\bar{A}\}_{7:}-a\{\bar{A}\}_{8:}} & \\ \multicolumn{4}{c}{\{\bar{A}\}_{7:}+b\{\bar{A}\}_{8:}} & \end{array}\right],$$

$$\bar{D}^T_{21_{\bar{p}}} = \left[\begin{array}{ccc} & & 0 \\ & & 0 \\ & & (J_{ch}+(-ab+ac-bc+c^2)M_t-abM_{ch})\psi \\ & & (J_{ch}+(b^2-2bc+c^2)M_t+b^2M_{ch})\psi \\ & & 0 \\ & & 0 \\ 0_{13\times 2} & \{\bar{D}^T_{11_{\bar{z}^*\bar{p}}}\}_{:1} & (J_{ch}+(-ab+ac-bc+c^2)M_t-abM_{ch})\psi \\ & & (J_{ch}+(b^2-2bc+c^2)M_t+b^2M_{ch})\psi \\ & & 0 \\ & & 0 \\ & & -(J_{ch}+(c^2-bc)M_t)\psi \\ & & ((-b+c)M_t-bM_{ch})\psi \\ & & -(J_{ch}+bcM_{ch})\psi \end{array}\right],$$

$$\bar{D}_{21_{\bar{w}^*}} = \left[\begin{array}{cc} 0_{2\times 2} & \\ \{\bar{B}_{1_{\bar{w}^*}}\}_{7:}-a\{\bar{B}_{1_{\bar{w}^*}}\}_{8:} & I_{4\times 4} \\ \{\bar{B}_{1_{\bar{w}^*}}\}_{7:}+b\{\bar{B}_{1_{\bar{w}^*}}\}_{8:} & \end{array}\right], \text{ and } D_{22} = \left[\begin{array}{c} 0_{2\times 2} \\ \{\bar{B}_2\}_{7:}-a\{\bar{B}_2\}_{8:} \\ \{\bar{B}_2\}_{7:}+b\{\bar{B}_2\}_{8:} \end{array}\right].$$

In the above, $\psi = 1/(M_{ch}J_{ch}+c^2M_{ch}M_t+M_tJ_{ch})$, $\{X\}_{i:}$ denotes the i-th row of X, $\{X\}_{k-l:}$ the k-th till l-th row of X, and $\{X\}_{:j}$ the j-th column of X.

Appendix C

Motivation for Tire Damping

Consider the 4 DOF vehicle in Fig. B.1 *without* tire damping, *i.e.*, $b_{tf} = b_{tr} = 0$. Suppose the only control goals are minimization of the front vertical and rotational chassis accelerations and suppose that besides the suspension deflections y_1 and y_2 their derivatives $\dot{y}_1$ and $\dot{y}_2$ are measured. The following is *incorrectly* conjectured in [45, Section 4.2]. The control law

$$u = \begin{bmatrix} u_1 \\ u_2 \end{bmatrix} = - \begin{bmatrix} k_{sf} & 0 & b_{sf} & 0 \\ 0 & k_{sr} & 0 & b_{sr} \end{bmatrix} \begin{bmatrix} y_1 \\ y_2 \\ \dot{y}_1 \\ \dot{y}_2 \end{bmatrix} = Ky \tag{C.1}$$

would make the TFM between the road inputs and the chassis accelerations equal to zero, since it compensates the forces generated by the suspension springs (k_{sf}, k_{sr}) and dampers (b_{sf}, b_{sr}). Although K in (C.1) is not an admissible $\mathcal{H}_\infty$ controller, because it does not *asymptotically* stabilize the system (closed-loop eigenvalues on $j\omega$-axis occur), it was expected in [45] that a stabilizing controller achieving $\|M\|_\infty \approx 0$ could be computed.

However, $\mathcal{H}_\infty$ design with μ-Tools rejected this conjecture: $\|M\|_\infty$ was lower bounded by 0.25, *unless* front and rear tire damping was introduced. This appears to be due to the fact, that at the eigenfrequencies of the front and rear axle/tire "subsystems," the input u with a *stabilizing* controller has no influence on the two accelerations and they cannot be arbitrarily small simultaneously. For a 2 DOF vehicle model in [13], this phenomenon is imputed to so-called "invariant points" in the transfer function between the single road input and the single acceleration to be controlled. A similar phenomenon occurs for a 7 DOF model in [13] and the 4 DOF model studied here. This explains the lower bound on $\|M\|_\infty$: at the invariant frequencies, $\bar{\sigma}(M)$ cannot be made arbitrarily small without endangering stability and the achievable performance expressed in the $\mathcal{H}_\infty$ norm is limited.

If tire damping is introduced, invariant points are avoided [23], the effect of which is clear from $\mathcal{H}_\infty$ designs with damping ratios $\beta = 0.01$: $\|M\|_\infty \approx 0$ results. Introduction of small tire damping is justified by the fact, that in practice they are always present. Moreover, the optimal performance levels for candidate IO sets are not "hindered" by a nonzero lower-bound, which serves a better assessment of the IO sets.

Appendix D

Sensor Noise and Actuator Weights in the Generalized Plant

Consider the generalized plant's state-space description in (3.5), *excluding* controller output weights (u-weights) and measurement noise (y-noise):

$$G: \begin{cases} \dot{x} = Ax + B_1 w + B_2 u \\ z = C_1 x + D_{11} w + D_{12} u \\ y = C_2 x + D_{21} w + D_{22} u. \end{cases} \tag{D.1}$$

Next, u-weights "$z_u = W_u u$" and y-noise "$\bar{w}_y = V_y w_y$" are defined, with W_u and V_y diagonal TFMs:

$$W_u: \quad \begin{cases} \dot{x}_u = A_u x_u + B_u u \\ z_u = C_u x_u + D_u u, \end{cases} \tag{D.2}$$

$$V_y: \quad \begin{cases} \dot{x}_y = A_y x_y + B_y w_y \\ \bar{w}_y = C_y x_y + D_y w_y. \end{cases} \tag{D.3}$$

Combining (D.1)–(D.3), the following state-space description results for the generalized plant *including* u-weights and y-noise:

$$\begin{bmatrix} \dot{x} \\ \dot{x}_u \\ \dot{x}_y \end{bmatrix} = \begin{bmatrix} A & 0 & 0 \\ 0 & A_u & 0 \\ 0 & 0 & A_y \end{bmatrix} \begin{bmatrix} x \\ x_u \\ x_y \end{bmatrix} + \begin{bmatrix} B_1 & 0 \\ 0 & 0 \\ 0 & B_y \end{bmatrix} \begin{bmatrix} w \\ w_y \end{bmatrix} + \begin{bmatrix} B_2 \\ B_u \\ 0 \end{bmatrix} u \tag{D.4}$$

$$\begin{bmatrix} z \\ z_u \end{bmatrix} = \begin{bmatrix} C_1 & 0 & 0 \\ 0 & C_u & 0 \end{bmatrix} \begin{bmatrix} x \\ x_u \\ x_y \end{bmatrix} + \begin{bmatrix} D_{11} & 0 \\ 0 & 0 \end{bmatrix} \begin{bmatrix} w \\ w_y \end{bmatrix} + \begin{bmatrix} D_{12} \\ D_u \end{bmatrix} u \tag{D.5}$$

$$y = \begin{bmatrix} C_2 & 0 & C_y \end{bmatrix} \begin{bmatrix} x \\ x_u \\ x_y \end{bmatrix} + \begin{bmatrix} D_{21} & D_y \end{bmatrix} \begin{bmatrix} w \\ w_y \end{bmatrix} + D_{22} u \tag{D.6}$$

The augmented matrices in these equations will again be referred to as "A, $B_1, \ldots, D_{21}$." The Hamiltonians H_X, H_Y in viability conditions 2 and 3 depend on these matrices:

$$H_X = H_X(A, B_1, B_2, C_1, D_{11}, D_{12}, \gamma); \qquad H_Y = H_Y(A, B_1, C_1, C_2, D_{11}, D_{21}, \gamma),$$

(see, *e.g.*, [12] for the exact expressions), as well as the Riccati equation solutions X_∞, Y_∞ in viability conditions 4 and 5: $X_\infty = \mathrm{Ric}(H_X)$, and $Y_\infty = \mathrm{Ric}(H_Y)$ (see, *e.g.*, [45, Section 2.4] for details on the function "Ric").

Hence, due to the influence of A_y and B_y, H_X and X_∞ depend on the output set. In analogy, H_Y and Y_∞ depend on the input set via A_u and C_u. This explains the first potential reason that the three-phase IO selection as mentioned in 1.II in Chapter 7 is impossible. Future research must be performed to support the conjecture, that these influences "drop out." If this conjecture holds, the efficiency of the IO selection can be improved, provided the second potential problem does not occur. In order to write D_{12} and D_{21} in the form (3.6), non-singular transformations are performed on u and y [30, Section 6.7]:

$$\tilde{u} = S_u u, \qquad \tilde{y} = S_y y, \tag{D.7}$$

together with unitary transformations on w and z:

$$\tilde{w} = T_w w, \qquad \tilde{z} = T_z z, \tag{D.8}$$

with $T_w T_w^* = I$, $T_z T_z^* = I$. These transformations are obtained via singular-value decompositions of D_{12} and D_{21}:

$$D_{12} = T_z^{-1} \begin{bmatrix} 0 \\ I \end{bmatrix} S_u, \qquad D_{21} = S_y^{-1} \begin{bmatrix} 0 & I \end{bmatrix} T_w. \tag{D.9}$$

Under these transformations, the generalized plant is rewritten as follows:

$$\begin{aligned} \dot{x} &= Ax + B_1 T_w^{-1} w + B_2 S_u^{-1} u \\ z &= T_z C_1 x + T_z D_{11} T_w^{-1} w + T_z D_{12} S_u^{-1} u \\ y &= S_y C_2 x + S_y D_{21} T_w^{-1} w + S_y D_{22} S_u^{-1} u. \end{aligned} \tag{D.10}$$

The effect of y-noise in T_w, S_y and u-weights in T_z, S_u is a second potential reason that the three-phase IO selection suggested in Chapter 7 is impossible. Moreover, due to the effects of T_z and T_w on D_{11} it is expected that the first viability condition in Section 3.1 must be checked for each IO set again, which was indeed found to be true for the active suspension example.